

**SYNTHESIS AND CHARACTERIZATION OF SOLUBLE  
CONDUCTING POLYMERS FOR OPTOELECTRONIC  
APPLICATIONS**

**HAMMED WASIU ADEBAYO**

**FACULTY OF SCIENCE  
UNIVERSITY OF MALAYA  
KUALA LUMPUR**

**2017**

**SYNTHESIS AND CHARACTERIZATION OF  
SOLUBLE CONDUCTING POLYMERS FOR  
OPTOELECTRONIC APPLICATIONS**

**HAMMED WASIU ADEBAYO**

**THESIS SUBMITTED IN FULFILMENT OF THE  
REQUIREMENTS FOR THE DEGREE OF DOCTOR OF  
PHILOSOPHY**

**FACULTY OF SCIENCE  
UNIVERSITY OF MALAYA  
KUALA LUMPUR**

**2017**

**UNIVERSITY OF MALAYA**  
**ORIGINAL LITERARY WORK DECLARATION**

Name of Candidate: **HAMMED WASIU ADEBAYO**

Registration/Matric No: **SHC120018**

Name of Degree: **DOCTOR OF PHILOSOPHY**

Title of Project Paper/Research Report/Dissertation/Thesis (“this Work”):

**SYNTHESIS AND CHARACTERIZATION OF SOLUBLE CONDUCTING  
POLYMERS FOR OPTOELECTRONIC APPLICATIONS**

Field of Study: **POLYMER CHEMISTRY**

I do solemnly and sincerely declare that:

- (1) I am the sole author/writer of this Work;
- (2) This Work is original;
- (3) Any use of any work in which copyright exists was done by way of fair dealing and for permitted purposes and any excerpt or extract from, or reference to or reproduction of any copyright work has been disclosed expressly and sufficiently and the title of the Work and its authorship have been acknowledged in this Work;
- (4) I do not have any actual knowledge nor do I ought reasonably to know that the making of this work constitutes an infringement of any copyright work;
- (5) I hereby assign all and every right in the copyright to this Work to the University of Malaya (“UM”), who henceforth shall be owner of the copyright in this Work and that any reproduction or use in any form or by any means whatsoever is prohibited without the written consent of UM having been first had and obtained;
- (6) I am fully aware that if in the course of making this Work I have infringed any copyright whether intentionally or otherwise, I may be subject to legal action or any other action as may be determined by UM.

Candidate’s Signature

Date:

Subscribed and solemnly declared before,

Witness’s Signature

Date:

Name:

Designation:

## ABSTRACT

Accelerated increase in growth of world energy consumption, the fast depletion of fossil fuel reserve and climatic change due to the burning of fossil fuel have called for sourcing alternative means to generate energy. Renewable energy sources are inexhaustible and occur naturally; the energy generated are non-polluting and economically viable thus, they are believed to be the befitting alternatives to non-renewable fossil fuels. The most salient method of exploiting the solar energy is via solar cells which directly convert solar radiation absorbed by semiconductors to electrical energy. Unlike silicon solar cells, polymer solar cells are solution processed, flexible and lightweight and therefore believed to offer the eventual solution to renewable energy. Challenges such as low power conversion efficiency and durability being overcome have made polymer solar cells suitable candidate for a future energy source. Backbone rigidity prevents many conjugated polymers from being processable from organic solvents creating major hindrances to their potential applications as donor materials for polymer photovoltaics. Side-chain functionalization is a common way of rendering conjugated polymers solution processed, however, factors such as structural modification can cause steric hindrance in the polymer molecule. Therefore, electrical, optical and mechanical properties of the polymers are greatly affected. Dodecyl benzene sulfonic acid, a surfactant anion, has been used to improve solubility of conducting polyaniline (PANI) and polypyrrole (Ppy) making them soluble in m-cresol, dimethyl sulfoxide (DMSO), dimethylformamide (DMF), and chloroform. This thesis addresses the use of DBSA as a dopant and stabilizer for the synthesis of solution processed conducting polymers. The materials studied in this project are intended for donor material in the active layer of polymer solar cells. Meanwhile, chemical oxidative polymerization of processable conducting polypyrrole using DBSA, a relatively large dopant anion, reduces intermolecular interaction between polypyrrole chains, leading to the organic soluble Ppy.

Therefore, in the present study, solution processable copolymer containing PNVC and Ppy was synthesized via chemical oxidative polymerization with DBSA as a dopant and stabilizer and ammonium persulfate the oxidant. It was found that the solubility of the resulting copolymer was greatly enhanced by the DBSA dopant. Furthermore, the result from the electrical and thermal analysis showed improved thermal behaviour with respect to the Ppy and electrical conductivity as regards the PNVC. Additionally, photovoltaic properties of the DBSA doped PNVC-Ppy copolymer was tested by fabricating BHJ solar cell using the copolymer product as the donor and a soluble fullerene derivative PC<sub>60</sub>BM as the acceptor. The effect of GO and rGO on the electrical properties of the DBSA-doped PNVC-Ppy copolymer was further investigated due to the fact that  $\pi$ -electron rich polymers can form  $\pi$ -stacking with the graphene sheets. The obtained nanocomposites exhibited appropriate optical and electrical properties to be used an active layer in polymer electronics. In conclusion, this thesis demonstrates that solubility of the PNVC-Ppy copolymer can be significantly improved by doping with DBSA and the doped copolymer can be applied in photovoltaics.

## ABSTRAK

Peningkatan penggunaan tenaga dunia, pengurangan rizab bahan api fosil dengan pantas serta perubahan iklim yang berpunca daripada pembakaran bahan api fosil menyebabkan perlunya sumber alternatif untuk menjana tenaga. Ini memastikan sumber tenaga boleh diperbaharui sentiasa ada dan terjadi secara semula jadi. Tenaga yang dihasilkan bukan sahaja tidak mencemar tetapi juga berdaya maju dari segi ekonomi. Oleh itu, ia dipercayai merupakan alternatif untuk bahan api fosil yang tidak boleh diperbaharui. Kaedah yang paling penting untuk mengeksploitasi tenaga solar adalah melalui serapan sel-sel solar yang ditukarkan oleh semikonduktor menjadi tenaga elektrik. Berlainan dari sel-sel solar silikon, sel-sel solar polimer mudah diproses, fleksibel dan ringan. Justeru, ia boleh menyumbang sebagai tenaga boleh diperbaharui. Ia juga berjaya mengatasi cabaran-cabaran seperti faktor kecekapan penukaran kuasa rendah serta ketahanan, lantas membuatnya sesuai digunakan sebagai sumber tenaga di masa depan. Ketegaran struktur tulang belakangnya menghalang banyak polimer konjugat daripada diproses oleh pelarut organik. Ini menghalang potensi aplikasinya sebagai bahan penderma untuk fotovolt polimer. Meskipun fungsi rantai polimer merupakan cara yang biasa digunakan untuk mempercepatkan proses larutan polimer konjugat, faktor seperti pengubahsuaian struktur boleh menyebabkan halangan sterik dalam molekul polimer. Justeru, sifat-sifat polimer seperti elektrik, optik dan mekanikal akan terjejas. Dodesil benzena asid sulfonik yang juga merupakan surfaktan anionik telah digunakan untuk meningkatkan kebolehlarutan polianilina (PANI) dan polipirol (Ppy) sekali gus melarutkannya di dalam m-cresol, dimetil sulfoksida (DMSO), dimetil formamida (DMF) dan kloroform. Tesis ini mengkaji penggunaan DBSA sebagai pendopan dan penstabil untuk sintesis larutan polimer konduktor yang diproses. Bahan-bahan yang dikaji dalam projek ini bertujuan untuk dijadikan bahan penderma untuk lapisan aktif dalam sel-sel solar polimer. Pempolimeran oksidatif kimia polipirol yang boleh diproses menggunakan DBSA, yang mana merupakan pendopan anionik besar, dikenal pasti dapat mengurangkan interaksi antara molekul antara rantaian polipirol lalu menghasilkan larutan Ppy organik. Oleh itu, dalam kajian ini, larutan kopolimer yang boleh diproses dan mengandungi PNVC dan Ppy telah disintesis melalui pempolimeran oksidatif kimia dengan DBSA sebagai pendopan dan penstabil serta ammonium persulfat oksida. Didapati bahawa kebolehlarutan kopolimer yang terhasil telah banyak dipertingkatkan oleh pendopan DBSA itu. Tambahan pula, hasil daripada analisis elektrik

dan haba yang menunjukkan tingkah laku haba lebih berkesan kerana penggunaan Ppy dan pengaliran elektrik untuk PNVC. Selain itu, ciri-ciri fotovolta daripada DBSA PNVC-Ppy kopolimer telah diuji dengan rekaan BHJ sel solar menggunakan produk kopolimer sebagai penderma dan fullerena larut PC<sub>60</sub>BM derivatif sebagai penerima. Kesan GO dan rGO pada sifat-sifat elektrik PNVC-Ppy kopolimer DBSA telah disiasat dengan lebih lanjut kerana kebolehan  $\pi$ -elektron polimer kaya membentuk  $\pi$ -susunan dengan lembaran graphene diragui. Komposit nano yang diperolehi mempamerkan ciri-ciri optik dan elektrik yang sesuai digunakan sebagai lapisan aktif dalam polimer elektronik. Kesimpulannya, tesis ini menunjukkan bahawa kebolehlarutan kopolimer PNVC-Ppy boleh ditingkatkan secara signifikan dengan pendopan DBSA manakala kopolimer yang didopan boleh digunakan dalam fotovolta.

University of Malaysia

## ACKNOWLEDGEMENTS

Alhamdulillah for the journey so far! A Ph.D. program is indeed a journey that requires everything. This journey wouldn't have been successful but with the help from Allah and the support and encouragement of many people. First and foremost, I would like to express my sincere gratitude to my supervisor Assoc. Prof. Ekramul Mahmud who provided me with the opportunity to work in conducting polymer group. Thank you for your sincere guidance, creative support, and gentle advice. I'm equally indebted to my co-supervisor Prof. Rosiyah bint Yahya for her words of encouragement, particularly when the going was very tough. It wouldn't have reached this level if not for her intervention.

I'm really grateful to Assoc. Prof. Khaula Sulaiman of Solar/Photovoltaic Materials Research Group (SPMRG), Department of Physics University of Malaya for giving me the chance to work with her group during the photovoltaic fabrication stage. I also like to thank Lim Lih Wei, her postgraduate student who assisted in the device fabrication. I'm grateful to my fellow group members with whom I have had the pleasure to work with during my Malaya life. Shafiq really assisted in the collation of research materials, he's always ready to render some help whenever needed. Obaid, Ali and I worked together to set up the polymer lab. Ali and I actually started together from the scratch.

My special thanks to my wife for her undiluted love, understanding, caring, and encouragement right from the MSc era till the moment. I really appreciate her help for making my life worthwhile. I'm deeply indebted to my parents for giving me the opportunity to explore this path. Their prayers, unconditional and endless love are the tonics for my survival. I equally appreciate the inputs of my in-laws, they showed up when I really needed a helping hand. I'm grateful to my siblings and my extended family members for their believe, prayers and support.



## TABLE OF CONTENTS

|  |          |
|--|----------|
| Abstract .....   | iii      |
| Abstrak .....  | v        |
| Acknowledgements .....   | vii      |
| Table of Contents .....  | viii     |
| List of Figures .....  | xii      |
| List of Tables.....  | xv       |
| List of Symbols and Abbreviations.....                                   | xvi      |
| <br>   |          |
| <b>CHAPTER 1: GENERAL INTRODUCTION .....</b>                             | <b>1</b> |
| 1.1 Background and Motivation .....                                      | 1        |
| 1.2 Objectives and thesis organization .....                             | 5        |
| <br>   |          |
| <b>CHAPTER 2: LITERATURE REVIEW.....</b>                                 | <b>7</b> |
| 2.1 Organic Semiconductors.....  | 7        |
| 2.1.1 Conjugated Polymers .....  | 7        |
| 2.1.1.1 Historical development .....                                     | 9        |
| 2.1.1.2 Electronic Properties of conjugated polymers .....               | 12       |
| 2.1.1.3 Doping of conjugated polymers .....                              | 14       |
| 2.1.1.4 Band structure and charge carriers in conjugated polymers.....   | 16       |
| 2.2 Heterojunction polymer solar cell .....                              | 19       |
| 2.2.1 Bilayer Heterojunction .....                                       | 19       |
| 2.2.2 Bulk Heterojunction .....  | 20       |
| 2.2.3 Morphology of bulk heterojunctions .....                           | 21       |
| 2.3 Architecture of organic solar cells and performance parameters ..... | 22       |
| 2.4 Rendering conjugated polymers solution processable.....              | 28       |

|       |  |    |
|-------|--|----|
| 2.4.1 | Side chain functionalization .....               | 29 |
| 2.4.2 | Functionalized protonic acid doping .....        | 29 |
| 2.5   | Conjugated polymer-graphene nanocomposites ..... | 31 |

**CHAPTER 3: PROCESSABLE DBSA-DOPED POLY(N-VINYL CARBAZOLE)-  
POLY(PYRROLE) COPOLYMER..... 34**

|       |  |    |
|-------|--|----|
| 3.1   | Introduction.....  | 34 |
| 3.2   | Materials and methods .....  | 38 |
| 3.2.1 | Materials .....  | 38 |
| 3.2.2 | Preparation of DBSA-doped PNVC-Ppy copolymer .....   | 38 |
| 3.2.3 | Characterization.....  | 39 |
| 3.3   | Results and Discussion .....   | 40 |
| 3.3.1 | Roles of APS concentration on conductivity and yield.....                                  | 40 |
| 3.3.2 | Roles of concentration of DBSA on solubility and conductivity of DBSA-doped PNVC-Ppy ..... | 45 |
| 3.3.3 | Optical properties of DBSA-doped PNVC-Ppy .....  | 49 |
| 3.3.4 | Infrared analysis of DBSA-doped PNVC-Ppy .....   | 52 |
| 3.3.5 | XRD pattern of DBSA-doped PNVC-Ppy .....   | 54 |
| 3.3.6 | Thermal property of the DBSA-doped PNVC-Ppy.....   | 55 |
| 3.3.7 | Morphology of DBSA-doped PNVC-Ppy.....   | 57 |
| 3.4   | Conclusion .....   | 59 |

**CHAPTER 4: PHOTOVOLTAIC PERFORMANCE OF SOLUTION  
PROCESSABLE DBSA-DOPED POLY(N-VINYL CARBAZOLE)-  
POLY(PYRROLE) COPOLYMER..... 60**

|     |                   |    |
|-----|-------------------|----|
| 4.1 | Introduction..... | 60 |
| 4.2 | Experimental..... | 63 |

|       |   |    |
|-------|---|----|
| 4.2.1 | Fabrication and characterization of organic solar cells ..... | 63 |
| 4.3   | Results and discussion .....                                  | 64 |
| 4.3.1 | Film-forming ability of the copolymer .....                   | 64 |
| 4.3.2 | Optical and electrochemical properties .....                  | 64 |
| 4.3.3 | Photovoltaic properties .....                                 | 69 |
| 4.3.4 | Conclusion .....  | 72 |

**CHAPTER 5: ENHANCING THE ELECTRICAL CONDUCTIVITY OF DBSA-DOPED POLY(N-VINYL CARBAZOLE)-POLY(PYRROLE) COPOLYMER ..74**

|       |   |    |
|-------|---|----|
| 5.1   | Introduction.....   | 74 |
| 5.2   | Experimental.....   | 77 |
| 5.2.1 | Materials .....   | 77 |
| 5.2.2 | Instrument.....   | 77 |
| 5.2.3 | Preparation of graphene oxide (GO) .....                        | 77 |
| 5.2.4 | Synthesis of PNVC-Ppy/GO Composites .....                       | 78 |
| 5.2.5 | Characterization.....   | 78 |
| 5.3   | Results and discussion .....                                    | 79 |
| 5.3.1 | Fourier transformed infrared spectroscopy (FTIR) analysis ..... | 82 |
| 5.3.2 | XRD study .....   | 83 |
| 5.3.3 | Raman spectroscopy .....  | 83 |
| 5.3.4 | Optical properties of PNVC-Ppy nanocomposite.....               | 85 |
| 5.3.5 | Electrical conductivity.....                                    | 87 |
| 5.4   | Conclusion .....  | 87 |

**CHAPTER 6: REDUCED GRAPHENE OXIDE-POLY(N-VINYL CARBAZOLE)-POLY(PYRROLE) COMPOSITES—SYNTHESIS AND CHARACTERIZATION FOR OPTOELECTRONIC APPLICATIONS..... 89**

|   |   |            |
|---|---|------------|
| 6.1   | Introduction.....                                 | 89         |
| 6.2   | Experimental.....                                 | 93         |
| 6.2.1   | Preparation of rGO .....                          | 93         |
| 6.2.2   | Preparation of PNVC-PPy/rGO nanocomposites .....  | 93         |
| 6.3   | Results and discussion .....                      | 94         |
| 6.3.1   | FTIR analysis .....                               | 94         |
| 6.3.2   | Raman spectroscopy .....                          | 95         |
| 6.3.3   | FESEM study .....                                 | 97         |
| 6.3.4   | Electrical conductivity.....                      | 99         |
| 6.3.5   | X-RD analysis .....                               | 100        |
| 6.3.6   | TGA analysis .....                                | 101        |
| 6.3.7   | Optical study of PNVC-PPy/rGO nanocomposite ..... | 102        |
| 6.4   | Conclusion .....                                  | 104        |
| <b>CHAPTER 7: CONCLUSION AND RECOMMENDATION .....</b> |   | <b>106</b> |
| 7.1   | Conclusions .....                                 | 106        |
| 7.2   | Recommendations.....                              | 108        |
| References .....                                      |   | 110        |
| List of Publications and Papers Presented .....       |   | 128        |

## LIST OF FIGURES

|  |    |
|--|----|
| Figure 2.1: (a) $sp^3$ hybridized carbon atoms forming diamond structure; (b) $sp^2$ hybridized carbon atoms forming graphite structure .....  | 12 |
| Figure 2.2: Balls and sticks model of polyacetylene.....   | 13 |
| Figure 2.3: $sp^2$ hybridization in conjugated polymers: both $sp^2$ hybridized carbons overlap along the nuclei to form a $\sigma$ bond and the remaining p orbitals interact laterally to form a $\pi$ bond..... | 14 |
| Figure 2.4: n-type (phosphorus-doped) and p-type (boron-doped) doping processes in silicon (inorganic semiconductor).....  | 15 |
| Figure 2.5: Band structure of organic semiconductors compared with those of conductors, inorganic semiconductors, and insulators. ....   | 17 |
| Figure 2.6: Molecular structure of buckminsterfullerene C <sub>60</sub> and its soluble derivatives; PC <sub>60</sub> BM and PC <sub>70</sub> BM. ....   | 21 |
| Figure 2.7: Typical device architecture of BHJ photovoltaic cell .....   | 23 |
| Figure 2.8: $\eta EQE$ for a P3HT : PCBM and P3HT:DPM-6 photovoltaic cell (Bolink et al., 2011).....   | 25 |
| Figure 2.9: Current-voltage (I-V) curve for a typical BHJ solar cell under illumination  | 26 |
| Figure 3.1: Thermal stability of PNVC–Ppy copolymer vs NVC concentration at different temperatures .....   | 42 |
| Figure 3.2: Electrical conductivity of PNVC–Ppy copolymer vs NVC concentration at different temperatures.....  | 43 |
| Figure 3.3: Electrical conductivity of DBSA-doped PNVC-Ppy vs APS concentration at different temperatures. ....  | 44 |
| Figure 3.4: Yield of the copolymers vs APS concentration at – 5 °C .....   | 45 |
| Figure 3.5: Solubility and electrical conductivity of DBSA-doped PNVC-Ppy synthesized with different DBSA concentrations .....   | 46 |
| Figure 3.6: Solubility of DBSA-doped PNVC-Ppy vs polarity indices of the solvents.....   | 48 |
| Figure 3.7: Optical absorption spectra of DBSA-doped PNVC-Ppy, Ppy, and PNVC.....  | 50 |
| Figure 3.8: Band gap estimation of DBSA-doped PNVC-Ppy .....   | 51 |

|   |    |
|---|----|
| Figure 3.9: UV-vis spectra of BDSA doped PNVC-Ppy at varying concentrations of BDSA.....  | 52 |
| Figure 3.10: FTIR spectrum of (a) PNVC, (b) Ppy and (c) BDSA-doped PNVC- Ppy..  | 53 |
| Figure 3.11: XRD patterns of PNVC, BDSA-doped PNVC- Ppy, and Ppy. ....  | 55 |
| Figure 3.12: TGA thermogram of PNVC, Ppy, doped PNVC-Ppy and undoped PNVC-Ppy. ....   | 56 |
| Figure 3.13: FESEM images of (a) Ppy, (b) PNVC, and (c) BDSA-doped PNVC–Ppy copolymer.....  | 58 |
| Figure 4.1. Photoluminescence (PL) spectra of BDSA-doped PNCV-Ppy, BDSA-doped PNVC-Ppy:PC60BM .....   | 69 |
| Figure 4.2: a, b) logarithmic J-V characteristics of the photovoltaic devices.....  | 71 |
| Figure 5.1: Photograph of (a) BDSA-doped PNVC-Ppy/GO dispersed in DMF; (b) PNVC-Ppy/GO (without BDSA) dispersed in DMF .....  | 80 |
| Figure 5.2: FESEM images of (a) GO, (b) BDSA-doped PNVC-PPy, and (c) BDSA-doped PNVC-PPy/GO.....  | 81 |
| Figure 5.3: FTIR spectra of (a) BDSA-doped PNVC-Ppy/GO, (b) GO, and (c) PNVC-Ppy copolymer .....  | 82 |
| Figure 5.4: X-RD spectra of (a) BDSA-doped PNVC-PPy/GO nanocomposite, (b) BDSA-doped PNVC-PPy copolymer and (c) GO. ....  | 83 |
| Figure 5.5: Raman spectroscopy of (a) nanocomposite PNVC-PPy/GO, (b) copolymer PNVC-PPy and (c) graphene oxide.....   | 85 |
| Figure 5.6: Optical absorption spectra of (a) BDSA-doped PNVC-Ppy copolymer and BDSA-doped PNVC-Ppy nanocomposite, (b) GO, (c) Photoluminescence excitation of copolymer and nanocomposite..... | 86 |
| Figure 6.1: FTIR of GO, rGO, BDSA-doped PNVC-Ppy, and BDSA-doped PNVC-PPy/rGO nanocomposite.....  | 95 |
| Figure 6.2: Raman spectra of a) BDSA-doped PNVC-Ppy/rGO-3, b) BDSA-doped PNVC-Ppy/rGO-2, c) BDSA-doped PNVC-Ppy/rGO-1 d) rGO, e) BDSA-doped PNVC-Ppy, and f) GO .....                           | 97 |
| Figure 6.3: FESM image of a) rGO, b) BDSA-doped PNVC-Ppy, and c) BDSA-doped PNVC-Ppy/rGO .....  | 98 |

|  |     |
|--|-----|
| Figure 6.4: X-RD spectra of a) PNVC-Ppy b) rGO c) PNVC-Ppy/rGO-1, d) PNVC-Ppy/rGO-2 and d) PNVC-Ppy/rGO-3 .....              | 101 |
| Figure 6.5: Thermogravimetry (TGA) micrograph of rGO, composite, and copolymer .....   | 102 |
| Figure 6.6: Optical absorption spectra of DBSA-doped PNVC-Ppy, DBSA-doped PNVC-Ppy/rGO, and rGO (in-set).....                | 103 |
| Figure 6.8 : Photoluminescence spectra of a) PNVC-Ppy, b) PNVC-Ppy/rGO-1, c) PNVC-PPy/rGO-2, d) PNVC-Ppy/rGO-3, e) rGO ..... | 104 |

University of Malaya

## LIST OF TABLES

|  |    |
|--|----|
| Table 2.1: Examples of a few conjugated polymers .....   | 11 |
| Table 3.1. Solubility of PNVC-Ppy in selected organic solvents (g/100ml) .....   | 48 |
| Table 3.2. FTIR band assignments of PNVC, Ppy, and PNVC-PPY .....  | 54 |
| Table 4.1: Absorbance maximum of copolymer films spin coated from different solvents (20 mg copolymer/mL). .....   | 66 |
| Table 4.2. Optical and electrochemical properties of DBSA-doped PNVC-Ppy copolymer .....   | 68 |
| Table 4.3. Photovoltaic performance of the solar cell based on DBSA-doped PNVC-Ppy:PC <sub>60</sub> BM thin film spin coated at 1000 or 500 rpm before and after annealing at 180 °C for 10 min..... | 72 |
| Table 6.1: Electrical conductivity of rGO compared to GO, copolymer and DBSA-doped PNVC-Ppy/rGO.....   | 99 |



## LIST OF SYMBOLS AND ABBREVIATIONS

|          |   |   |
|----------|---|---|
| ACN      | : | Acetonitrile                                |
| AM       | : | Air mass                                    |
| APS      | : | Ammonium persulphate                        |
| BHJ      | : | Bulk heterojunction                         |
| BP       | : | British petroleum                           |
| CdS      | : | Cadmium sulphide                            |
| CdTe     | : | Cadmium telluride                           |
| CHP      | : | N-cyclohexyl-2-pyrrolidone                  |
| CIGS     | : | Copper indium gallium selenide              |
| CP       | : | Conducting polymer                          |
| CP/G     | : | Conducting polymer-graphene                 |
| CuPc     | : | Copper phthalocyanine                       |
| DA       | : | Donor-acceptor                              |
| DMF      | : | Dimethyl formamide                          |
| DMSO     | : | Dimethyl sulphoxide                         |
| $E_g$    | : | Electronic band gap                         |
| FESEM    | : | Field emission scanning electron microscope |
| FET      | : | Field-effect transistor                     |
| FF       | : | Fill Factor                                 |
| FTIR     | : | Fourier transforms infrared                 |
| GO       | : | Graphene oxide                              |
| GOR(rGO) | : | Reduced graphene oxide                      |
| HOMO     | : | Highest occupied molecular orbital          |
| IPCE     | : | Incident photon-to-current efficiency       |

|                     |   |  |
|---------------------|---|--|
| ITO                 | : | Indium tin oxide                           |
| $J_{sc}$            | : | Short circuit current                      |
| K                   | : | Kelvin                                     |
| LUMO                | : | Lowest unoccupied molecular orbital        |
| NMP                 | : | N-methyl pyrrolidone                       |
| NVC                 | : | N-vinyl carbazole                          |
| OLED                | : | Organic light-emitting diode               |
| OPV                 | : | Organic photovoltaic                       |
| OSC                 | : | Organic semiconductor                      |
| P3AT                | : | Poly (3 alkyl) thiophene                   |
| P3HT                | : | Poly(3-hexylthiophene)                     |
| PA                  | : | Polyacetylene                              |
| PANI                | : | Polyaniline                                |
| PC <sub>60</sub> BM | : | [6,6]-phenyl-C61-butyric acid methyl ester |
| PCE                 | : | Power conversion efficiency                |
| PEDOT               | : | Polyethylene dioxythiophene                |
| PI                  | : | Polarity index                             |
| PL                  | : | Photoluminescence                          |
| PNVC                | : | Poly n-vinyl carbazole                     |
| PPP                 | : | Poly(p-phenylene)                          |
| PPV                 | : | Poly(phenylenevinylene)                    |
| Ppy                 | : | Polypyrrole                                |
| PSC                 | : | Polymer solar cell                         |
| PSS                 | : | Polyparaphenylene sulphide                 |
| PT                  | : | Polythiophene                              |
| PV                  | : | Photovoltaic                               |

|          |   |                            |
|----------|---|----------------------------|
| SR       | : | Spectra response           |
| TGA      | : | Thermogravimetric analysis |
| THF      | : | Tetrahydrofuran            |
| TW       | : | Terawatt                   |
| $V_{oc}$ | : | Open circuit voltage       |
| W        | : | Watt                       |
| XRD      | : | X-ray diffraction          |

University of Malaya

## CHAPTER 1: GENERAL INTRODUCTION

### 1.1 Background and Motivation

Optoelectronics is a branch of electronics that combines optical and electronic properties of semiconducting materials to fabricate devices that operate on both light and electrical currents. Optoelectronic devices produce electrical energy on exposure to light energy in the visible and infrared regions of the electromagnetic spectrum. These class of devices includes light-emitting diodes and laser diodes that produce light when activated electrically, photovoltaic cells that convert light to an electrical energy, and devices that can control the propagation of light using electronics. When an incident light in form of photon strikes a surface, the surface produces photoluminescence. Devices such as photoresistors applicable as twilight switches, security, and counting systems are common examples of photoconductive devices. Their operational principle is based on detecting variations in the light intensities and subsequently, deactivate or activate electronic circuits. Devices such as phototransistors and photodiodes are in this category as they generate current upon illumination using reverse bias junctions. On the other hand, photovoltaic devices produce electricity on exposure light using potential difference generated across the p-n junction.

To be potentially useful in optoelectronics, a conducting polymer must possess excellent mechanical and electronic properties, solution processability, and high environmental stability. However, a fundamental problem hindering the processes and application of conducting polymers is the difficulties involved in rendering conjugated polymer solution processable. Although conjugated polymers are relatively infusible and insoluble in organic solvents because of the backbone rigidity resulting from the conjugated double bonds, solubility can be achieved through chemical modifications of the polymeric chain with little effect on the electrical conductivity. From the industrial point of view, achieving solubility will enable processing of conducting polymer blends,

nanocomposites or copolymer films or fibre for various electronic and mechanical applications.

Furthermore, the ability to process conjugated polymer from solution has introduced a new era in terms of fundamental research areas, such as the spectroscopic origin of charge storage difference between conducting polymer in solid state and dissolved form. Fundamentally, the conjugated polymer is doped in order to achieve a reasonable state of conduction. However, mechanisms for the inherent restacking of doped conducting polymer have been linked to two possible causes; (1) the direct impact of doping on the polymer rigidity (2) the increased inter-chain interaction due to increase in polarity. Conducting polymer chain rigidity can be influenced by an increase in electron density of the region around the double bond.

Owing to the synergistic effect of composite materials, conducting polymer blends, copolymers or nanocomposites exhibit exceptional properties. Thus, various forms of conducting polymers are expected to be applicable in many areas, such as energy storage devices, sensors, catalysis, microwave absorption and EMI shielding, ER fluids and optoelectronics. Optoelectronic applications of conducting polymers especially polymer solar cells require the conjugated polymer to be solution processable from organic solvents. As mentioned earlier, the extent of solubility of a given conjugated polymer is governed by factors such as chain length, backbone rigidity, the degree of polymerization, the polarity of the substituent groups, and interchain interaction. Apart from solution processability, conducting polymer solubility also contributes to the morphology, and crystallinity of the active layer material, which eventually govern the optimal performance of optoelectronic devices.

In 1839, a French experimental physicist Edmund Becquerel discovered that certain materials could display photovoltaic effect by generating a weak electrical current on

exposure to sunlight (Becquerel, 1839). In 1873 Smith discovered photoconductivity in selenium (Adams & Day, 1876; Spanggaard & Krebs, 2004). later in 1883 Fritts fabricated photovoltaic cell by coating gold with selenium (Chandrasekaran et al., 2011). Although 1 % efficiency was recorded for Fritts' solar cell, materials involved were very costly and thus the cell was never adopted on a large scale. The discovery of the first practical silicon solar cell by a team of scientists at Bell Laboratory in 1953 revolutionized the solar cell technology with power conversion efficiency of 6 % (Chapin et al., 1954).

The photovoltaic effect is the basic process in which electron-hole pairs are created when solar photons fall on semiconductors. Upon light absorption, the electron is displaced from the valence band to the conduction of a semiconductor leaving behind a positive charge called the hole. If the semiconductor material is connected to two charge collection points (electrodes), electricity can be generated. The electrical energy generated is clean and renewable.

For many years, inorganic solar cell consist of mainly crystalline silicon has been the most circulated solar power outlet. In terms of power conversion efficiency ( $\approx 26\%$ ) (Green et al., 2015) and life cycle ( $> 20$  years), (Bundgaard & Krebs, 2007; Gong et al., 2015) silicon-based solar cell is still a reference point. Despite high efficiency, very expensive materials and the high cost of production of silicon-based solar cells remain the challenges to the industry. For example, the cost of production of the photon absorber in silicon-based solar cells is almost half of the total cost (Hammed et al., 2013; Rahimi et al., 2013).

In the quest for reducing materials and production costs of the first-generation wafer based photovoltaic technologies, the second-generation solar cell technology is currently under active scientific investigation. The new technology involves direct deposition of thin film of amorphous silicon, cadmium telluride (CdTe), copper indium gallium

selenide (CIGS) or cadmium sulphide (CdS) onto a large area substrate by either sputtering, physical or chemical vapour deposition. Apart from the lower cost of production, ease of fabrication into a thin film and higher photon absorption render second generation solar cells stiff competitor to the silicon wafer. However, the efficiency of the thin film photovoltaic cell which is currently in the range of 15-20% (Lu et al., 2015) and its commercial use are some of the challenges to overcome.

Simultaneously, since the discovery of intrinsic semiconducting polymers in the 1970s, (Heeger, 2001; MacDiarmid, 2001) research focuses on conjugated polymers has increased immensely. As a result, a range of applications of organic thin film and organic solid based devices have emerged. Among them are biosensors, photodiodes, organic light-emitting diodes (OLEDs) (Gross et al., 2000), field-effect transistors (FETs) (Horowitz, 1998), supercapacitors (Bispo-Fonseca et al., 1999) and photovoltaic cells. The early stage of OPV witnessed devices with very low power conversion efficiency and short life span (Kallmann & Pope, 1959; Nicholson & Castro, 2010). Recently, organic based solar cells have demonstrated capabilities in terms of efficiency (11 %) (Green et al., 2015) and stability comparable to their inorganic counterparts making them suitable candidates for future renewable energy source as they are not only solution processable but also suitable for high-throughput large area production via screen printing (Krebs et al., 2009).

Owing to their numerous advantages such as low cost of production, ease of fabrication into a thin film, mechanical flexibility and high photon absorption, organic semiconductors are expected to be suitable for various electrical and electronic applications including generation of portable and domestic electricity. Polymer solar cells can be used as building materials, combine with textile or plastic materials, for cost reduction and effective usage (Bedeloglu, 2011).

## 1.2 Objectives and thesis organization

This project aims at testing the hypothesis that copolymerization of n-vinyl carbazole and pyrrole monomers in the presence of dodecyl benzene sulfonic acid will yield soluble conducting polymers applicable as active layer materials in polymer bulk-heterojunction solar cells.

It is well-known that side chain functionalization is one of the common ways of rendering conjugated polymers solution processable. However, such structural modification often leads to steric hindrance on the conjugated backbone, especially if the side chains are big alkyl groups. As a result, electrical, optical and mechanical properties of the polymers are significantly affected.

The prime focus of this work is to devise an easy route to polymerizing soluble conducting polymers using organic acid, dodecyl benzene sulfonic acid. This novel material is expected to be solution processable due to the stabilizing effect of the organic acid making it possible to spin cast a thin film from the polymer product. Another focus of the present work is to investigate the optical, electrochemical and morphological properties of the polymer products as required for their applications as donor materials in solar cells. Lastly, the present work also emphasizes the application of the copolymer products as donor materials in the active layer of polymer bulk heterojunction solar cells.

In Chapter 2, a brief historical background of solar cells *vis-à-vis* the emergence of organic based solar is discussed. The second part of the chapter addresses the concept of polymer photovoltaic cells, its working principle, and characterization. In the last part of the chapter, deep insight into the chemistry of  $\pi$ -conjugated polymers, their preparation and the state of the art polymers in the field of organic electronics are addressed. The last part of the chapter addresses the various methods of rendering conjugated polymers



solution processable by evaluating side chain functionalization and the use of functional protonic acid dopants.

In Chapter 3, synthesis and characterization methods of solution processable  $\pi$ -conjugated polymers are discussed. The film forming abilities of the polymer in various organic solvents are tested to investigate their potentials as donor materials in polymer bulk-heterojunction solar cells.

In Chapter 4, having studied the optical and electronic bandgaps as well as photoluminescence properties of the copolymers, photovoltaic cells with solution processable DBSA-doped PNVC-Ppy copolymer as the donor material and PC<sub>60</sub>BM as the electron acceptor are fabricated. Photovoltaic properties of these cells such as fill factor, open circuit voltage, short circuit current and power conversion efficiency are measured.

Due to the low conductivity of poly n-vinyl carbazole, the electrical conductivity of the copolymer product is lower than that of polypyrrole. Therefore, in Chapter 5 and 6, graphene, a single layer of graphite that is well known due to its high electrical and excellent mechanical properties is used to form a composite with the copolymer. The effects of graphene oxide and reduced graphene oxide on the electrical property of the polymer are thus investigated.

## CHAPTER 2: LITERATURE REVIEW

### 2.1 Organic Semiconductors

Organic solar cells are new technology whereby optically active organic materials are used to replace inorganic semiconductors in order to reduce production cost and increase domestic application of solar cells. Among the advantages of organic materials is molecular design flexibility resulting from the ability to easily modify their physical and chemical orientations.

Organic materials are readily available and can be solution processable. Thus, a large volume of organic solar cells can be fabricated at low cost via spin coating, inkjet printing, screen printing doctor blading, and roll to roll printing (Krebs, 2009). Organic molecules readily absorb photons because of their high optical absorption coefficient. Therefore, the ratio of material quantity to light absorbed is very low. The main shortcomings of organic solar cells are low device efficiency and low stability.

Organic solar cells can be grouped into two categories based on the size of the constituent molecules. While solar cells fabricated from small molecules are usually synthesized by thermal evaporation and then vacuum-deposited in the form of thin film, polymer solar cells are generally solution-processed from single or a mixture of two or three organic solvents. However, recent studies have shown that small molecule organic photovoltaic cells with excellent efficiency are also solution processable (Sun et al., 2012; Zhou et al., 2012). The discussions in this thesis will be limited to polymer-based solar cells.

#### 2.1.1 Conjugated Polymers

Based on their electrical behaviours, materials are generally classified as conductors (conductivity  $> 10^3$  S/cm), insulators (conductivity  $< 10^{-10}$  S/cm), and semiconductors ( $10^{-10} < \text{conductivity} < 10^{-4}$  S/cm based on doping level). The general belief about polymers

was that they were insulating in nature, unable to transport electrical charges and thus their usage was confined to packaging, electrical insulations, and fabric where their flexibility and inert properties were tapped. Insulating polymers contain long chains of saturated hydrocarbons with surface resistivity above  $10^{12}$  ohm-cm. In these polymers, all the valence electrons of the carbon atoms forming the backbone are used for covalent bonding. Hence, no free electrons and therefore, the polymers are insulating.

Development of conjugated polymers that displays conductivity when doped changed “all-insulating” perception about polymers. First of such attempt was the conductivity of doped polypyrrole reported by McNeill *et al* (1963) and was measured to be  $1 \text{ S cm}^{-1}$ . Later in 1977, Heeger *et al.* (2000) accidentally discovered that polymers (plastics) can conduct in a similar way to inorganic semiconductors or even metals. They were thus awarded the Nobel Prize in Chemistry in 2000 for the ground-breaking discovery.

The discovery of polyacetylene in 1977 subsequently lead to further investigations into the electrical properties of conducting polymers and more conjugated polymers and their derivatives were discovered in early years. Nowadays, apart from conduction mechanism of conjugated polymers, other intriguing properties of conjugated polymers such as photoluminescence, optical behaviour, and film forming ability are being investigated. The accelerating popularity is due to molecular tunability, a key factor to collaborative research and to the evolving technological applications of these novel materials in supercapacitors (Snook *et al.*, 2011; Wang *et al.*, 2014), electromagnetic shielding (Thomassin *et al.*, 2013; Vyas & Chandra, 2016), molecular electronics (Kim *et al.*, 2013), sensors (Ates, 2013; Green *et al.*, 2010), organic solar cells (Coughlin *et al.*, 2014), and non-linear optics (Prasad & Ulrich, 2012).

Unlike other conducting polymers which are made conducting by forming a composite with conducting particles such as metal, carbon, or graphite (Croce *et al.*, 1990; Huo *et*

al., 2014); intrinsically conducting polymers possess conjugated double bonds in their backbone and can be made conducting via doping. Conjugated polymers, similar to other organic compounds, contain single bonds built from  $\sigma$  (sigma) bonds and double bonds built from  $\pi$  (pi) bonds.  $\sigma$  bonds between the nuclei of the carbon atoms that make up the polymer chain are immobile and therefore, give the polymer its firmness and rigidity. By introducing dopant materials, the  $\pi$ -electrons can easily be delocalized, the reason for their electrical conductivity. Figure 2.1 shows a few conjugated polymers that serve as the basis for the research into the field of conducting polymers. The remaining part of this chapter will address the historical developments of conjugated polymers with a deep insight on their characteristic properties.

#### **2.1.1.1 Historical development**

Mankind has been using natural polymers in the form of wood, fibre, bone, and fur since the primeval periods. However, these materials were not known as macromolecules until a Nobel Prize winner, Hermann Staudinger coined the word 'macromolecule' when working on a molecule with large polymeric chains. Later, the macromolecular chemistry was brought to a limelight by the contribution of Nobel laureates Karl Ziegler, Giulio Natta, and Paul Flory. However, the products of their investigations were insulating polymeric material devoid of electrical characteristics. Hence, they were deemed not interesting from conducting polymer perspective. Meanwhile, many conducting polymers have been known and used without being aware of their conductivity perhaps due to the improper characterization that obscured their electronic properties. As an example, Poly (p-phenylene sulphide), PSS branded as Rayton by Phillips Chemicals has been commercially produced and applied as an insulator since the past three decades.

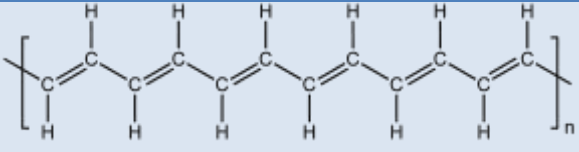
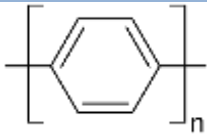
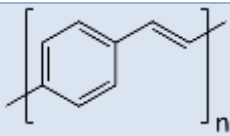
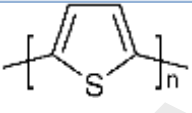
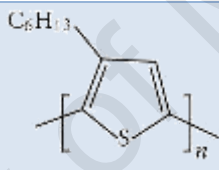
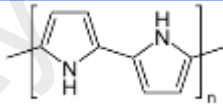
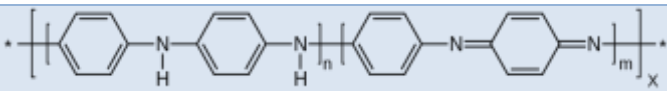
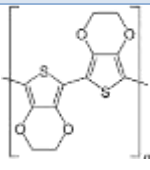
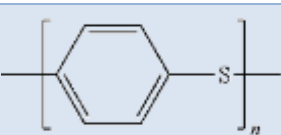
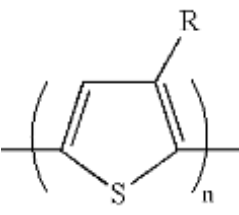
The ground-breaking efforts of Shirakawa and co-workers on the preparation of polyacetylene as well as doping it to assume metallic conductivity by MacDiarmid and

Heeger research group shifted research focus towards conjugated polymers and their applications (Heeger, 2001; Shirakawa, 2001). While these investigations opened a new door into the world of plastics, it should be noted that investigation into conducting behaviour of conjugated polymers can be traced back to the work of René Buvet and Marcel Jozefowicz on polyaniline as well as Donald Weiss on polypyrrole in the 19<sup>th</sup> century when they were not known as polymers.

McNeill and Weiss (1959) investigated conducting polymers to obtain adsorbents that can be activated electrically. Using hydroquinone and phthalic anhydride reagents, they obtained insoluble xanthene polymers that exhibited semiconductor properties. Later based on a report that upon heating, thermally unstable tetraiodopyrrole liberates iodine vapour to produce a black solid mass, Weiss and McNeill isolated and then polymerized an insoluble black powder from tetraiodopyrrole (McNeill et al., 1963). Characterizing the structural and electrical properties of the product (polypyrrole), they observed 'a three-dimensional network of pyrrole rings' that contain 'iodine substitution' (Bolto & Weiss, 1963; Rasmussen, 2011). Their work proposed a tentative structure of (iodine substituted) polypyrrole with good electrical conductivity having resistivity ranged between 11-200  $\Omega$  cm (Bolto et al., 1963).

Aniline, on the other hand, has been known since the mid-1800s (Inzelt, 2012) owing to its oxidation into coloured substances. Its ability to easily undergo redox process was the major reason why it was used to study the mechanism of oxidative polymerization in the early 1900s (Inzelt, 2012). To understand the electronic properties and subsequently, the redox behaviour of oligoaniline, Jozefowicz and his group devoted to finding a reproducible synthetic route to obtain aniline oligomer (Rasmussen, 2011). This later leads to the chemical polymerization of emeraldine form of polyaniline using ammonium persulfate as the oxidizing agent.

Table 2.1: Examples of a few conjugated polymers

|  |  |
|--|--|
| <p><b>Polyacetylene (PA)</b></p>   |    |
| <p><b>Poly(p-phenylene) (PPP)</b></p>  |     |
| <p><b>Poly(phenylenevinylene) (PPV)</b></p>                                  |     |
| <p><b>Polythiophene (PT)</b></p>   |     |
| <p><b>poly(3-hexylthiophene) (P3HT)</b></p>                                  |    |
| <p><b>Polypyrrole (PPy)</b></p>  |   |
| <p><b>Polyaniline (PANI)</b></p>   |  |
| <p><b>Polyethylene dioxythiophene (PEDOT)</b></p>                            |   |
| <p><b>Polyparaphenylene sulfide (PSS)</b></p>                                |  |
| <p><b>Poly (3 alkyl) thiophene (P3AT)</b></p> <p>R = methyl, butyl, etc.</p> |   |

### 2.1.1.2 Electronic Properties of conjugated polymers

Carbon is the element number 6 of the Periodic Table with ground state electronic configuration of  $1s^2 2s^2 2p^2$ . Therefore, it belongs to group 4 having its valence electrons in 2s and 2p orbitals. In a typical organic molecule where carbon is the central atom, the 2s and 2p orbitals in the atomic carbon may hybridize into tetrahedral  $sp^3$  orbital, planar hexagonal  $sp^2$  orbital or  $sp$  orbital which is linear. Diamond represents the simplest  $sp^3$  structure of carbon materials while polyacetylene and graphite are in  $sp^2$  form.

In diamond, the tetravalency of carbon atom is satisfied with single covalent bonds ( $\sigma$  bonds) only whereas in graphite (figure 2.1) and polyacetylene, only 3 electrons are hybridized. The 4<sup>th</sup> electron which is unhybridized occupies the empty  $2p_z$  orbital. Therefore, the free  $\pi$ -electrons in graphite are responsible for its conductivity. Likewise, Polyacetylene 'is in the metallic conducting regime' when doped (MacDiarmid, 2001). However, in diamond, all the valence electrons of carbon are used for  $\sigma$  bond. Hence no mobile electrons and diamond is an insulator.

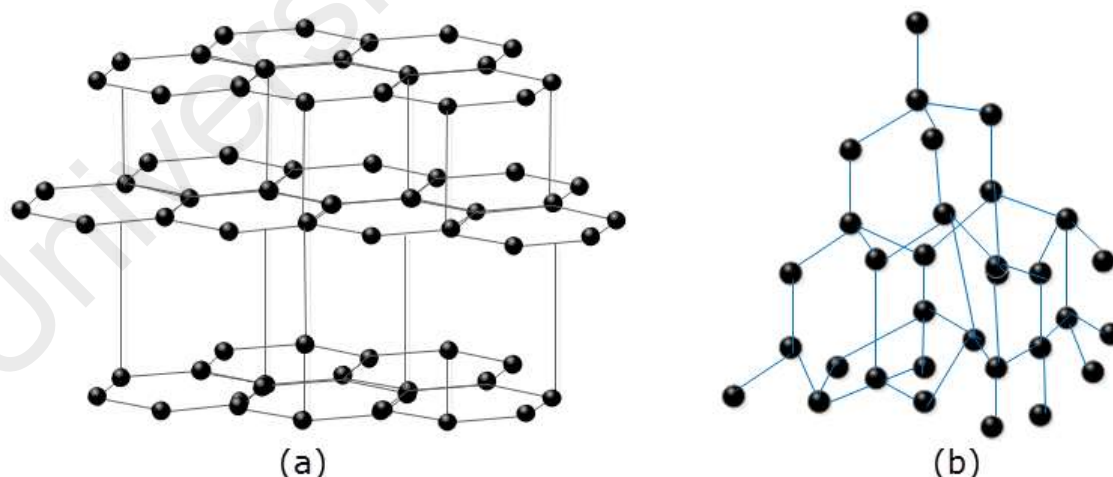


**Figure 2.1: (a)  $sp^3$  hybridized carbon atoms forming diamond structure; (b)  $sp^2$  hybridized carbon atoms forming graphite structure**

In polyacetylene molecule (figure 2.2), the 3 hybridized valence electrons of carbon atom form 3  $\sigma$ -bonds, one each with the adjacent carbons and one with a hydrogen atom.

The inter-carbon  $\sigma$ -bonds responsible for the stability of the carbon chains (backbone) and other structural properties of the polymer. The remaining  $2p_z$  orbitals occupied by the 4<sup>th</sup> electron overlap laterally (figure 2.3) with that of adjacent carbon atoms in the polymer chain forming the weaker  $\pi$ -bonding orbitals that are responsible for optoelectronic properties of the polymer.

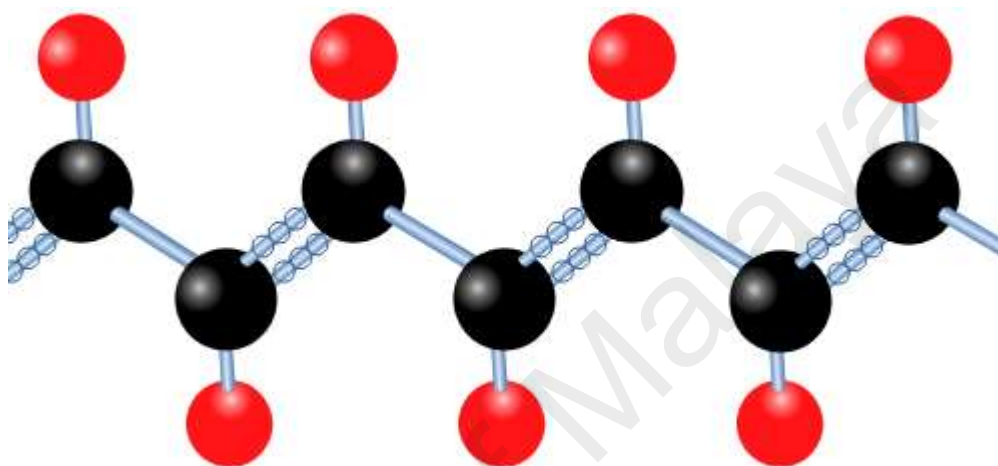


**Figure 2.2: Balls and sticks model of polyacetylene**

Overlapping of  $\pi$ -orbitals allows molecular rotation at the  $\pi$ -bonding sites which facilitate planarity of the molecule giving rise to a phenomenon called conjugation. In conjugation system, the  $\pi$ -electrons are delocalized along the backbone of the polymer. Therefore, conjugated polymers are carbon-based materials with backbones consisting of carbon atoms linked together by  $sp^2$  hybridized  $\sigma$ -bonds with delocalized unpaired electrons ( $\pi$ -electrons) that allow charge transfer along the backbone of the polymer.



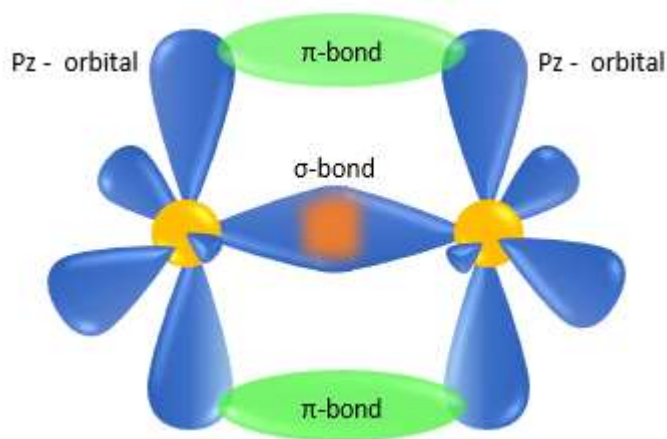


**Figure 2.3:  $sp^2$  hybridization in conjugated polymers: both  $sp^2$  hybridized carbons overlap along the nuclei to form a  $\sigma$  bond and the remaining p orbitals interact laterally to form a  $\pi$  bond**

They are considered  $\pi$ -conjugated because their backbones are mainly alternating (C–C) single and (C=C) double bonds. Among the so-called intrinsically conducting polymers, only polyacetylene [trans-(CH) $_x$ ] can be called a semiconductor in its neutral state. Others are low semiconductors or insulators with poor electrochemical properties. To consider conjugated polymers useful in their potential application areas, enhanced conductivity is required. The conductivity of conjugated polymers can be increased by several magnitudes via a process called doping. Doping dramatically transforms conjugated polymers from low semiconductors or insulators ( $10^{-10}$  S/cm) to conductors (1 to  $10^4$  S/cm).

### 2.1.1.3 Doping of conjugated polymers

Conjugated polymers popularity continues to grow and they have become very relevant on account of doping concept that has not only differentiates them from other forms of polymers, also enhances their scientific and technological importance (Chiang et al., 1977). The first doping process on conjugated organic polymer was carried out on trans-polyacetylene in 1977. Trans-polyacetylene was doped with iodine vapour and conductivity of the polymer increased from  $10^{-5}$  to  $10^3$  S/cm (Shirakawa et al., 1977). Doping of conjugated polymers is carried out in order to initiate charge transfer process

by introducing electron acceptor or electron donors into the polymer chain to partially oxidize or reduce the polymer. As a result, charged defects such as solitons, polarons or bipolarons are formed in the polymer chain and thus serve as charge carriers. By inserting polymeric organic salts as counterions into the conjugated polymer structure, the conducting polymers can undergo oxidation or reduction reaction and thus converted to conducting polymer salts. The counter ions (dopants) are either oxidants or reductants donating electrons to or accepting electrons from the polymers; they allow the conducting polymers to maintain their charge neutrality. This is quite different to what obtains in inorganic semiconductors (figure 2.4) where a small quantity of the dopant is introduced into the lattice of the semiconductor to significantly enhance its electrical conductivity. Another difference between doping in conducting polymers and the inorganic semiconductors is reversibility. Doped conjugated polymers can be de-doped chemically or electrochemically to restore the original properties of the polymer without degrading the polymeric chain (McCullough & Jayaraman, 1995).

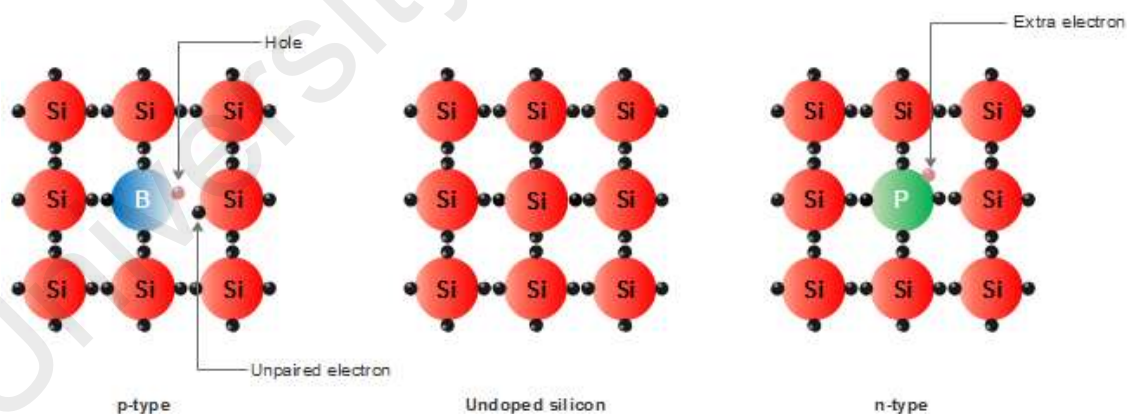


**Figure 2.4: n-type (phosphorus-doped) and p-type (boron-doped) doping processes in silicon (inorganic semiconductor)**

Doping of conducting polymers can be classified according to the chemical nature of the dopant species or the mechanism of doping. Redox, non-redox, ion implantation, and thermal doping represent a different mechanism of doping conducting polymers.

Meanwhile, dopant could be organic, inorganic or polymeric in nature. Organic dopants can enhance both the solubility and conductivity of the conjugated polymer. Their effects on the solubility of conjugated polymers will be fully discussed in section 2.5.2 of this thesis.

#### **2.1.1.4 Band structure and charge carriers in conjugated polymers**

In inorganic semiconductors, mobile electrons are delocalized in the continuous energy bands formed due to the interaction of atomic orbitals of the atoms of the semiconductor. However, in conjugated polymers, overlapping of several  $\pi$ -electrons of the carbon atoms that constitute the polymer backbone results in the formation of broad quasi-continuous energy bands. These energy bands are analogous to the conduction and valence bands of inorganic semiconductors (figure 2.5). In the electronic structure of inorganic semiconductors, the lower energy level is referred to as the valence band while the energy level that contains free electrons is called the conduction band. This is a similitude of the highest occupied molecular orbital (HOMO) and the lowest unoccupied molecular orbital (LUMO) in organic semiconductors. Assuming that the  $\sigma$ -bonds along the polymer backbone are equal with evenly distributed  $\pi$  electrons between the bonds, the band structure of the polymer would have been metallic and the polymer would have displayed metallic character. However, due to Peierls Instability, the structure of polyacetylene is dimerized with unequal bond lengths that are displayed as alternation of carbon to carbon single bonds (C–C) and carbon to carbon double bonds (C=C) respectively (MacDiarmid, 2001).

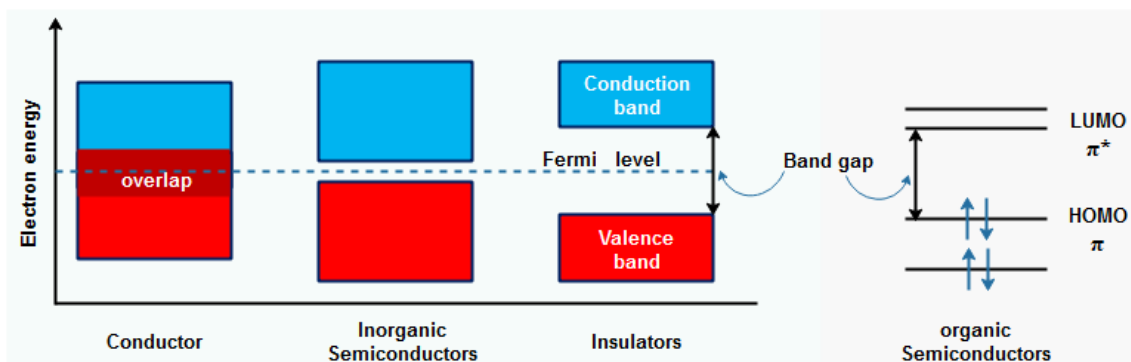


**Figure 2.5: Band structure of organic semiconductors compared with those of conductors, inorganic semiconductors, and insulators.**

Carbon to carbon single bonds (C–C) is longer than carbon to carbon double bonds (C=C). Thus, dimerized polyacetylene is seen as a semiconductor not like a metal because there are no partially filled  $\pi$ -electron bands. Rather, the  $\pi$  molecular orbital is split into two: fully occupied bonding ( $\pi$ ) orbitals otherwise known as (HOMO) and empty antibonding ( $\pi^*$ ) orbitals (LUMO) (figure 2.5). The energy difference between HOMO and LUMO is called the band gap ( $E_g$ ) (Heeger, 2010; Skotheim & Reynolds, 2006).

Band gap of the conjugated polymer is directly affected by its conjugation length which in turn, dictates its electrical properties. The higher the degree of the conjugation length, the wider the delocalized  $\pi$ -electrons band and the lower the optical band gap of the polymer.

Electron delocalization within and between the molecules of conjugated polymers facilitates absorption in the visible spectral range. In order to transport electrons across the bandgap, the polymer must absorb a photon. If the energy of the absorbed photon is greater than or equal to the bandgap of the polymer, an electron is photoexcited from the HOMO to the LUMO creating a tightly bound electron-hole pair called exciton. Generally, in solar cells, the generated exciton is further separated into a hole and an electron which is then transported to their respective electrodes for charge collection.

Because anode and cathode of the cell are chosen based on their work function differences, they facilitate the charge separation and transportation to each electrode.

Unfortunately, this general process only works for inorganic solar cells due to the low binding energy of inorganic semiconductors where electrons are excited from the valence band to the conduction band leading to the generation of an electron-hole pair that can easily dissociate into free charge carriers. Meanwhile, the dielectric constant of organic semiconductors is low ( $\epsilon \sim 3-4$ ) giving rise to the high binding energy of the electron-hole pair. Thus, rather than separation into free charge carriers, exciton remains tightly bound resulting in distortion of the physical state of the molecule by changing its electronic structure. The next stage in the existence of exciton is diffusion. As a result of charge neutrality of the exciton, it diffuses  $\sim 10$  nm (diffusion length of most conjugated polymers) through the conjugated polymer chain. Within this very short distance, exciton can either decay (radiatively or nonradiative) or dissociate into free charge carriers. If exciton decay radiatively, it emits a photon of lower energy. The difference between the energy of absorbed and emitted light is termed Stoke shift, a measure of energy loss by thermalization.

One of the earliest investigations on organic photovoltaic effect was carried out by Kallmann and Pope (1959) when they sandwiched a single crystal of anthracene between two electrodes of different work functions and illuminated the device from the transparent electrode. They observed that only a tiny part of the crystal was excited giving a photovoltage value of 200mV with efficiency less than 0.1 %.

Device performance and that of subsequent ones (Silinsh et al., 1974) derived their built-in potential that split the generated exciton either from the difference in energy potentials of the metal electrodes or from the Schottky diode behaviour of the cell. In Schottky diode, exciton splits due to the build-up of the electric field close to one of the

metal-organic interfaces creating an asymmetric device. Thus, the reported low efficiency of the device is due to short exciton lifetime and ineffective dissociation of the excitons as a large percentage of them are quenched at the metal interface.

## **2.2 Heterojunction polymer solar cell**

### **2.2.1 Bilayer Heterojunction**

A landmark work was the introduction of heterojunction by Tang (1986) and it is recognized as the pioneered endeavour in the field of OPVs. Tang demonstrated that higher efficiencies and better fill factor are obtainable by inserting two layers of organic semiconductors with different but compensating energy bands between the electrodes. The layers consisted of copper phthalocyanine (CuPc) as the donor (*p*-type semiconductor) and a perylene tetracarboxylic derivative (PV) as the acceptor (*n*-type semiconductor) sandwiched between an indium tin oxide (ITO) coated glass substrate and a silver electrode, ~1% efficiency was reported.

In Tang's device, the driving force behind the splitting of the photogenerated exciton is derived from energy level alignment of the donor and acceptor materials. Thus during exciton diffusion process, the electron is promoted from HOMO to the LUMO of the donor material to create positively charged hole. If the promoted electron dissociates from the hole and the LUMO of the acceptor is properly aligned to that of the donor in order to accommodate the excited electron, the electron relaxes onto the LUMO of the acceptor and thus collected at the anode. Also, the positively charged hole remains on the donor material HOMO is collected at the cathode to generate photovoltage ( $V_{OC}$ ). The driving force behind this charge collection process is either the concentration gradient of the charge carrier or the drift built by internal electric fields.

### 2.2.2 Bulk Heterojunction

Although Tang reported a better power conversion efficiency for bilayer device when compared with monolayer device, however, the efficiency is still far below that of a typical inorganic solar cell. Bilayer heterojunction devices suffer from “exciton diffusion bottleneck” (Forrest, 2005) because in almost all organic materials useful for OPV, optical absorption length is  $> 100$  nm (Halls et al., 1996; Haugeneder et al., 1999; Pettersson et al., 1999) while the diffusion length of exciton is only  $\sim 10$  nm. The implication is that in planar heterojunctions, the distance covered by diffusing exciton is much less than the length of optical absorption. As a result, photogenerated excitons formed further away from DA interface are likely to dissociate into free carriers before they reach the interface. Whereas exciton dissociation occurs within a very short timescale (100-1000 ps) and efficient charge carrier creation occurs only at the heterojunction interface; thus, inefficient dissociation into electron and hole within this timescale can lead to recombination or decaying (Yu et al., 1995). To overcome this limitation, bulk heterojunctions were independently introduced by Yu et al. (1995) and Halls et al. (1995).

With the aim of ‘bringing the heterojunction to the exciton’, the donor-acceptor materials were intimately blended together to create a large interface for exciton dissociation throughout the device. Earlier in 1992, Yoshino *et al.* and Sariciftci *et al.*, independently reported the observed photoinduced electron transfer from conjugated polymer to fullerene derivatives (Morita et al., 1992; Sariciftci et al., 1992). The reports signify a major breakthrough in organic solar cell technology due to the replacement of n-type organic molecules with fullerene and its derivatives (figure 2.6), characterized by strong electron affinity and high electron mobility material.

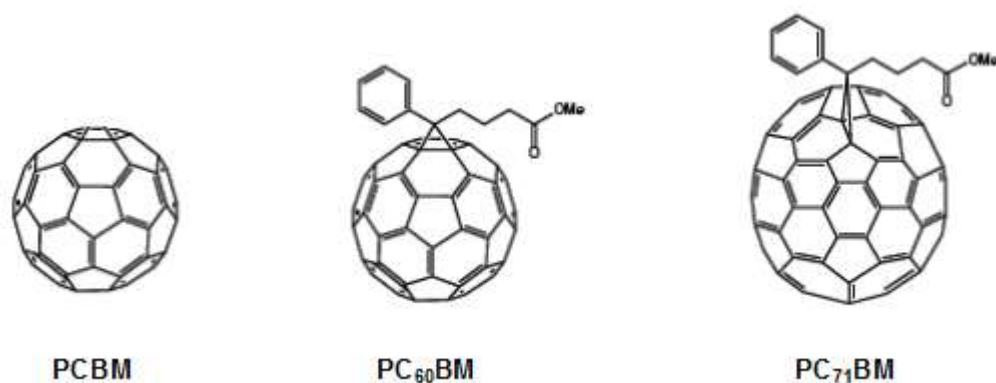


**Figure 2.6: Molecular structure of buckminsterfullerene C<sub>60</sub> and its soluble derivatives; PC<sub>60</sub>BM and PC<sub>70</sub>BM.**

Therefore, in polymer-fullerene blend bulk heterojunction solar cell devices, electron rich and readily oxidized  $\pi$ -conjugated polymers are light absorbers as well as hole transport materials while soluble fullerene derivatives (such as [6,6]-phenyl-C<sub>61</sub>-butyric acid methyl ester, PC<sub>60</sub>BM or PC<sub>70</sub>BM), with potential of accepting up to 6 electrons (Allemand et al., 1991) are the acceptors. HOMO-LUMO transition is better in C<sub>70</sub> compares to C<sub>60</sub>. Thus, extrasolar photons can be harvested and thus better efficient solar cells are realized by replacing symmetrical C<sub>60</sub> with C<sub>70</sub> which has a larger absorption coefficient (Wienk et al., 2003). At present, polymer-fullerene blends represent the state of the art with efficiencies approaching 10%, a positive indication that PSCs indeed have promising future.

### 2.2.3 Morphology of bulk heterojunctions

Although the concept of BHJ addresses exciton dissociation problem that limits the efficiency of bilayer heterojunction system, however, some requirements need to be met to avoid of minimizing various loss mechanisms that accompany charge generation, transport, and extraction. Studies show that a finely mixed morphology with a large donor/acceptor interface not only favours charge carrier generation, space charge can build up thereby increase the chances of non-germinate recombination. Therefore, it is necessary to comprehend the importance of manipulating the morphology, as the



performance of BHJ solar cells depends largely on the nanoscale morphology of the photoactive layer. Controlling the interpenetrating network morphology, and optimizing the charge transport mobility and solar absorption of the polymer are essential for achieving devices with improved performances. With regard to the solar absorption and charge mobility, the introduction of molecular band gap engineering has yielded notable successes (Bakhshi et al., 2012; Roncali, 2007; Roncali et al., 2006) in the synthesis of new low band gap polymers (donors) with balanced charge-carrier transport in relation to PCBM (acceptor). However, difficulties in characterizing and optimizing organic film morphology make it difficult to understand and control the morphology (Chen et al., 2011). With little or no application of post-deposition treatments, it is difficult to obtain an environmentally stable and perfect morphology of which the composite film forming the active layer is naturally assembled to a required level of phase separation. Therefore, processing conditions such as solvent effect (Weerakoon et al., 2012), the blend ratio of the constituents (Balderrama et al., 2011; Hau et al., 2010; Haung et al., 2010), as well as post-deposition treatments, have to be considered.

### **2.3 Architecture of organic solar cells and performance parameters**

A typical BHJ solar cell device (figure 2.7) is fabricated in a modular arrangement where hole conducting layer consisting of Poly(ethylene dioxythiophene) doped with polystyrene sulphonic acid (PEDOT:PSS) is spin coated on top of indium tin oxide (ITO) coated glass substrate. Due to its high electrical conductivity and high work-function, ITO is the most commonly used transparent electrode in OPVs. However, ITO is fragile and expensive. Therefore, researchers are working on better alternatives to ITO in optoelectronics. Graphene (Zhang et al., 2013), metal nanowires (Kholmanov et al., 2013), carbon nanotubes (Kim et al., 2010) and conducting polymers (Yeo et al., 2013) are among the promising alternatives. Subsequently, a solution of the conducting polymer donor and an electron acceptor material (soluble fullerene) spin cast from a common

organic solvent is sandwiched between the PEDOT:PSS coated ITO substrate and a thin layer of lithium fluoride (LiF) and a layer of aluminium (Al). LiF serves as a hole blocking layer while Al or silver (Ag) is usually the top electrode.

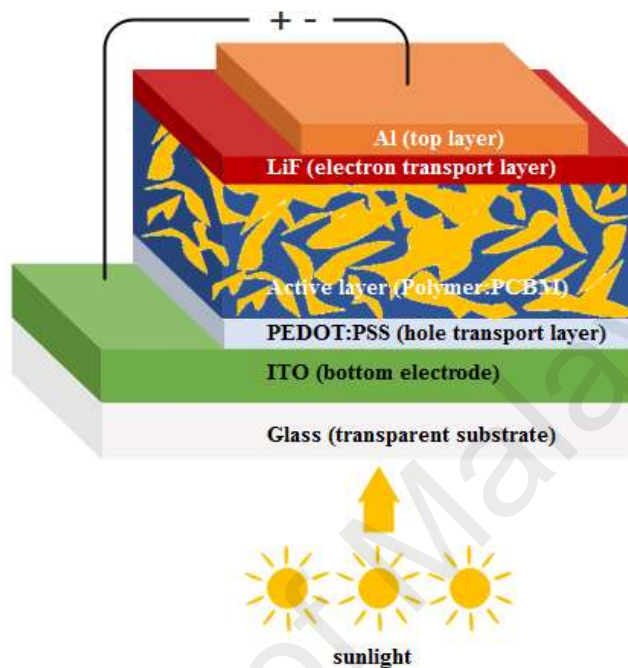


**Figure 2.7: Typical device architecture of BHJ photovoltaic cell**

As indicated previously, absorption of photon promotes an electron from HOMO to LUMO; thus create exciton which undergoes series of processes to generating electricity. These processes can be explained in four major steps: The first step is photon absorption with efficiency  $\eta_A$  which generates Coulombically bound electron-hole pair called exciton with binding energy  $E_{ex}$ , smaller than the band gap of the photoactive material (conjugated polymer) and that of separated electron and hole. Light absorption efficiency  $\eta_A$  is a function of the absorption spectra of the photoactive material. Device configuration also plays an important role in photon absorption. Next, the generated exciton diffuses towards the donor-acceptor interface with efficiency  $\eta_{ED}$  based on the diffusion length of the exciton. Diffusion length must not be too long as exciton can either decay or dissociate through internal mechanism. Therefore, the active layer thickness should be within the exciton diffusion length. Here, bulk heterojunction concept greatly

enhances  $\eta_{ED}$  as the interface is always next to exciton generation domain. The third step involves exciton separation into free charge carriers as a result of energy level offset between the donor and the acceptor material. Efficiency governing this step is represented by  $\eta_{CS}$ . Lastly, charges are transported to their respective electrodes using the force generated as a result of work function difference between the electrodes. Morphology also plays a crucial role in this step. Donor-acceptor blend needs to provide continuous pathways for the mobile hole and electron on their way to the electrodes where they are collected with efficiency  $\eta_{CC}$ .

From photon absorption to charge collection at the electrodes, energy conversion processes of PSCs depend on external quantum efficiency  $\eta_{EQE}$ , otherwise known as the incident photon-to-current efficiency (IPCE). Calculated as a function of wavelength,  $\eta_{EQE}$  is the ratio of the number of charge carriers collected at the electrodes to the number of incident photons falling on the device. Device loss mechanisms are analysed using  $\eta_{EQE}$ . The equation that defines  $\eta_{EQE}$  is derived from cell's spectra response (SR):

$$SR(\lambda) = \frac{J_{sc}(\lambda)}{P_{in}} \quad (2.1)$$

Considering the energy of photon  $\left(\frac{hc}{\lambda}\right)$  and elementary charge ( $e$ ):

$$\eta_{EQE}(\lambda) = \frac{\text{number of electron}}{\text{number of photon}} = \frac{J_{sc}}{P_{in}} \times \frac{hc}{\lambda e} \quad (2.2)$$

$\eta_{EQE}$  is thus written as a product of the efficiencies ( $\eta$ ) described above: light absorption ( $\eta_A$ ), exciton diffusion ( $\eta_{ED}$ ), charge splitting ( $\eta_{CS}$ ), and charge collection ( $\eta_{CC}$ ) represented as:

$$\eta_{EQE} = \eta_A \times \eta_{ED} \times \eta_{CS} \times \eta_{CC} \quad (2.3)$$

Figure 2.8 shows a graph of  $\eta_{EQE}$  vs wavelength for solar cells based on P3HT:PCBM and P3HT:DPM-6.

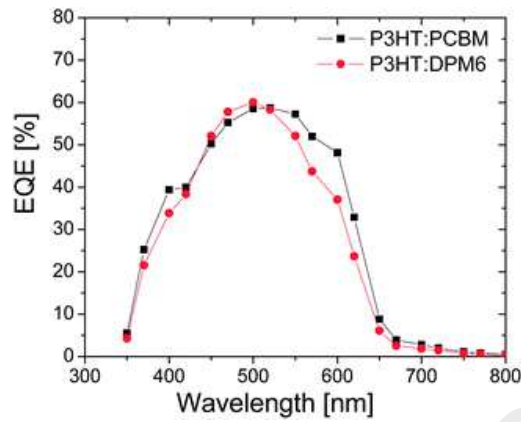


**Figure 2.8:  $\eta_{EQE}$  for a P3HT : PCBM and P3HT:DPM-6 photovoltaic cell (Bolink et al., 2011)**

Current density measured as a function of voltage in the dark and under illumination is used to determine the electrical properties of a solar cell. Figure 2.9 shows the four photovoltaic parameters of a typical solar cell. The open-circuit voltage  $V_{OC}$ , short circuit current  $J_{sc}$ , maximum power point  $P_m$ , and fill factor FF.

Open circuit voltage,  $V_{OC}$  is the maximum voltage delivered by the solar cell at zero current. It can be measured directly when the electrodes are not in contact and it is limited by the difference between the work functions of the electrodes and the strength of the acceptor. (Brabec et al., 2002; Marks et al., 1994) Because the  $V_{OC}$  depends on the active layer materials (donor and acceptor), it is therefore linked to the energy difference between the HOMO of the donor and the LUMO of the acceptor.  $V_{OC}$  provides the energy needed for charge separation. The equation below shows the relationship between typical conjugated polymer donor and PCBM acceptor.

$$V_{oc} = E_{HOMO}^{Donor} - E_{LUMO}^{PCBM} - \frac{kT}{q} \ln \left[ \frac{(1-P)\gamma N_C^2}{PG_M} \right] \quad (2.4)$$

where  $q$  is the elementary charge,  $P$  is the dissociation probability of a bound electron-hole pair into free charge carriers,  $G_M$  is the generation rate of the bound electron-hole pairs,  $\gamma$  is the Langevin recombination constant,  $N_c$  is the effective density of states,  $k$  is the Boltzmann constant, and  $T$  is the temperature. (Kroon et al., 2008)

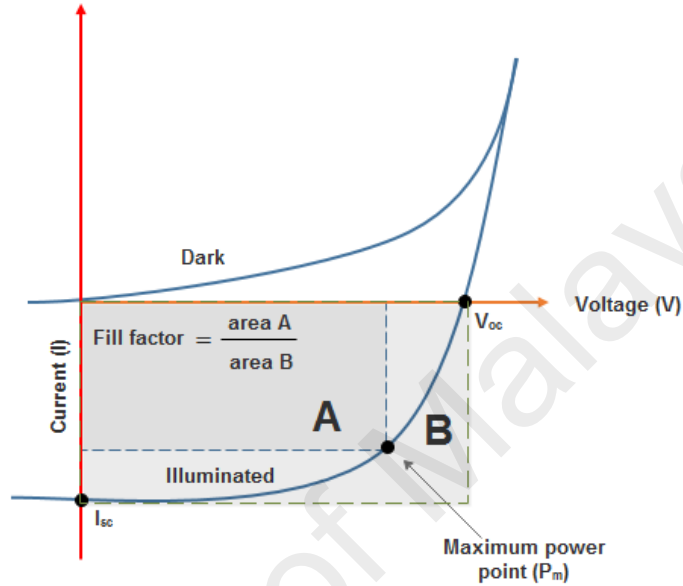


**Figure 2.9: Current-voltage ( $I$ - $V$ ) curve for a typical BHJ solar cell under illumination**

If the metal electrode and the donor material are not properly matched, or there is increase in charge carrier loss,  $V_{OC}$  decreases. Interfacial effect created by electrode-donor mismatched can be rectified by deposition of a low work function interlayer such as lithium fluoride (LiF).

Short circuit current  $J_{sc}$ , is the current density of the solar cell when no external field is applied. It can be determined by the integral of the product between cell spectra response and incident photon power ( $P_{in}$ ).

$$J_{sc} = \frac{q}{hc} \int_{\lambda_{min}}^{\lambda_{max}} \eta_{EQE} P_{in}(\lambda) \lambda d\lambda \quad (2.5)$$

Therefore, it is more advantageous to use broader solar spectrum, donor polymer with high absorption coefficient and enlarged  $E_{HOMO}^{Donor} - E_{LUMO}^{Acceptor}$  in order to have higher photon absorption and consequently better  $J_{sc}$  and  $V_{oc}$  respectively.

Along the  $J - V$  curve, the point at which the product of the current density and the voltage is at the maximum,  $J_m \times V_m$ , is the point at which the solar cell delivers the maximum power ( $P_m$ ):

$$P_m = J_m \times V_m \quad (2.6)$$

The fill factor (FF) is the ratio of  $J_m \times V_m$ , the measured maximum power and the maximum theoretical power output ( $J_{sc} \times V_{oc}$ ):

$$FF = \frac{P_m}{J_{sc} \times V_{oc}} = \frac{J_m \times V_m}{J_{sc} \times V_{oc}} \quad (2.7)$$

The intersection of the abscissa and the ordinate describes the  $J_{sc}$  and the  $V_{oc}$  respectively. Fill factor measures the “squareness” of the  $J - V$  curve. Parameters such as active layer morphology, interface recombination, and charge carrier mobility and balance. (Li, Zhu, et al., 2012)

Power conversion efficiency ( $\eta$ ) of the device is a measure of maximum power of the device relative to the incident photon power ( $P_{in}$ ). Relating the efficiency to the parameters described previously,  $\eta$  of can be described as:

$$\eta = \frac{P_m}{P_{in}} = \frac{FF \times J_{sc} \times V_{oc}}{P_{in}} \quad (2.8)$$

The incident photon power is usually fixed at 100 mW/cm<sup>2</sup> under an air mass (AM) of 1.5 G. Thus, building efficient polymer solar cell requires understanding of strategies to control nanoscale morphology of the active layer, proper design of active layer materials

and processing and stability of the device (and interface of the device). The following section will focus on the important factors needed to building efficient PSCs.

#### **2.4 Rendering conjugated polymers solution processable**

Although conducting polymers possess semiconductors properties as expected, the presence of conjugated backbone which is responsible for their conducting properties is the reason behind some of their drawbacks. Conjugated polymers are intractable and insoluble in common organic solvents causing a great limitation to their potential applications. For instance, CP that is applicable as active layer materials in BHJ solar cells is expected to be solution processable to facilitate ease of fabrication and deposition onto flexible substrates using any of the various established thin film coating technologies.

Structural factors such as length of aliphatic groups in the chain, the degree of polymerization, the polarity of the substituent groups, intermolecular attractions and rigidity of polymer backbone are the contributors to the degree of solubility of conducting polymers. Apart from processability, morphology, crystallization, degree of phase segregation and interaction of the polymer with other materials particularly in the active layer of PSCs are also influenced by the solubility of the polymer. Insolubility of conjugated polymers has been traced to backbone rigidity associated with strong inter-chain  $\pi$ -stacking interactions which prevent solvation but favours aggregation. Another explanation to the rigidity of conjugated polymer is the measure of angular correlation factor along the chain which is not found in saturated polymers. Angular correlation can be determined by measuring the statistical length of the polymer chain. The higher the value of statistical length, the more rigid the polymer (Bhattacharya & De, 1999).

#### 2.4.1 Side chain functionalization

An early method of rendering conjugated polymer solution processable is by incorporating side chain on the backbone. Side chain functionalization increases entropy and also lowers the interchain coupling of the resulting polymer making it processable from melt or solution. However, decorating conducting polymer backbone with long alkyl or alkoxy substituent group can cause steric hindrance that distorts the planarity of the polymer structure thereby destroys its charge mobility characteristic. As a result, the conductivity of the polymer is affected because  $\pi$ -orbitals that responsible for conductivity are less available to allow smooth movement of charges along the polymer backbone (Cheng et al., 2009).

#### 2.4.2 Functionalized protonic acid doping

A number of conjugated polymers have successfully been doped by protonic acids through protonation of the polymer backbone (Han & Elsenbaumer, 1989; Lang et al., 2010; Walton et al., 1991). In protonic acid ( $H^+ M^-$ ) doping of polyaniline, the overall charge neutrality is maintained by  $M^-$  from the acid which act as the counter ion. While protonic acid doping truly enhanced the conductivity of polyaniline, solution processability of high molecular weight polyaniline remained a challenge (Cao et al., 1993). Despite being doped to conducting form, high molecular weight polyaniline remained insoluble when dissolved in common organic solvents. However, upon doping with dodecylbenzene sulfonic acid, a functionalized protonic acid, polyaniline became not only highly conductive but soluble in common organic solvents such as xylene, chloroform, m-cresol, and DMSO (Cao et al., 1993). According to Cao and co-workers, functionalized protonic acid can be designated as  $H^+(M^- - R)$ . Unlike ordinary protonic acids, the counter-ion ( $M^-$ ) of functionalized protonic acid contains a hydrophobic functional group,  $R$ , an alkyl group which facilitates interactions between the polymer and nonpolar or weakly organic solvent. Usually, counter-ions on the protonic are big to



prevent the doped conjugated polymer chain from close packing because when expanded, organic solvents can easily diffuse into the polymer backbone thus induce processability of the doped polymer. However, studies show that solubility of the protonic acids doped conducting polymers is greatly affected by the increased concentration of the doping agents. That the solubility of DBSA-doped polymer was remarkably affected when the concentration of the DBSA per mole of pyrrole monomer increased beyond 1 mol (Lee et al., 1995; Song et al., 2000).

Soluble, high molecular weight doped polyaniline has been synthesized using functionalized protonic acid as the doping agent. The polymer product was soluble in common organic solvents and free standing polyaniline films with excellent electrical conductivity were prepared from the solution of the polymer (Cao et al., 1992). The solubility was due to the interaction between the organic functional group present in the functionalized protonic acid. The incorporation of protonic acid reduces the forces of attraction between and within the polymer chain. Also, the functional group being organic, can easily interact with polar or non-polar organic liquids thus dissolving the polymer in the chosen solvent. In 1995 Kim's group chemically polymerized soluble and electrically conductive polypyrrole doped with DBSA. The polymer was soluble in common organic solvent and a film cast from the polymer solution was subsequently used as a transparent anode in polymer light emitting diodes with external quantum efficiency of 0.5 % (Gao et al., 1996; Lee et al., 1995). After the breakthrough, other research groups have employed different forms of organic sulfonic acids to synthesize solution processable conducting polymers to enable various potential applications of conducting polymers (Lee et al., 2002; Lee et al., 2000; Oh et al., 2001; Song et al., 2004). This synthetic route is simple and efficient when compared to other methods of obtaining solution processable conducting polymers.

## 2.5 Conjugated polymer-graphene nanocomposites

Nanoparticles have been known since the 12th century when they were used for glazes on Ming Dynasty (1368-1644) ceramics. In the early 1900s, nanocomposites comprised of carbon black and rubber were used to enhance durability and effectiveness of automobile tires though with no understanding of the material properties. The investigation into properties of nanocomposites started around 1950 and its commercial viability came into the limelight in the 80s when Toyota Motor Corporation introduced automobile timing belts made from nylon-montmorillonite nanocomposite (Singh et al., 2012). Later in the 90s, nylon-carbon nanotube nanocomposites were used in other areas such as computer read-write heads and to provide static dissipative protection in auto fuel systems. Nanocomposites are materials with at least a component having a dimension within nanoscale (Nel et al., 2006). Composite materials are usually biphasic; a matrix and a dispersed phase. The matrix is a continuous phase that envelops the dispersed phase to give a 'hybrid' material that displays the combining properties of both components. In polymer nanocomposites, the processability and mechanical properties of the composite are derived from the polymeric component. The blended properties of polymer nanocomposites afford new materials with electrical and morphological features enhanced or completely different from the individual parent components due to their electronic interactions at the nanoscale level.

Owing to the improved processability, mechanical strength, and electrical behaviours of the resulting composite, research interests in conducting polymer-graphene (CP/G) nanocomposites is growing by the day. For example, in the case of energy storage and production applications, the unique band structure and electrons mobility of graphene in synergy with optical, high conductivity and light weight properties of conducting polymers were employed to fabricate a memory device based on graphene oxide-poly{[9,9-di(triphenylamine) fluorene]-[9,9-dihexylfluorene]-[4,4'-(9H-fluorene-9,9-

diyl) dibenzenamine]] (GO-PTHF) applicable for non-volatile rewritable memory (Zhuang et al., 2014). By applying negative electrical sweep, this novel material can be switched to the ON or OFF state, by applying negative or positive electrical sweep. Meanwhile, most of the combining properties of conducting polymers and graphene manifest in the excellent thermal and electrical properties of the nanocomposite (Gómez et al., 2011; Song et al., 2012; Zhang et al., 2010). Various preparations routes such as in-situ polymerization, colloidal dispersion, solution mixing, or melt mixing have been employed to obtain conducting polymer nanocomposites. Of all these preparation methods, in-situ chemical oxidative polymerization is the most common.

For instance, functionalized graphene doped with polypyrrole (Ramasamy et al., 2015) was prepared via in-situ polymerization to investigate the effect of the surface chemistry of the resulting nanocomposite on its performance as a supercapacitor. Graphene was serially functionalized with an amine ( $\text{NH}_2\text{-G}$ ) and nitrogen (NG) and their capacitive performance was compared with that of graphene oxide/polypyrrole (GO/PPy) and reduced (GO/PPY). while all the composites displayed good capacitive performance, the performance of NG-PPy was the best ( $3.67 \text{ Fg}^{-1}$ ) (Lai et al., 2012). In situ chemical oxidation polymerization is a well-adopted technique to obtain graphene-conducting polymer nanocomposites (Asadian et al., 2014; Wang et al., 2013). However, the high tendency for aggregation and poor solubility of graphene and some conducting polymers are some of the drawbacks of this preparation route. owing to successful application of DBSA to prepare solution processable polyaniline (PANI) and polypyrrole polymers together with synergistic properties of conducting polymer-graphene nanocomposites, DBSA has recently been applied to facilitate interaction between graphene and polyaniline. The in-situ polymerization of PANI-DBSA/reduced graphene oxide (GOR) was carried out using ammonium persulfate as the oxidant and DBSA as a dopant.

The resulting solution processable nanocomposite exhibited a high electrical conductivity making it applicable in optoelectronics (Basavaraja et al., 2012).

University of Malaya

## CHAPTER 3: PROCESSABLE DBSA-DOPED POLY(N-VINYL CARBAZOLE)-POLY(PYRROLE) COPOLYMER

### 3.1 Introduction

In recent years, vast research interests have led towards preparing new composites based on conducting polymers to harness their excellent properties and simple synthetic routes. Conducting polymers are useful in optoelectronics, sensors, as well as chemical displays, such as biosensors, photodiodes, organic light-emitting diodes (OLEDs), field-effect transistors (FETs), supercapacitors, and photovoltaic cells (Camurlu & Guven, 2015; Chandrasekhar, 2013; Das & Prusty, 2012; Guo, Glavas, et al., 2013; Livi et al., 2014; Rodrigues et al., 2015). In a  $\pi$ -conjugated polymer, such as polypyrrole, polythiophene or polyaniline, alternating single and double bonds of the polymer backbone control both the transfer of electron and the energy levels (Dou et al., 2013; Po et al., 2010). Also, the delocalized  $\pi$ -bonds electrons in conducting polymer backbones are responsible for strong interchain charge transfer interactions, thereby characterizing their exceptional combination of electrical and mechanical properties (Cao & Xue, 2014). However, poor processability from organic solvents, environmental instability, and poor mechanical properties are among the limitations to potential applications of conducting polymers (Das & Prusty, 2012; Facchetti, 2010; Kumar & Chand, 2012).

Furthermore, previous reports have shown that copolymerization of pyrrole (Py) with n-vinyl carbazole (NVC) yielded copolymer with improved thermal stability, conductivity, electrophotography, (Shattuck & Vahtra, 1969) and dielectric properties. In the case of poly(N-vinyl carbazole) (PNVC), the justifications were based on its good photoconductivity (Basavaraja et al., 2011; Thinh et al., 2012) and thermal stability (up to 300°C), albeit it possesses a wide band gap and poor electrical conductivity ( $10^{-10}$  to  $10^{-16}$  S/cm<sup>-1</sup>). PNVC is a hole conductor, which has also demonstrated electron mobility upon doping with iodine (Safoula et al., 1996). In fact, studies have suggested that PNVC

possesses the ability for the effective hole and/or electron mobility (Andrey et al., 2006; Govindraju et al., 2016; Zhou et al., 2017). Nevertheless, a major drawback to these properties is the extreme brittleness, which, however, has prompted many efforts towards improving both the mechanical and the chemical processing of PNVC. Many research efforts have focused on the development of copolymers, composites or blends containing PNVC moiety in order to harness its hole transport and thermal stability properties. Such materials have been developed via chemical or electrochemical polymerization of NVC monomer with inorganic and high electrical conducting materials, such as graphene (Pernites et al., 2011), fullerene (Chen et al., 1996; Ramar & Saraswathi, 2015) or carbon nanotubes (Chemek et al., 2014) to achieve composite material with excellent luminous and conducting properties. On the other hand, due to its solubility in common organic solvents like chloroform, benzene, tetrahydrofuran, and toluene, researchers have considered copolymerizing PNVC with conducting polymers that are inherently intractable, perhaps, the presence of PNVC can induce solubility of the resulting copolymer (Jang et al., 2005). In 1997, Narayan and Murthy studied the absorption, the emission, and the short circuit current of bilayer device based on PNVC-P3HT. The device displayed additional PL features with respect to PNVC single layer device. In addition, recently, Alimi et al., synthesized copolymers based on PNVC and polymers, such as poly(3-methyl thiophene),(Chemek et al., 2010) poly(3-hexyl thiophene),(Chemek et al., 2014) and poly(p-phenylene vinylene).(Mbarek et al., 2013) All the copolymers products are solution processable with PNVC-P3HT and PNVC-PPV exhibited optical and electrical properties suitable for optoelectronic applications. The earliest work on copolymer and composite based on NVC and Py was reported by Toppare et al.(Geissler et al., 1991) PNVC-Ppy copolymer and composite were prepared via electrochemical polymerization. They reported that the conductivity of the products was within  $10^{-1}$  and  $10^{-3}$  S/cm without mentioning the solubility of their products. Later,

Biswas and Roy (Biswas & Roy, 1993b, 1994, 1995, 1996) conducted extensive findings on the properties of PNVC-Ppy by using different oxidants and in varying the reaction medium, although the copolymer showed improvement in thermal stability, as well as morphological and conductivity properties. However, none of the polymer products was soluble in organic solvent. On top of that, the further attempt made by Biswas and Ballav to copolymerize NVC and TP also resulted to intractable polymer nanocomposite, but with improved thermal properties in relation to the homopolymers (Ballav & Biswas, 2003). Besides, Wan et al. synthesized a flexible film of PNVC-Ppy with room temperature electrical conductivity as high as 10 S/cm by using laser-electrochemical polymerization. Yet, the authors did not mention any report about the solubility of the resulting polymer (Li et al., 1995)

Polypyrrole (Ppy) has been given wide focus and its commercial application is expanding by the day; owing to its excellent electrical conductivity<sup>21, 22</sup> and superior environmental stability. (Lin et al., 2008) However, polypyrrole is obtained as an intractable powder that is difficult to process in solution. Conjugated backbone, the condition for its metallic conductivity, is also responsible for its insolubility. Thus, in order to obtain soluble polypyrrole product while maintaining its electrical conductivity, non-substituted pyrrole monomers are replaced with alkyl substituted monomers, which are proposed to reduce the interchain interaction between the chains of polypyrrole molecules in a doped state. Unfortunately, the presence of long alkyl chain on the pyrrole causes a steric hindrance that affects the planarity of the resulting polymer. As a result,  $\pi$ -orbital overlaps are greatly affected and they are less available; causing a significant reduction in the polymer conductivity. The soluble polypyrroles obtained, nonetheless, exhibited low electrical conductivity.

However, limitations to commercial applications of conducting polymers, especially polypyrrole and polyaniline, have recently been reduced by successful synthesis of conducting polymers that are soluble in common organic solvents, such as m-cresol, chloroform, and dimethylformamide (DMF). Moreover, surfactant anions were used as counter ions that induced their solubilities.(Van der Sanden, 1997) At present, dodecylbenzene sulfonic acid (DBSA) and camphor sulfonic acid are used as dopants to obtain free-standing polyaniline film from emeraldine base solution.(MacDiarmid & Epstein, 1994) In addition, soluble polypyrrole has been synthesized via one-step chemical oxidative polymerization.(Kim et al., 1996) Incorporation of surfactant anions into the backbone of polypyrrole allows the long alkyl chain of the dopant anions to serve as a spacer that expands the polymer chain to enable diffusion of organic solvents into the spaces created by the dopant molecule.(Lee et al., 1995) In optoelectronics, especially organic solar cell fabrication, conjugated polymers are often used as the donor (or acceptor) materials in the device active layer. In fact, properties, such as good redox potential, high electrical conductivity, environmental stability, and solution processability, which are also characteristics of doped polypyrrole, can be harnessed if doped polypyrrole is used in the active layer of the organic solar cell.

Dopant stabilized polypyrrole are usually prepared in water by using ammonium persulfate oxidant. Hence, we hypothesized that if the polymerization is carried out in the presence of NVC, solution processable copolymers soluble in common organic solvents could be yielded. This could widen the potential applications of pyrrole/carbazole derivatives, especially in optoelectronics. NVC is insoluble in water but soluble in various organic solvents, including acetonitrile, which is miscible with water. Therefore, in order to facilitate an interaction between NVC and ammonium persulfate oxidant, polymerization medium could be a mixture of water and acetonitrile. In this regard, this paper presents the chemical synthesis of the soluble PNVC-Ppy copolymer in a doped



state. The copolymer was synthesized in a biphasic system that consisted of both water and acetonitrile with a controlled amount of ammonium persulfate oxidant to initiate the polymerization process and DBSA, attached to pyrrole molecule, to induce solubility. As a result, the copolymer displays solubility in dimethyl sulfoxide (DMSO), dimethylformamide (DMF), and chloroform. In addition, the new copolymer exhibits other properties application as an active layer in optoelectronic devices. Data obtained from x-ray diffraction analysis (XRD), FTIR spectroscopy, FESEM, and TGA are presented to examine its structural, morphological, and thermal properties.

## **3.2 Materials and methods**

### **3.2.1 Materials**

Pyrrole (Merck) was freshly distilled and stored in dark cool condition. N-vinyl carbazole (Aldrich Chemistry), ammonium persulfate (Acros Organics), and dodecylbenzene sulfonic acid (DBSA, Acros Organics) were used as received. All the solvents were of analytical grade.

### **3.2.2 Preparation of DBSA-doped PNVC-Ppy copolymer**

Polymerization of NVC and pyrrole monomers was carried out at 0°C by using ammonium persulfate as the oxidant. 0.01 mole DBSA was dissolved in 80 ml of acetonitrile. To the above solution, 0.02 mole of NVC and 0.02 mole of pyrrole dissolved in 80 ml of acetonitrile were added. The mixture was stirred vigorously for 5 min and then kept at 0 °C. 0.004 mole of APS in 40 ml ACN/water (1:1) mixture was added dropwise. The gradual addition of the oxidant turned the monomer solution to a dark-green colour, indicating the onset of polymerization. The solution, later, turned dark-brown after 6 h of reaction. The chemical oxidative polymerization of the copolymer proceeded for 6 h and was terminated by the addition of methanol. The dark-brown polymer product was filtered and sequentially washed with 10% HCl, distilled water,

acetone (to leach out excess DBSA), and toluene (to remove unreacted NVC monomer and PNVC homopolymer). The final product was filtered and dried in a vacuum oven at 60 °C. For comparison, PNVC and Ppy homopolymers were separately synthesized using the same procedure with 0.02 mole of one monomer in the absence of the other. Also, undoped PNVC-Ppy copolymer synthesized similar to the doped copolymer though, without DBSA.

### 3.2.3 Characterization

The polymerization yield was calculated based on the following formula:

$$yield(\%) = \left(\frac{m_1}{m_2}\right) \times 100\% \quad (3.1)$$

where  $m_1$  is the weight of PNVC–Ppy copolymer, and  $m_2$  is the weight of NVC + pyrrole monomers. The current-voltage measurements were performed by using a Jandel RM3000 Test Unit and the electrical conductivity was calculated by using the following equation:

$$\sigma = V^{-1}I \left(\frac{\ln 2}{\pi d_n}\right) \quad (3.2)$$

where  $V$  is the applied potential measured in volt,  $d_n$  is the thickness of the pellet measured in  $cm$ , and  $I$  is the current in ampere.

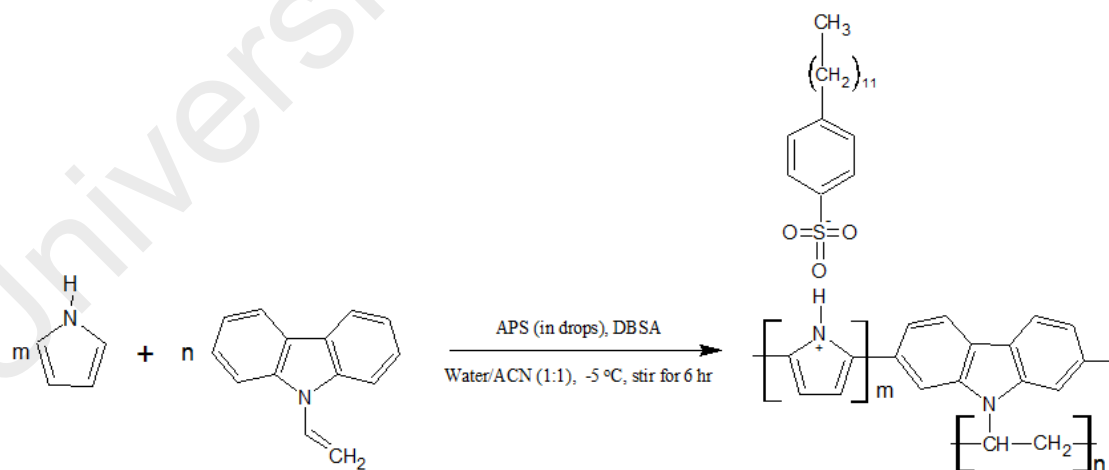
Field-emission scanning electron microscopy (FESEM) images were taken to examine the morphology of the PNVC-Ppy by using Hitachi SU-8220 microscope, while FT-IR spectra were measured with Perkin Elmer FTIR-Spotlight 400 spectrometer. Optical density measurement was performed by using a Shimadzu UV-2600 spectrometer, in the range of 200-1100 nm. The XRD spectra were measured on a PANalytical EMPYREAN model diffractometer with Cu-K radiation. Meanwhile, thermogravimetry was performed on a Perkin Elmer TGA 6 model instrument from 25 – 900 °C at a heating rate of 10 °C

/ min under atmospheric condition, whereas electrical conductivity measurement was taken by using four-point probe method on the pellets (0.15 g, diameter 1cm) of the homopolymers and the copolymers compressed (pressure, 15 bar) from their respective powdered samples.

In this work, molar ratios APS/NVC–Py = 1 and DBSA/NVC–Py = 0.5 were used for all the characterizations. The reaction temperature and the time were -5 °C and 18 hr respectively. The solubility of the solvent was determined by dissolving 10 mg of the copolymer product in 20 ml of each of the selected solvents (DMSO, DMF, chloroform, THF, chlorobenzene) and then, ultrasonicated for 20 min. The solution was then filtered through a 1 µm Teflon membrane filter and the filtrate was transferred to a previously weighed glass plate where the solution was left to evaporate and solubility was determined.

### 3.3 Results and Discussion

#### 3.3.1 Roles of APS concentration on conductivity and yield



**Scheme 1: Synthesis of DBSA-doped PNVC-Ppy**

The synthesis of doped PNVC–Ppy copolymer is shown in scheme 1. The polymerization medium was carefully chosen to facilitate an interaction between the monomers and ammonium persulfate oxidant. Interestingly, no precipitate was formed

when ammonium persulfate was added to the mixture of water and acetonitrile. Moreover, the solubility of ammonium persulfate in water did not prevent the miscibility of water and acetonitrile.

It has been established that the yield and the conductivity of conducting polymers are affected by certain factors, such as monomer to oxidant ratio, duration, solvent, oxidant, and reaction temperature. For instance, P. A. Steven (Armes, 1987) obtained 100% yield of polypyrrole at an optimum ratio (2.4) of iron(III) to pyrrole monomer. Also, polymerization at a short period of time yielded an enhanced result when carried out at low temperature. (Rapi et al., 1988)

Additionally, in order to establish the effect of the APS concentration on the yield and the conductivity of DBSA-doped PNVC-Ppy, we first investigated the relationship between the amount of NVC and the thermal stability of the polymer product. As expected, there was a linear relationship between the weight ratio of NVC and the thermal degradation of copolymer chain (Figure 3.1). Besides, the copolymer with the highest NVC content was the most stable to heat, while the copolymer with the least content of NVC degraded faster.

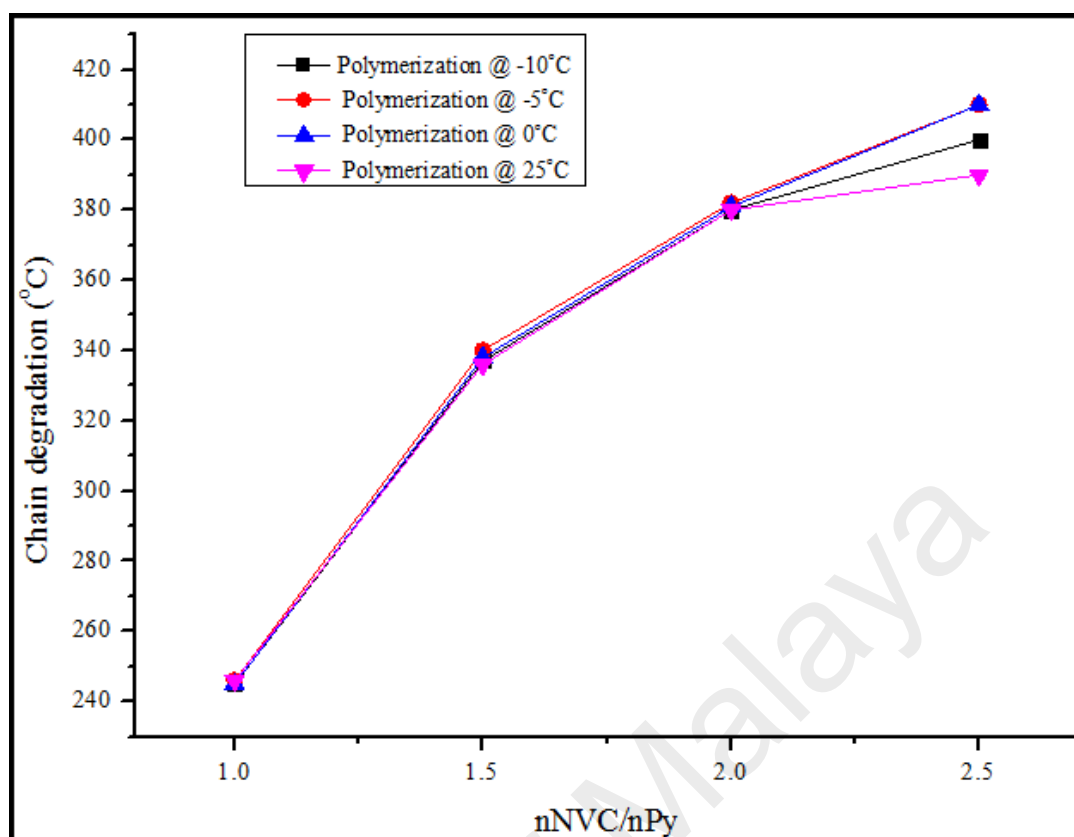


**Figure 3.1: Thermal stability of PNVC–Ppy copolymer vs NVC concentration at different temperatures**

This result was further compared with the electrical conductivity of the copolymer with varying concentrations of PNVC (Figure 3.2). The electrical conductivity of the copolymer decreased with increasing concentration of PNVC. However, the copolymer synthesized at mole ratio  $n_{NVC}/n_{Py} = 1.0$  had better thermal stability and moderate electrical conductivity at all the chosen temperatures. Hence, we investigated the role of APS concentration on electrical conductivity of PNVC-Ppy at a constant ratio of  $n_{NVC}/n_{Py} = 1.0$  and  $DBSA = 0.01 \text{ mol/dm}^3$  while varying the APS concentration from  $0.001 - 0.004 \text{ M}$  at different temperatures.

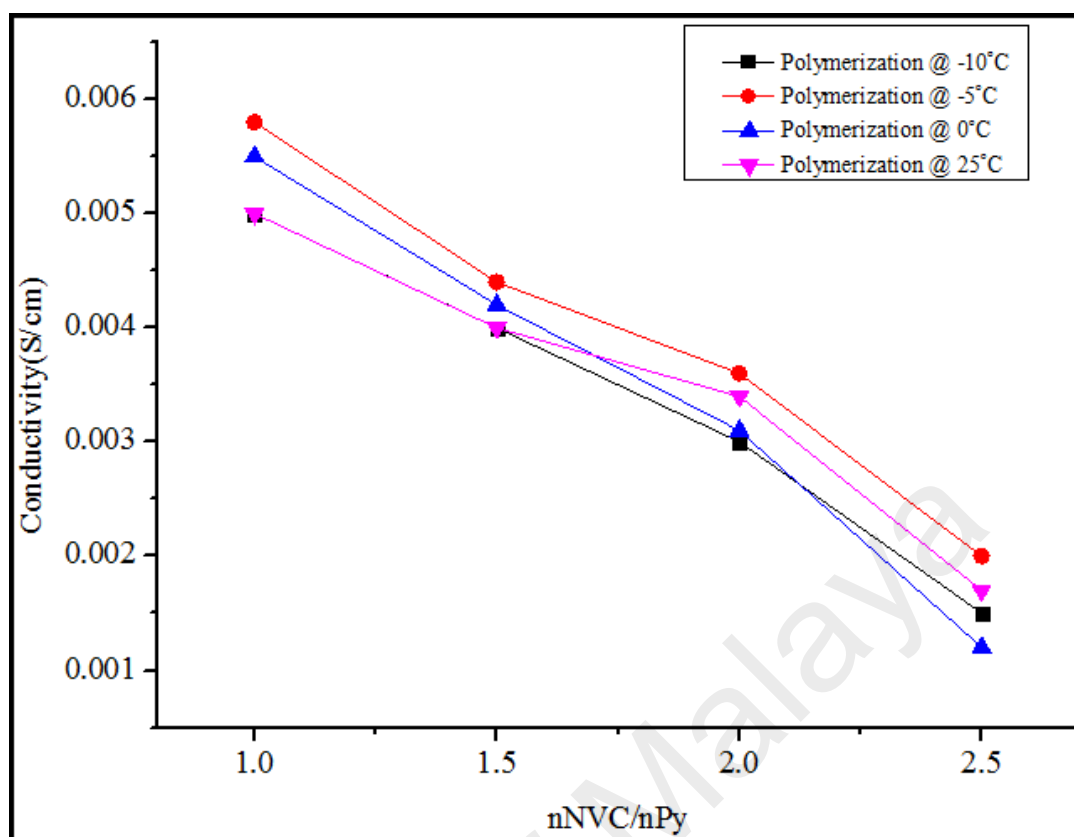


**Figure 3.2: Electrical conductivity of PNVC–Ppy copolymer vs NVC concentration at different temperatures.**

Moreover, the electrical conductivity of PNVC-Ppy increased as the polymerization temperature decreased and with an increase in the concentration of APS oxidant (Figure 3.3). Polymerization carried out at  $-5^{\circ}\text{C}$  with an APS concentration of  $0.004\text{ mol/dm}^3$  gave a better conductivity value,  $0.095\text{ S/cm}$ . At a temperature below the room temperature ( $-10$ ,  $-5$ , and  $0$ ), the conductivity of PNVC-Ppy followed a similar trend. Slow addition of APS resulted in progressive chain growth; causing a gradual increase in chain length over a prolonged period of time. Also, polymerization at a lower temperature extended the half-life of pyrrole free-radical cation or pyrrole oligomer for further random reaction either with each other or with carbazole unit.

The conductivity, nonetheless, increased gradually until a maximum value of  $9.5 \times 10^{-2}\text{ S/cm}$  was reached with  $0.004\text{ mol/dm}^3$  APS at a polymerization temperature of  $-5^{\circ}\text{C}$  and then, it started to decrease. However, since the polymerization was proceeded

randomly, even at low temperature, a high concentration of APS led to high oxidation of both pyrrole and NVC carbazole. On one hand, excessive oxidation of NVC could disrupt the pyrrole chain, thereby decreasing the conductivity of the copolymer. Also, pyrrole chain may be ruptured due to the high conversion rate to polypyrrole. Therefore, either or both of these conditions might lead to a decrease in conductivity of the copolymer while the concentration of APS increases.

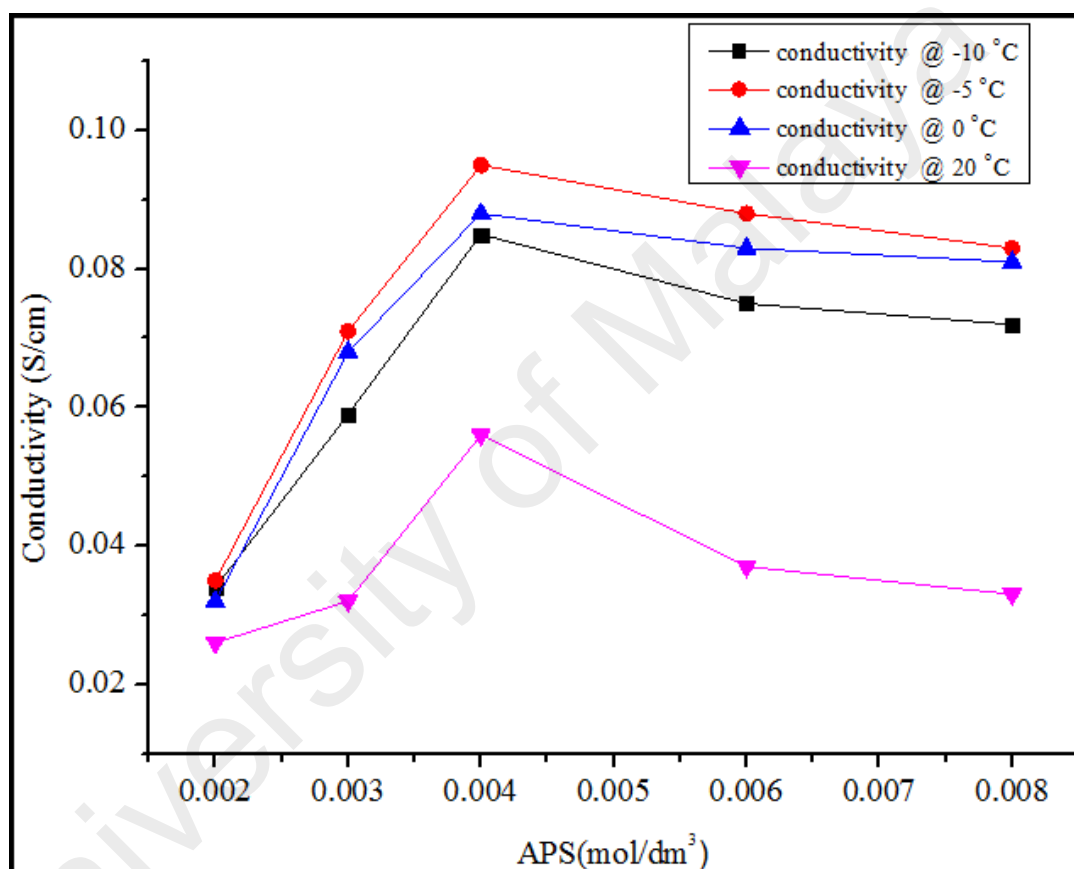


**Figure 3.3: Electrical conductivity of DBSA-doped PNVC-Ppy vs APS concentration at different temperatures.**

The highest conductivity was recorded at a temperature of  $-5^{\circ}\text{C}$ . Thus, in order to obtain relevant information about the correlation between the oxidant concentration and the polymerization yield, the polymerization was carried out at temperature  $-5^{\circ}\text{C}$  at a fixed concentration of DBSA ( $0.01 \text{ mol/dm}^3$ ) while changing the concentration of APS oxidant. The change in yield, with a corresponding change in concentration of APS oxidant, followed a similar pattern to that of conductivity (figure 3.4). The yield of

PNVC-Ppy at the polymerization temperature of  $-5^{\circ}\text{C}$  first increased as the APS concentration changed from  $0.002$  to  $0.004 \text{ mol/dm}^3$ . It then started to decrease at a higher APS concentration within the concentration range chosen in the present investigation.

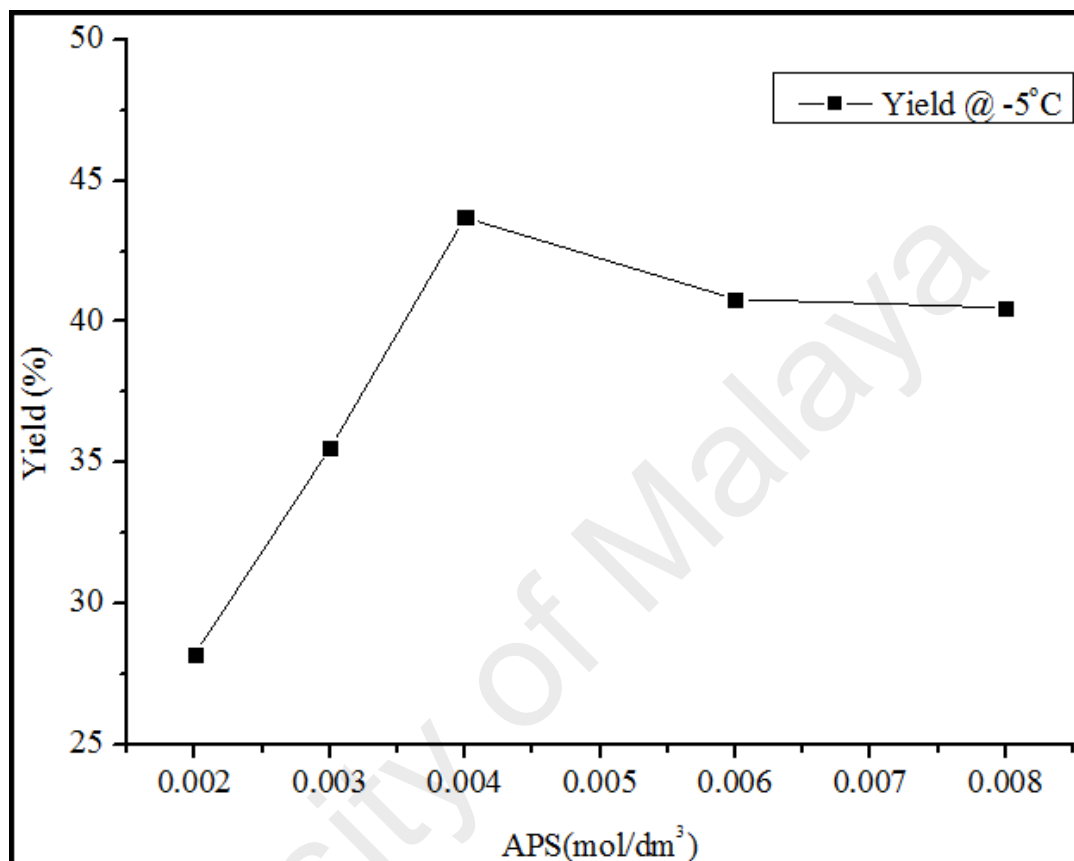


**Figure 3.4: Yield of the copolymers vs APS concentration at  $-5^{\circ}\text{C}$**

The rapid increase in yield, thus, can be attributed to the rapid generation of radicals due to increased initiator concentration. (Song et al., 2000) At concentration higher than  $0.004 \text{ mol/dm}^3$ , lower yield was obtained, perhaps because the equivalent amount of effective APS needed for polymerization had already reached  $0.004 \text{ mol/dm}^3$  and there was insignificant contribution from the extra concentration of APS.

### **3.3.2 Roles of concentration of DBSA on solubility and conductivity of DBSA-doped PNVC-Ppy**

DBSA was used as a dopant to stabilize the copolymer in organic solvents in order to obtain a soluble form of DBSA-doped PNVC-Ppy. While the concentration of persulfate



oxidant was kept at  $0.004 \text{ mol/dm}^3$  and the temperature at  $-5 \text{ }^\circ\text{C}$ , the concentration of DBSA, with respect to conductivity and solubility of the polymer, was varied to obtain the optimum amount of DBSA required as a dopant. Moreover, since the copolymer dissolved better in DMSO, it was used as a solvent for this investigation. The conductivity of the copolymer showed a little increase as DBSA concentration increased from  $0.005 \text{ mol/dm}^3$  to  $0.015 \text{ mol/dm}^3$  (Figure 3.5).

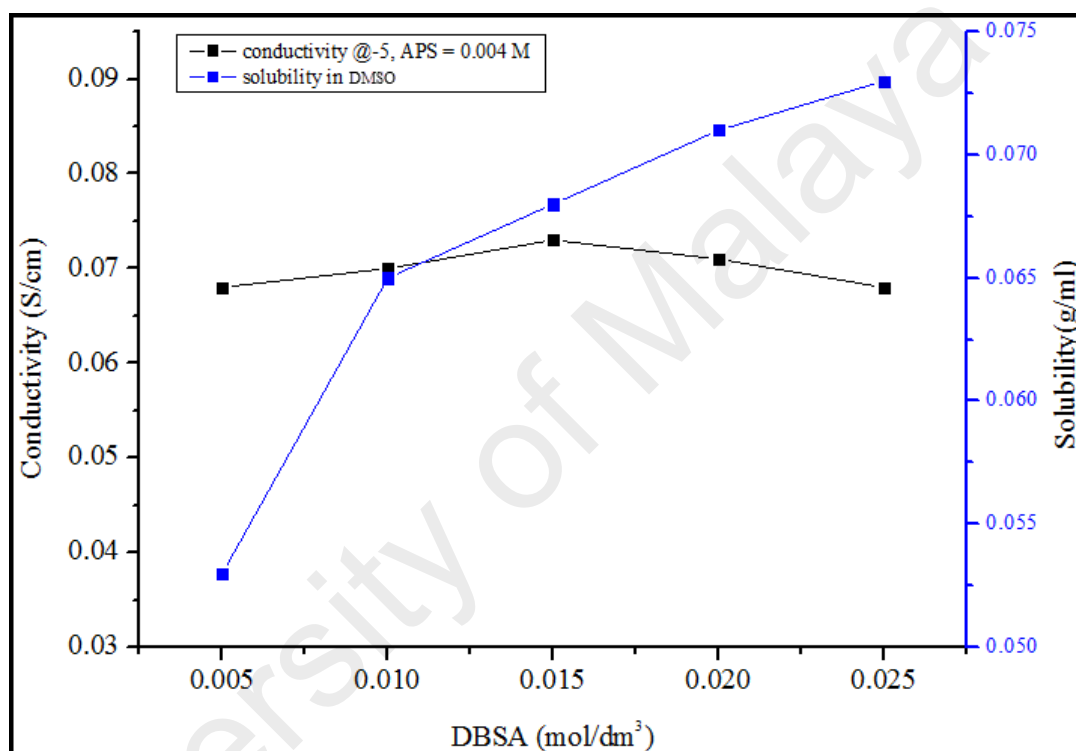


**Figure 3.5: Solubility and electrical conductivity of DBSA-doped PNVC-Ppy synthesized with different DBSA concentrations**

At DBSA concentration higher than  $0.015 \text{ mol/dm}^3$ , the conductivity followed a similar trend by decreasing at a slow rate. However, the conductivity was found to increase because raising DBSA concentration implied increasing the doping level of the PNVC-Ppy copolymer until an optimum concentration of DBSA was reached at  $0.015 \text{ mol/dm}^3$ . It then started to decline at a higher doping level, perhaps, as a result of percolation of DBSA molecules into the chain of PNVC-Ppy, which hindered the intermolecular interaction of the copolymer chains that limited the charge carrier mobility

of the chains (Wen et al., 2013). This same effect, however, facilitates the interaction of PNVC-Ppy with organic solvents. The solubility of the copolymer, nevertheless, increased with increasing concentration of DBSA because the incorporated surfactant anion (DBSA) expanded the polymer molecule, thereby allowing the organic solvent to diffuse into the spaces between the polymer backbones, and therefore, increased the interaction between the copolymer and the solvent (Lee et al., 1995). Besides, PNVC-Ppy was synthesized chemically by using different oxidants and various reaction media. Although PNVC homopolymer is soluble in a number of organic solvents, its solvating effect did not have any effect on the solubility of PNVC-Ppy prepared earlier (Biswas & Roy, 1994). None of the investigations reported that the copolymer had been soluble in any organic solvent. This means that the polypyrrole part of the copolymer had a stronger influence on the overall solubility of the copolymer. Thus, the interaction between Ppy molecule and the molecule of DBSA dopant influenced the solubility of DBSA-doped PNVC-Ppy.

Relative solubility of the copolymer in selected organic solvents was further investigated. Table 1 shows the solubility of PNVC-Ppy in the selected solvents. Solubilities with a value  $< 0.6$  g/100 ml were considered as partially soluble (PS) and the values within the range of  $0.6 - 0.9$  g/100 ml were termed soluble (S). It should be noted that despite the presence of long alkyl chain of DBSA, which induced polymer-solvent interaction, the copolymer dissolved in the selected solvents based on the polarity indices of the respective solvents (Figure 3.6).

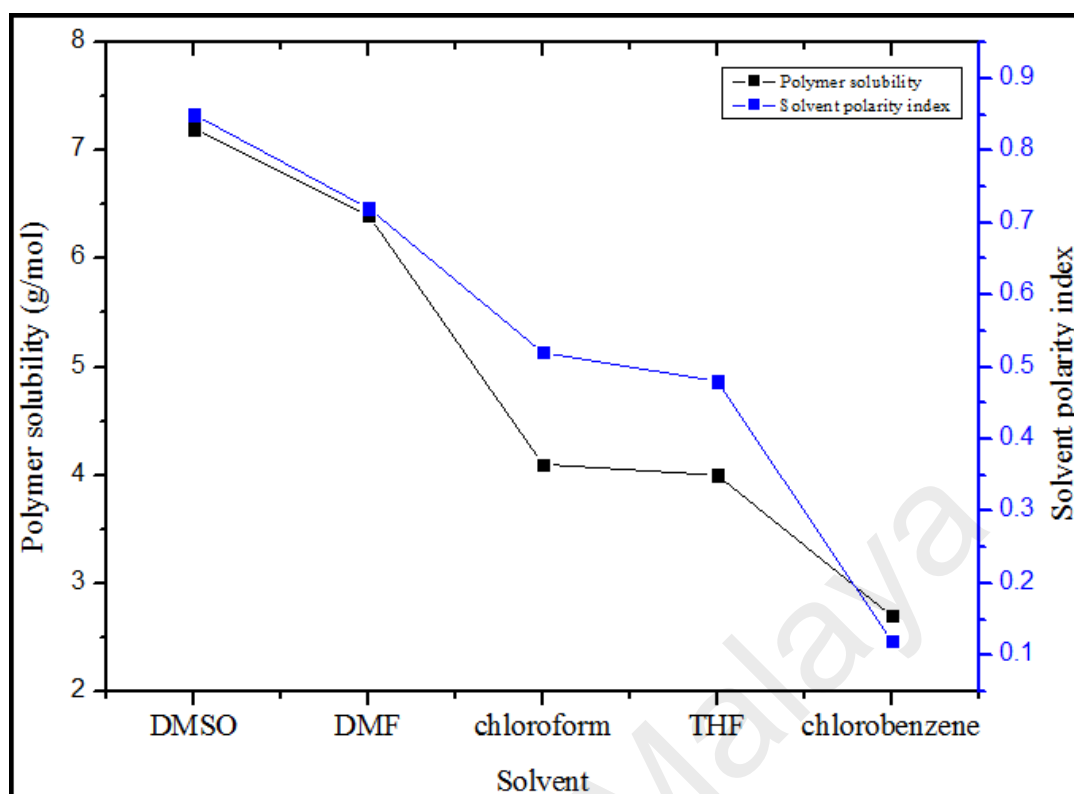


**Figure 3.6: Solubility of DBSA-doped PNVC-Ppy vs polarity indices of the solvents.**

The dissolution of the copolymer in high polar solvents, such as DMSO and DMF, was facilitated by hydrogen bond interaction between the DBSA of the copolymer and the solvent. Thus, no such strong hydrogen bond interaction was detected between the copolymer and the weakly polar solvents (PI = 4.1) or relatively non-polar solvent (PI = 2.7).

**Table 3.1. Solubility of PNVC-Ppy in selected organic solvents (g/100ml)**

|             | DMSO | DMF  | chloroform | THF  | chlorobenzene |
|-------------|------|------|------------|------|---------------|
| Solvent P.I | 7.2  | 6.4  | 4.1        | 4.0  | 2.7           |
| PNVC-Ppy    | 0.85 | 0.72 | 0.52       | 0.48 | 0.12          |

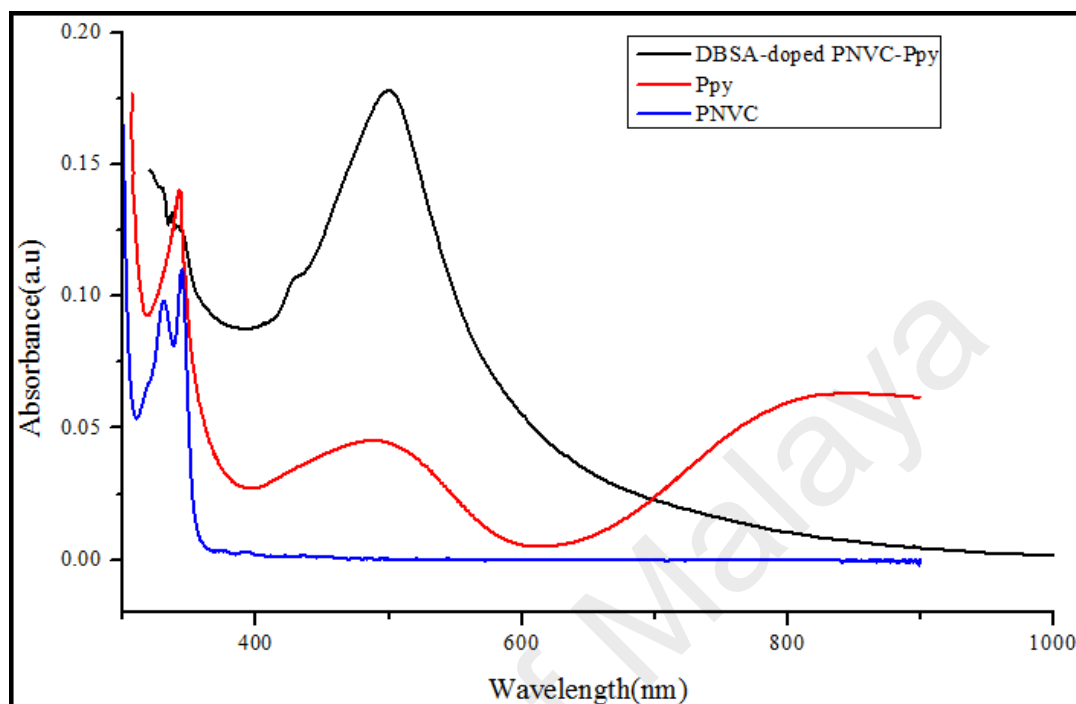
P.I = Polarity index

### 3.3.3 Optical properties of DBSA-doped PNVC-Ppy

The UV-vis spectra recorded for doped PNVC-Ppy, PNVC, and Ppy samples in chloroform are illustrated in Figure 3.7. The solution of Ppy in chloroform (Figure 3.7b) projected a strong absorption peak at 340 nm, one spectrum band of lower intensity between 436 nm and 645 nm, and a free carrier tail at 907 nm. The peak at 340 nm was attributed to the excitation of  $\pi - \pi^*$  transition in the pyrrole ring. Besides, the broad peak at 480 nm corresponded to the pyrrole polaronic band, while the broad free carrier tail was due to bipolaronic transition. Furthermore, the presence of polaron and bipolaron in the spectra of polypyrrole confirmed that the polypyrrole had been doped with DBSA. Polaron and bipolaron are known to be charge carriers in doped Ppy. Therefore, high conductivity of doped polypyrrole was due to band gap reduction because of formation of (bi)polaron (Bilal et al., 2014; Shen & Wan, 1998).

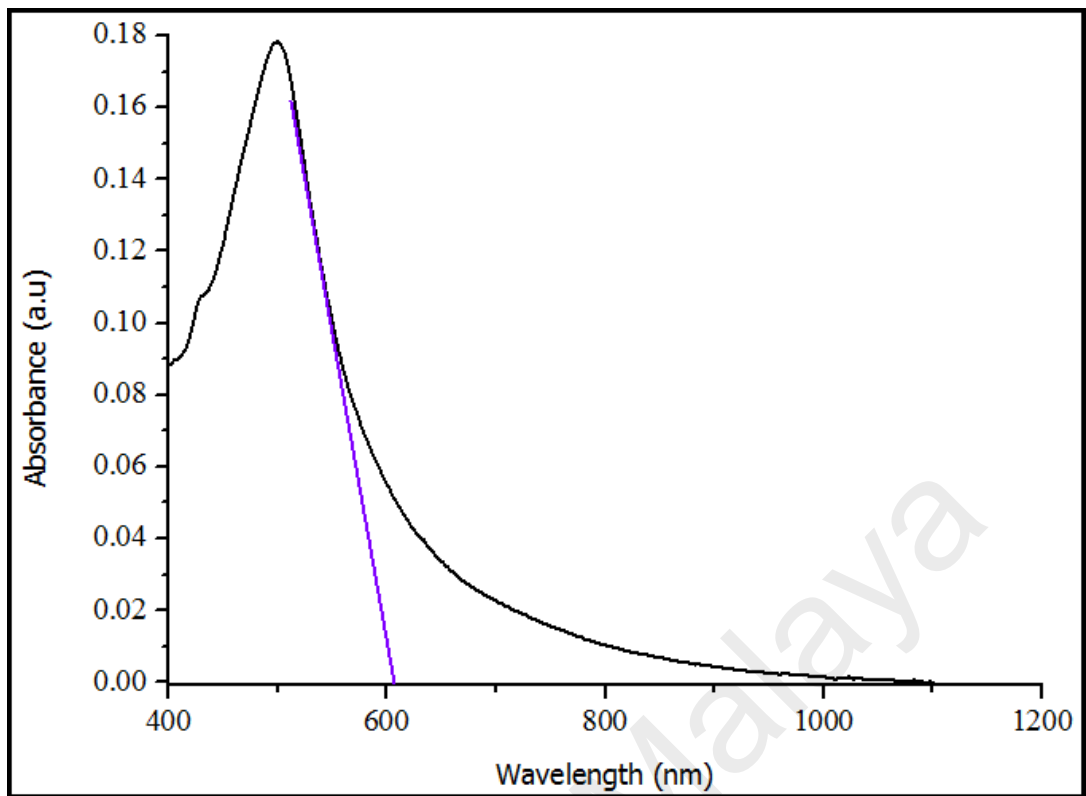
Moreover, typical absorption spectra of PNVC were observed at 295, 328, and 345 nm in the UV region of the electromagnetic spectrum (Figure 3.7c) (Mbarek et al., 2013; Zaidi et al., 2010). The free carrier tail, which is responsible for the high degree of conjugation in doped polypyrrole, was not found in the spectra of DBSA-doped PNVC-Ppy (Figure 3.7a). The presence of PNVC in polypyrrole chain shortened polypyrrole conjugation length, and therefore, the conductivity of the DBSA-doped PNVC-Ppy was reduced relative to that of polypyrrole because the incorporation of NVC into the chain of pyrrole affected the mobility of charge carrier along the Ppy backbone. This observation is in good agreement with the result obtained from the electrical conductivity test of the copolymer. Meanwhile, the optical bandgap of the copolymer was estimated to be 2.04 eV as deduced using the absorption spectrum fitting method (Figure 3.8). Compare with a band gap of Ppy ( $\sim 2.7$  eV) and PNVC (3.6 eV), the new copolymer exhibits a reduced band gap, indicating that PVNC truly incorporated into the Ppy chain to form the new copolymer. To select a polymer as a potential active layer material for

optoelectronic devices, solution processability, and the moderate band gap is parts of the criteria. Thus, the DBSA-doped PNVC-Ppy under study can be applied for the purpose.



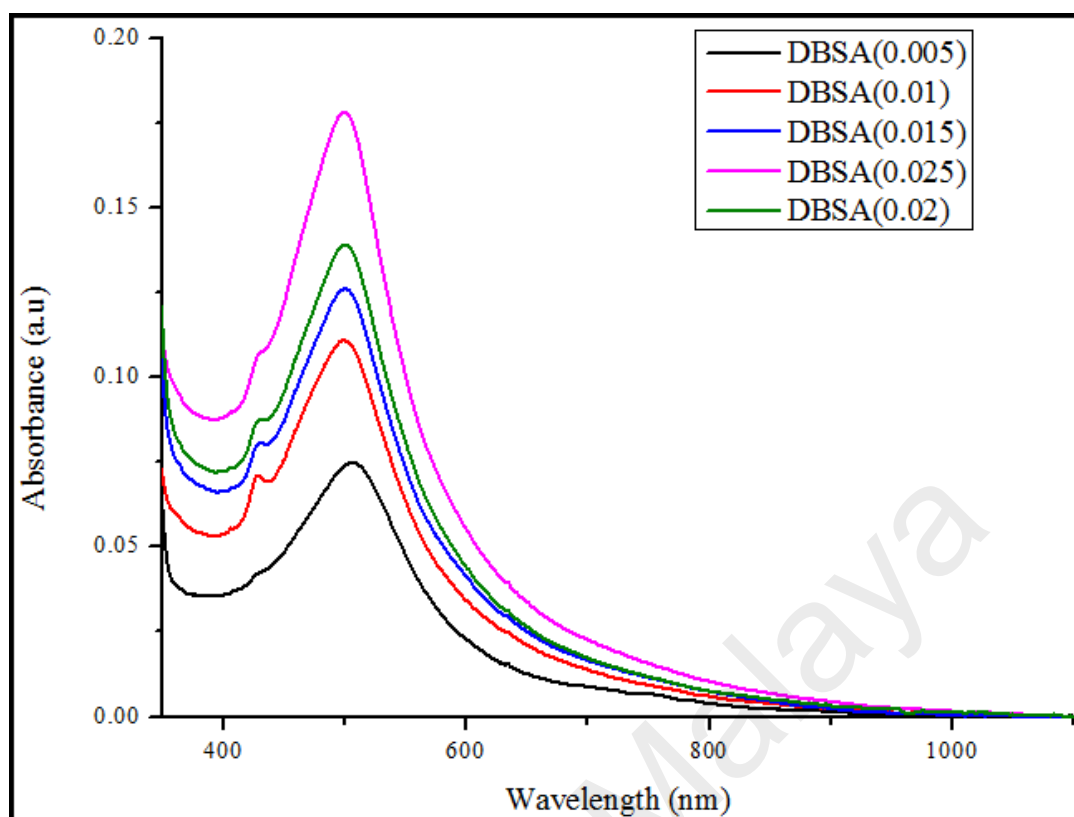
**Figure 3.7: Optical absorption spectra of DBSA-doped PNVC-Ppy, Ppy, and PNVC.**

Figure 3.9 shows the effects of varying DBSA concentrations on the UV-vis absorption of DBSA-doped PNVC-Ppy. Maximum absorption of all the spectra appeared at relatively similar wavelength (500 nm), but with different levels of intensities. The intensities varied with the concentration of the dopant and the copolymer doped with the highest concentration of DBSA recorded the highest conductivity.



**Figure 3.8: Band gap estimation of DBSA-doped PNVC-Ppy**

University of Malaya



**Figure 3.9: UV-vis spectra of BDSA doped PNVC-Ppy at varying concentrations of DBSA**

### 3.3.4 Infrared analysis of DBSA-doped PNVC-Ppy

The FTIR spectra of PNVC, Ppy, and DBSA-doped PNVC-Ppy are shown in Figure 3.10, while the details of the assigned peaks are presented in Table 3.2. The band at  $1454\text{ cm}^{-1}$  was attributed to C=C stretching vibration of polypyrrole ring. Also, the bands at  $770$  and  $668\text{ cm}^{-1}$  corresponded to C-C out of plane ring deformation or C-H rocking of Ppy. In addition, the band located at  $1162\text{ cm}^{-1}$  was assigned to C-N stretching vibration of Ppy. (Basavaraja et al., 2011) The next band at  $1330\text{ cm}^{-1}$  was ascribed to C-C stretching vibration of Ppy moiety. The absorption at  $2918\text{ cm}^{-1}$  was attributed to C-H asymmetric vibration. Hence, the presence of these bands in the spectra of DBSA-doped PNVC-Ppy confirmed the incorporation of PNVC into the backbone of Ppy. Furthermore, the Ppy bands at  $1555$  and  $921\text{ cm}^{-1}$ , as well as the PNVC bands at  $1596$  and  $3046\text{ cm}^{-1}$ , were not located in the spectra of DBSA-doped PNVC-Ppy. In the case of PNVC, the

band located at  $723\text{ cm}^{-1}$  was attributed to ring deformation of substituted aromatic structure,(Ballav & Biswas, 2003; Biswas & Roy, 1996) whereas the band at  $1483\text{ cm}^{-1}$  had been ascribed to ring vibration of NVC moiety. Generally, the peak intensities of copolymer were lowered compared to PNVC. This indicated that not only pyrrole participated in the oxidation process, but carbazole also oxidized via carbazole ring upon the addition of ammonium persulfate oxidant to form the copolymer. In addition, since NVC possesses double bond, free radical polymerization via the double bond is possible. Moreover, bands at  $1035$  and  $1008\text{ cm}^{-1}$  were observed in the spectrum of the copolymer, were due to S=O and a benzoid ring of DBSA. These bands confirmed that the PNVC-Ppy was in a doped state.(Han et al., 2005)

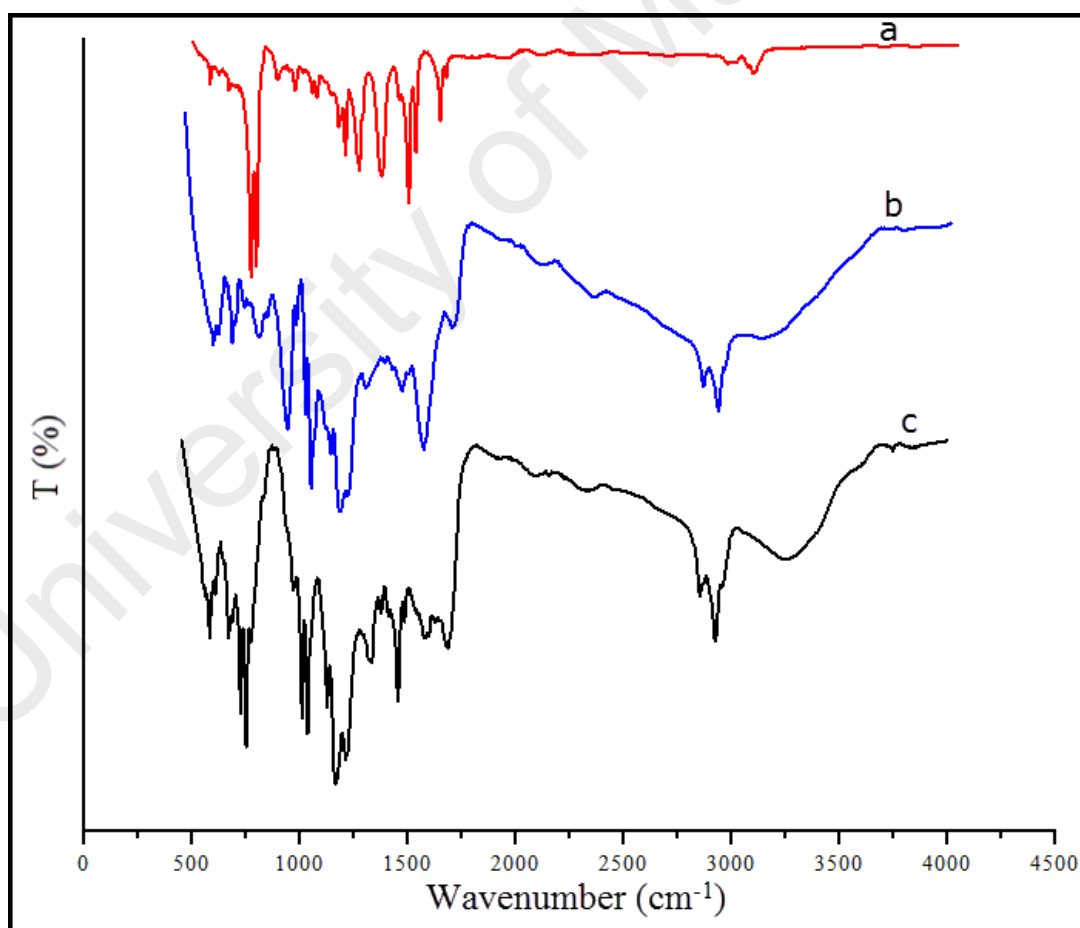


**Figure 3.10: FTIR spectrum of (a) PNVC, (b) Ppy and (c) DBSA-doped PNVC-Ppy.**



**Table 3.2. FTIR band assignments of PNVC, Ppy, and PNVC-PPY**

| Ppy  | PNVC-Ppy | PNVC | Peak Assignment   |
|------|----------|------|---|
| -    | -        | 3046 | C-H asymmetric stretching of aromatic structure                 |
| 2916 | 2918     |      |   |
| 2848 | 2851     |      |   |
| -    | 1664     | 1626 | C=C stretching vinylidene group                                 |
| -    | -        | 1596 |   |
| 1555 | -        | -    | C=C stretching of polypyrrole ring                              |
| 1454 | 1454     | 1452 |   |
| 1165 | 1162     | 1155 | C-H in-plane deformation of aromatic ring                       |
| 1123 | 1125     | 1125 |   |
| 790  | 770      | -    | C-C out of plane ring deformation or C-H rocking                |
| 668  | 668      | -    |   |
| 1287 | 1330     | 1323 | =C-N planar vibration   |
| 1032 | 1035     | 1025 | S=O of DBSA   |
| 1009 | 1008     | 1004 | Benzoid ring of DBSA  |
| -    | 1483     | 1482 | Ring vibration of NVC moiety                                    |
| -    | 749      | 743  | >CH <sub>2</sub> rocking vibration due to tail to tail addition |
| -    | 723      | 718  | Ring deformation of substituted aromatic structure              |

### 3.3.5 XRD pattern of DBSA-doped PNVC-Ppy

XRD measurements were performed to investigate the crystal structure of DBSA-doped PNVC-Ppy. The XRD patterns of PNVC, Ppy, and the copolymer are shown in Figure 3.11. The broad diffraction band of Ppy, which appeared at  $2\theta = 20.1^\circ$ , clearly indicated that polypyrrole was totally amorphous. The pattern of PNVC was dominated by a narrower and a more intense peak at  $2\theta = 20.8^\circ$ , which revealed the presence of semi-crystalline phase. As for the copolymer, the broad peak centred at  $2\theta = 19.3^\circ$  revealed that the DBSA-doped PNVC-Ppy was amorphous. Moreover, the interaction between the NVC and the monomers, which gave rise to the copolymer, was confirmed by a peak shift of PNVC from  $2\theta = 20.8^\circ$  to  $2\theta = 19.3^\circ$  of the copolymer upon copolymerization.

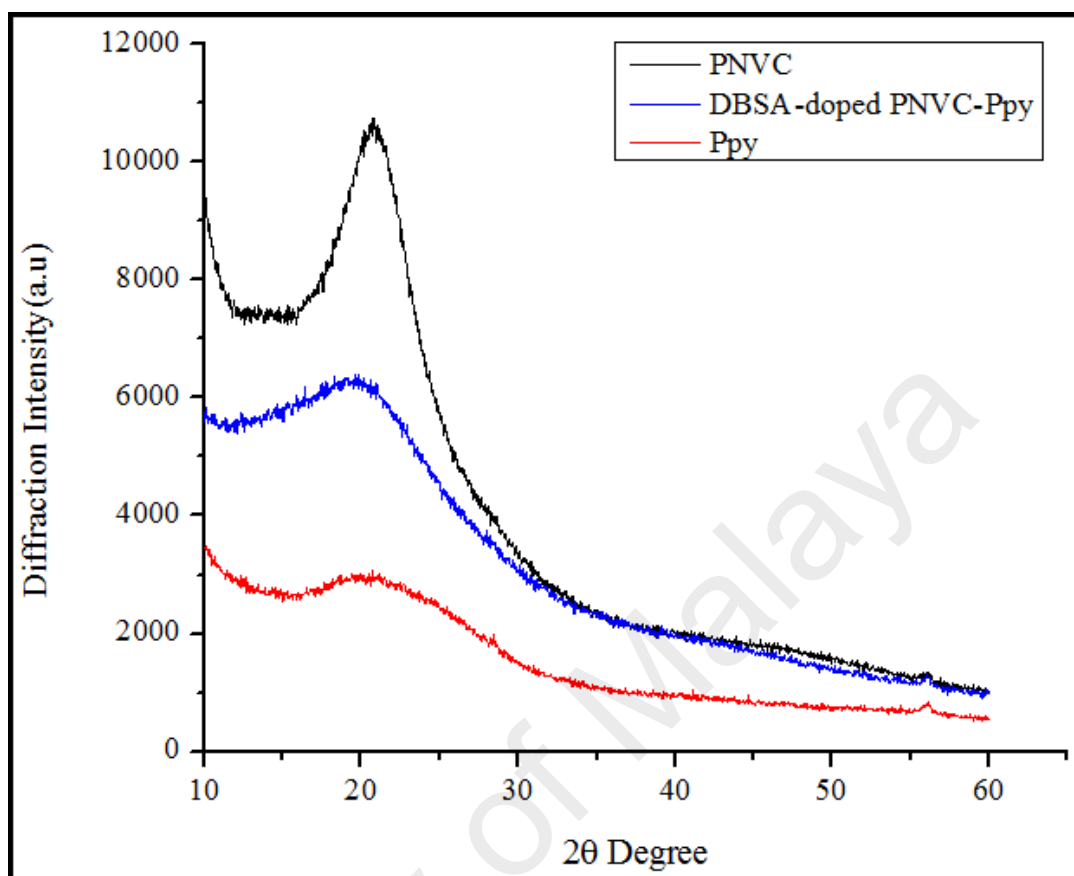


**Figure 3.11: XRD patterns of PNVC, DBSA-doped PNVC- Ppy, and Ppy.**

### 3.3.6 Thermal property of the DBSA-doped PNVC-Ppy

The thermal behaviour of DBSA-doped PNVC-Ppy was investigated via TGA analysis under nitrogen atmosphere. Figure 3.12 shows the TGA curves for the homopolymers, as well as the DBSA-doped and undoped copolymers. The measurement was taken at a temperature range of 50°C to 900°C at 20.00°C/min. Ppy was the least stable to heating with the highest rate of decomposition. The first stage of decomposition started at 81°C and it lost 16% of its weight at 173°C. Decomposition at this stage is usually attributed to the loss of physical moisture content (Lee et al., 2000). Further decomposition between 173°C and 500°C, where Ppy has lost almost 60%, was due to degradation of polypyrrole backbone and other interchain bonds. Between 500°C and 900°C, Ppy lost 70% of its

total mass, leaving behind carbonized polymer residue, a phenomenon that is common to infusible conjugated polymers (Donnet & Bansal, 1998).

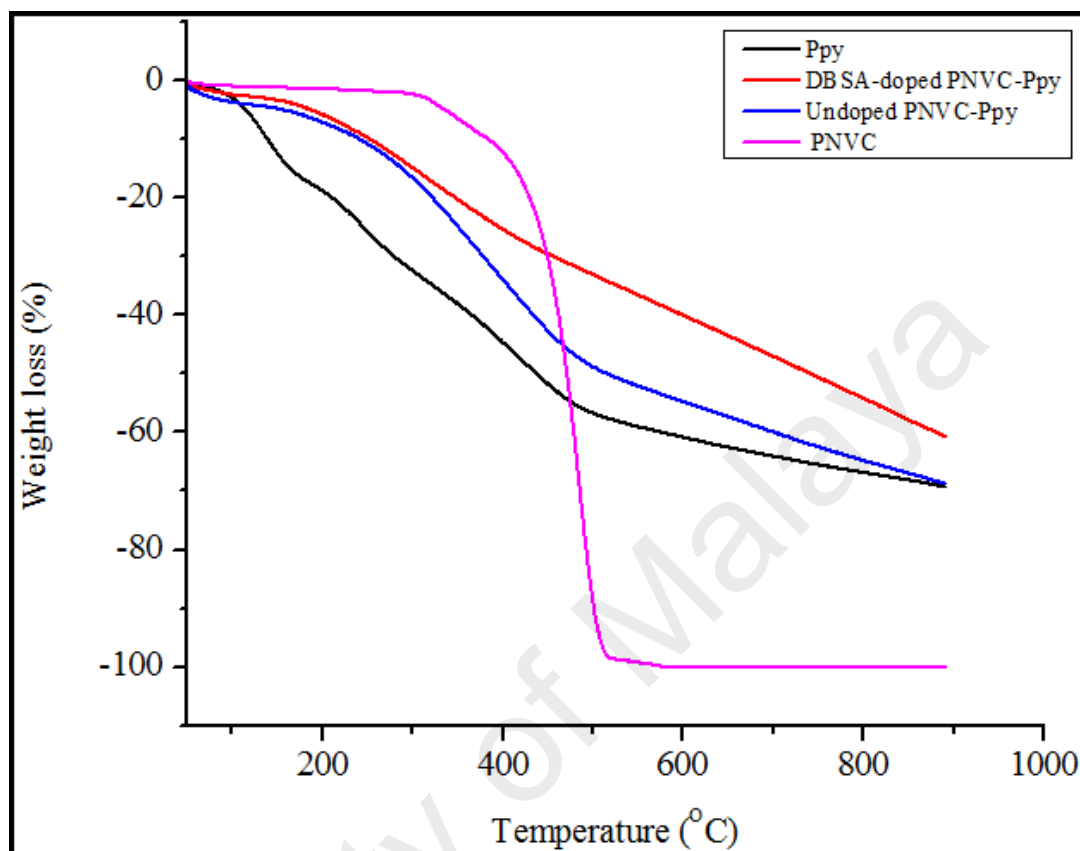


**Figure 3.12: TGA thermogram of PNVC, Ppy, doped PNVC-Ppy and undoped PNVC-Ppy.**

Conjugated polymers possess high carbon content due to double bonds alternation. Hence, the thermal stability of undoped PNVC-Ppy was enhanced. Besides, the effect of the DBSA dopant on thermal stability of the PNVC-Ppy was revealed by the thermogram of DBSA-doped PNVC-Ppy. Although, both doped and undoped PNVC-Ppy had initial thermal degradation at the same temperature range (50°C–200°C), DBSA-doped PNVC-Ppy appeared to be more thermally stable because 75% of its weight remained after the second stage of thermal degradation, which occurred between 200°C and 400°C. Other than that, the decomposition of polymer backbone took a longer temperature range (200°C–470°C) in undoped PNVC-Ppy and almost half the polymer weight had already lost to thermal degradation. Moreover, the superior thermal stability of PNVC was

displayed as it remained stable until up to 300°C with less than 2% loss of surface moisture content. However, PNVC decomposed completely before 600°C with no carbonized residue after decomposition, as indicated by the thermogram. In summary, not only PNVC contributed to the thermal stability of DBSA-doped PNVC-Ppy, but the presence of DBSA in the copolymer molecule also further enhanced the thermal stability of the copolymer.

### **3.3.7 Morphology of DBSA-doped PNVC-Ppy**

Figure 3.13 shows the SEM images of PNVC, Ppy, and DBSA-doped PNVC-Ppy all at  $\times 10$  magnification. PNVC showed spherical particles of larger size. The morphology revealed less tendency for agglomeration, which is perhaps the reason why PNVC was readily soluble in common organic solvents. Besides, preparation condition and method usually influence the surface morphology of Ppy (Shen & Wan, 1998). Ppy also displayed a porous morphology with agglomeration of tiny globules. Meanwhile, the DBSA-doped PNVC-Ppy presented a morphology that completely differed from those of homopolymers. PNVC-Ppy copolymer showed a distinctly formed and densely packed globular structure without voids in-between. The particles were uniformly arranged with similar diameters. The uniform size revealed that copolymerization actually took place between NVC and pyrrole monomers; forming a new product with distinctively a different structure.

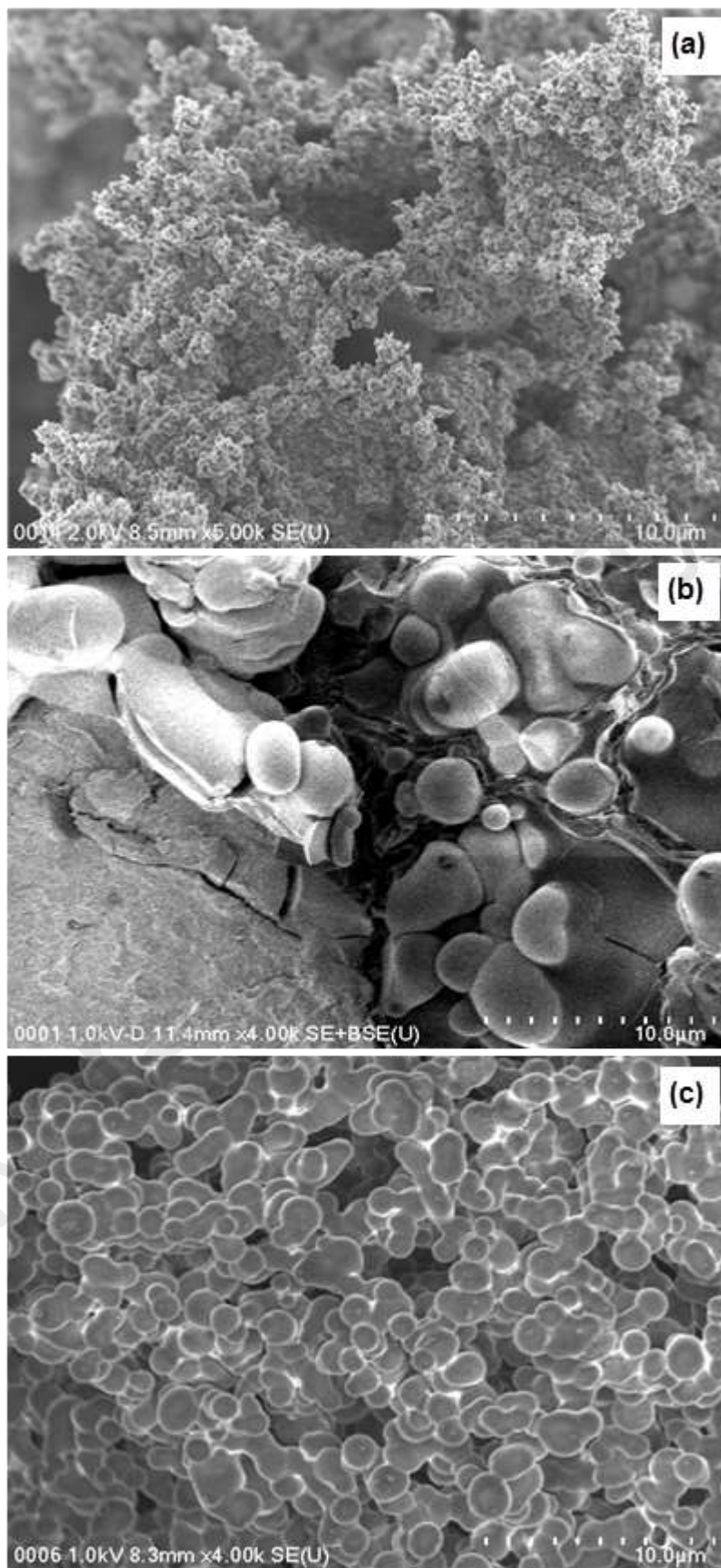


**Figure 3.13: FESEM images of (a) Ppy, (b) PNVC, and (c) DBSA-doped PNVC–Ppy copolymer**

### 3.4 Conclusion

In summary, this study had demonstrated that intractable copolymer of NVC and pyrrole could be rendered soluble in polar organic solvents by the counterion effect of DBSA. DBSA-doped PNVC-Ppy can now be seen as a solution processable conducting polymer, which can be simply obtained via chemical oxidation of NVC and Py monomers using ammonium persulfate oxidant. The new soluble copolymer should be better than PNVC in terms of electrical conductivity and optical absorption; Ppy in terms of thermal stability. Furthermore, the solubility of DBSA-doped PNVC-Ppy in some polar organic solvents allows further studies to look into its interaction with other organic solvents that are less polar in order to widen its area of applications. In fact, the easy synthetic route, solution processability, and low band gap of the soluble copolymer further enable the study of film forming ability of this product for applications as an active layer material or transparent electrodes in optoelectronics.

## CHAPTER 4: PHOTOVOLTAIC PERFORMANCE OF SOLUTION PROCESSABLE DBSA-DOPED POLY(N-VINYL CARBAZOLE)-POLY(PYRROLE) COPOLYMER

### 4.1 Introduction

Research focus on organic photovoltaic cells has increased over the past decade. Among the advantages of organic photovoltaics (OPVs) over the inorganic counterpart, are tunability and solution processability (Hu & Karasz, 2003; Mbarek et al., 2013; Udum et al., 2009) of organic semiconductors (OSCs) via copolymerization. Thus, large surface area production and mechanical flexibility can be realized when working with OSCs (Choi et al., 2015; Krebs et al., 2009). The effective solubility of solution processed conducting polymers in organic solvents makes them useful as donor materials in the active layer of BHJ solar cells. The active layer comprises conjugated polymer, the donor, blended with a soluble fullerene derivative (PC<sub>60</sub>BM or PC<sub>70</sub>BM), functionalized graphene, or polymer as an acceptor material. BHJ concept is an intimate mixing of the donor and acceptor materials to reduce the distance covered by the exciton to reach the donor/acceptor interface without sacrificing the active layer thickness. Soluble polythiophene, polyphenylenevinylene (PPV), and their derivatives are among the earliest donor materials for BHJ polymer solar cells (Li, Zhu, et al., 2012). Poly(3-hexylthiophene) (P3HT) possesses high hole mobility and broad solar absorption range, it is now used as a standard for OPV materials (Li, Zhu, et al., 2012; Price et al., 2011). For instance, power conversion efficiencies up to 5 % have been reported for solution processed BHJ solar cells based on P3HT and PCBM (Dang et al., 2011). Building efficient BHJ solar cells requires efforts on (Beaujuge & Frechet, 2011; Coughlin et al., 2014; Ye et al., 2014) towards achieving new donor (and acceptor) materials with strong absorption within the solar spectrum, tunable in the processing solution, and high charge carrier mobility as well as, processing and fabrication (Guo, Baumgarten, et al., 2013; Scharber & Sariciftci, 2013). Meanwhile, despite the electron-donating and electro-

optical properties of carbazole-based polymers, poly (n-vinyl carbazole) (PNVC), a popular carbazole-containing polymer has received little attention as donor material for BHJ solar cells (Chemek et al., 2010; Mbarek et al., 2013). Although used as a non-conjugated polymer, PNVC is a good hole transporting material that can be employed in photovoltaic devices. Due to its luminescence property (Chemek et al., 2012; Narayan & Murthy, 1997; Nishino et al., 1995), PNVC has been combined with other materials (organic or inorganic) to fabricate organic light emitting diodes (Brunner et al., 2004; Kido et al., 1994; Kido et al., 1995). Another advantage is the ease of copolymerization with conjugated polymers via chemical oxidative polymerization. As mentioned earlier, forming copolymer is a part of the tunability of conducting polymers to access their complementary properties in the new material. Recently, PNVC copolymers have been prepared via chemical oxidative polymerization using anhydrous  $\text{FeCl}_3$  as the oxidant (Chemek et al., 2014). As an example, PNVC-PPV copolymer applicable for optoelectronic devices was chemically synthesized by Mbarek et al., (2013) using  $\text{FeCl}_3$ . The resulting copolymer was not only solution processed but exhibited unique absorption and emission properties.

On the other hand, polypyrrole (Ppy) is a highly conducting  $\pi$ -conjugated polymer owing to its remarkable optical and electrical properties, easy processability, and facile polymerization (Tat'yana & Oleg, 1997). Its importance is demonstrated by wide area of potential applications such as (Gao et al., 1996), electrochromic devices (De Paoli et al., 1997; Takagi et al., 2012; Talaie et al., 2000), electrodes for batteries (Kim et al., 2012; Wang et al., 2011; Wang et al., 2006), supercapacitors (Zhao et al., 2013; Zhou et al., 2013), photovoltaics (He et al., 2014; Kim et al., 2009; Kwon et al., 2004), sensors (Li et al., 2016; Ramanavičius et al., 2006; Turco et al., 2015; Zhou et al., 2015) and so on. Although Ppy is often obtained as an intractable black powder via oxidative chemical polymerization, most of its potential applications are based on solution processing



techniques to obtain a thin film. Polypyrrole can be prepared via electrochemical or chemical polymerization using ferric chloride ( $\text{FeCl}_3$ ) or ammonium persulfate (APS) oxidant. Chemical polymerization is advantageous over electrochemical because it offers mass production at low-cost (Kiebooms et al., 2001). Owing to this advantage, efforts are being made to prepare solution processable polypyrrole via copolymerization with soluble polymers, functionalization with alkyl substituent groups, or doping with functional dopants. Soluble polypyrrole prepared with functional dopants such as DBSA possesses enhanced conductivity because the charge carriers are not only  $\pi$ - $\pi$  electrons but polarons and bipolarons generated by counterion effect of the dopants during polymerization. Copolymerization is another effective method to obtain soluble polypyrrole as it can weaken pyrrole chain rigidity and intermolecular interactions. Moreover, a copolymer with enhanced possible properties can be realized by copolymerizing pyrrole with other monomers. Although, PNVC possesses a wide band gap, (Jang et al., 2005) when copolymerized with other electrically conducting polymers such as polypyrrole, its good electron donating property can be useful in solar cell devices. Moreover, NVC and pyrrole monomers have comparable oxidative potential thus, PNVC-Ppy copolymers have been synthesized successfully via electrochemical oxidation of their mixed monomers (Sarac et al., 2005). Past studies have shown that PNVC-Ppy copolymers possess improved electrical conductivity (Sezer et al., 1999), high thermal stability (Biswas & Roy, 1993a), and good mechanical properties. Furthermore, it had been shown that core-shell nanoparticles of Ppy-PNVC synthesized via micelle templating exhibited remarkable optical and electrical properties. Meanwhile, the copolymers obtained by copolymerizing pyrrole with NVCs were reported to be insoluble masses (Biswas & Roy, 1996) or solubility information was not mentioned (Jang et al., 2005). However, when we carried out the copolymerization using DBSA as a dopant and ammonium persulfate as the oxidant, the resulting copolymer became

soluble in selected organic solvents and an enhanced conductivity was also recorded. Thus, in this chapter, we report the photovoltaic properties of the DBSA-doped PNVC-Ppy by fabricating a BHJ solar cell using the copolymer as the donor and PC<sub>60</sub>BM the acceptor.

## 4.2 Experimental

### 4.2.1 Fabrication and characterization of organic solar cells

Polymer BHJ solar cells based on DBSA-doped PNVC-Ppy (scheme 1) were fabricated following the conventional fabrication process. The indium tin oxide (ITO) coated glass substrate was sequentially ultrasonicated with acetone, ethanol, and distilled water and dried with a stream of nitrogen gas. Next, an aqueous solution of poly(3,4-ethylene dioxythiophene) doped with polystyrene sulfonic acid (PEDOT:PSS), the buffer layer, was spin coated at 1000 rpm onto the ITO surface of the precleaned glass substrate and then dried in air at 120 °C for 20 min. Having stirred on a hotplate at 60 °C for 24 hrs, a chloroform solution of the active layer containing a blend of DBSA-doped PNVC-Ppy and PC<sub>60</sub>BM (1:1 or 1:2) were spin coated at 500 rpm on top of the PEDOT:PSS and annealed at 120 °C for 10 min. Finally, aluminium (Al) approximately 80-100 nm thick was vacuum ( $10^{-5}$  Pa) deposited on the surface of the photoactive layer to yield ITO/PEDOT:PSS/DBSA-doped PNVC-Ppy:PC<sub>60</sub>BM/Al BHJ solar cell device. The active layer of the device was 4.5 mm<sup>2</sup>. The current-voltage (J-V) in the dark and under illumination were measured using a Keithley 236 source measuring unit. A Xenon light source acted as an irradiation source and the J-V characteristics were measured under AM1.5G. The electrochemical measurement of the DBSA-doped PNVC-Ppy copolymer was carried out at a scan rate of 75 mV/s at room temperature on a Zahner IM electrochemical workstation. 0.1M of tetrabutylammonium phosphorus hexafluoride (TBAPF<sub>6</sub>) in anhydrous acetonitrile (CH<sub>3</sub>CN) solution was used as the supporting electrolyte. The copolymer film was prepared by drop casting on a pre-cleaned working

electrode (glass/ITO) with Ag/Ag<sup>+</sup> and glassy carbon as reference and counter electrode respectively. The optical bandgap of the copolymer was estimated using the optical absorption spectrum fitting method.

### **4.3 Results and discussion**

#### **4.3.1 Film-forming ability of the copolymer**

For efficient photon harvesting, the donor material (polymer) is required to dissolve well in the processing solution in order to form a smooth film with absorption more than 0.25. The film-forming potential of DBSA-doped PNVC-Ppy copolymer was determined by separately dissolving 20 mg of the copolymer in 1 ml of chloroform, chlorobenzene, and dichlorobenzene. Table 4.1 summarizes the absorptions of the copolymer in the selected solvents. The copolymer exhibited film-forming ability in this order: chloroform > THF > chlorobenzene > dichlorobenzene. The poor film forming ability in chlorobenzene and dichlorobenzene is due to the poor solubility of the copolymer in the solvents. Therefore, the photovoltaic properties of the copolymer were investigated by using chloroform as the processing solution.

#### **4.3.2 Optical and electrochemical properties**

The UV-visible absorption spectra of the copolymer in both chloroform solution and thin film are presented in Figure 4.1. The spectrum of the DBSA-doped PNVC-Ppy copolymer displayed maximum absorption at 500 nm for solution and 525 nm for thin film. This can be attributed to  $\pi$ - $\pi^*$  electron transition along the copolymer main chain. The observed red shift by 25 nm is due to solid state intermolecular interactions as the thin film formed aggregates. The thin film exhibited a wider absorption spectrum showing absorption onset at 650 nm. The optical band gap ( $E_g^{opt} = 1.91 \text{ eV}$ ) of the copolymer was deduced from the absorption onset using the following equation:

$$E_g^{opt} = h * \frac{c}{\lambda} \quad (4.1)$$

Where h = Planks constant =  $6.626 \times 10^{-34}$  joules sec, C = speed of light =  $3.0 \times 10^8$  meter/sec, and  $\lambda$  = cut off wavelength =  $650 \times 10^{-9}$  meters. This value ( $E_g^{opt} = 1.91$  eV) shows that the copolymer is applicable as a donor material in the active layer of polymer solar cells.

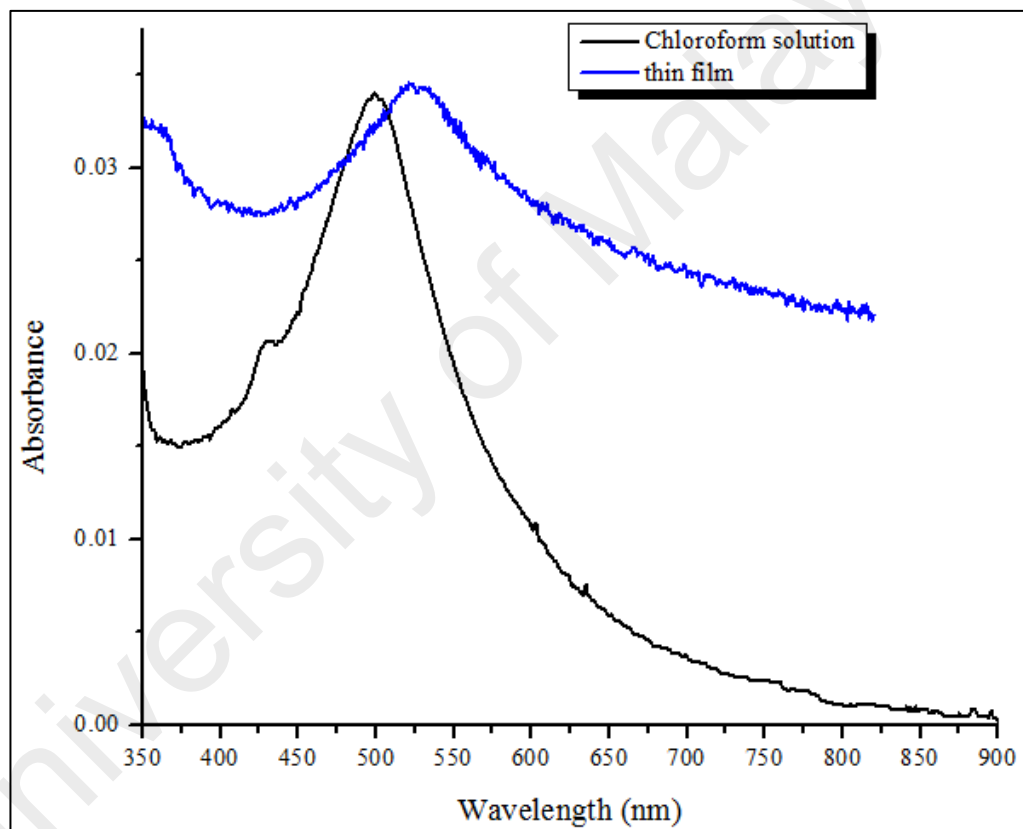


**Figure 4.1. UV-vis spectra of DBSA-doped PNVC-Ppy in chloroform solution and thin film**

The relative positions of the highest occupied molecular orbital (HOMO) and the lowest unoccupied molecular orbital (LUMO) of conducting polymers are crucial to the design of polymer solar cells. The HOMO and LUMO energy levels were calculated from

the onset oxidation ( $E_{onset}^{ox}$ ) and reduction ( $E_{onset}^{red}$ ) potentials of the voltammogram (figure 4.2) using the following equation:

$$E_{HOMO} = -q(E_{onset}^{ox} + 4.7)eV \quad (4.2)$$

$$E_{LUMO} = -q(E_{onset}^{red} + 4.7)eV \quad (4.3)$$

With the  $E_{onset}^{ox} = 0.50 V$  and  $E_{onset}^{red} = -1.43 V$ , the HOMO and LUMO energy levels were estimated to be  $-4.49 eV$  and  $-2.97 eV$  respectively. Thus, the electronic band gap was calculated from  $E_g^{ele} = E_{HOMO} - E_{LUMO} = 1.93 eV$ . This value is closed to the estimated value of the optical band gap.

**Table 4.1: Absorbance maximum of copolymer films spin coated from different solvents (20 mg copolymer/mL).**

| Solvent                | Film absorbance |
|------------------------|-----------------|
| <b>chloroform</b>      | 0.28            |
| <b>THF</b>             | 0.18            |
| <b>chlorobenzene</b>   | 0.005           |
| <b>Dichlorobenzene</b> | 0.005           |

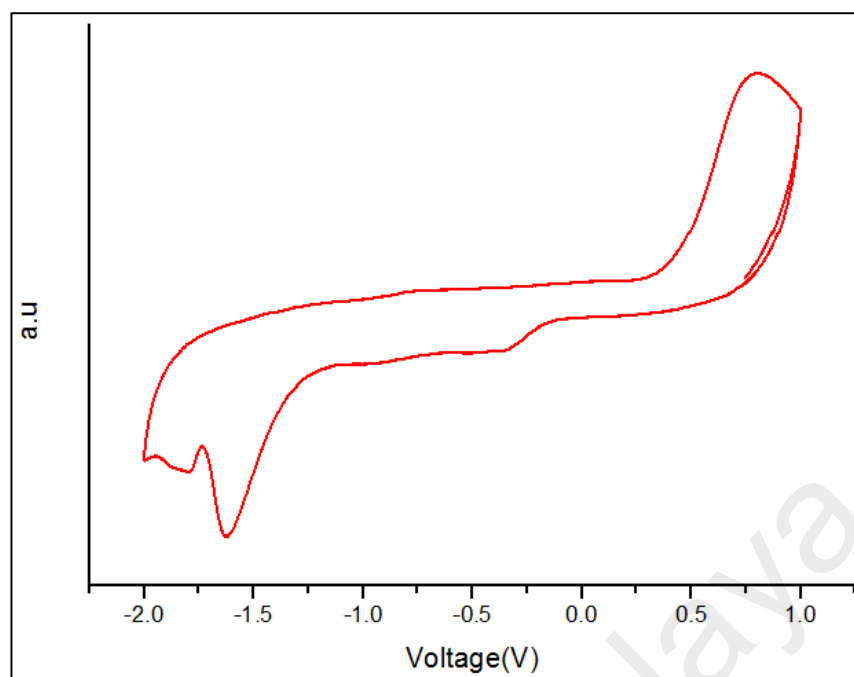


**Figure 4.2. Cyclic voltammogram of DBSA-doped PNVC-Ppy copolymer**

Table 4.2 summarizes the optical and electrochemical properties of the copolymer. The HOMO level of the copolymer (-4.49 eV) is close to that of P3HT, one of the conjugated polymers commonly used as donor materials in BHJ polymer solar cells. Meanwhile, the theoretical open circuit voltage ( $V_{oc}$ ) of solar cells with donor materials being conjugated polymers can be calculated as the difference between the  $E_{HOMO}$  of the donor and the  $E_{LUMO}$  of the acceptor:

$$V_{oc} = |E_{HOMO(donor)} - E_{LUMO(PC60BM)}| - 0.3 \quad (4.4)$$

For an efficient photoinduced electron transfer between the polymer donor and PC<sub>60</sub>BM acceptor, LUMO-LUMO offset of 0.3 eV is desirable. The LUMO-LUMO offsets between the copolymer (-2.97 eV) and PC<sub>60</sub>BM (-3.57 eV) is more than the desirable value. Therefore, a good exciton dissociation at the interface between the DBSA-doped PNVC-Ppy and PC<sub>60</sub>BM is expected.

**Table 4.2. Optical and electrochemical properties of DBSA-doped PNVC-Ppy copolymer**

|  |            |
|--|------------|
| <b>Ab<sub>Smax</sub> in solution (nm)</b>  | <b>500</b> |
| <b>Ab<sub>Smax</sub> in thin film (nm)</b> | 525        |
| <b>Thin film absorption onset (nm)</b>     | 650        |
| <b><math>E_g^{opt}</math> (eV)</b>         | 1.91       |
| <b><math>E_{onset}^{ox}</math> (V)</b>     | 0.50       |
| <b><math>E_{onset}^{red}</math> (V)</b>    | -1.43      |
| <b><math>E_{HOMO}</math> (eV)</b>          | -4.49      |
| <b><math>E_{LUMO}</math> (eV)</b>          | -2.97      |
| <b><math>E_g^{ele}</math> (eV)</b>         | 1.93       |

Photoluminescence (PL) spectra of the DBSA-doped PNVC-Ppy in chloroform solution without PC<sub>60</sub>BM and in a combination of 1:2 with PC<sub>60</sub>BM were investigated as shown in Figure 4.3. It can be seen that the DBSA-doped PNVC-Ppy solution shows strong photoluminescence between 475 and 680 nm, with excitation wavelength at 450 nm. The PL emission is moderately quenched when PC<sub>60</sub>BM (1:2, w/w) was blended with the copolymer indicating efficient photoinduced charge transfer along the interface between the photoexcited copolymer and PC<sub>60</sub>BM. This phenomenon, according to previous reports, shows the excited states in the DBSA-doped PNVC-Ppy backbone is quenched due to intermolecular electronic interactions at the donor-acceptor interface, a condition for efficient organic photovoltaic cells.

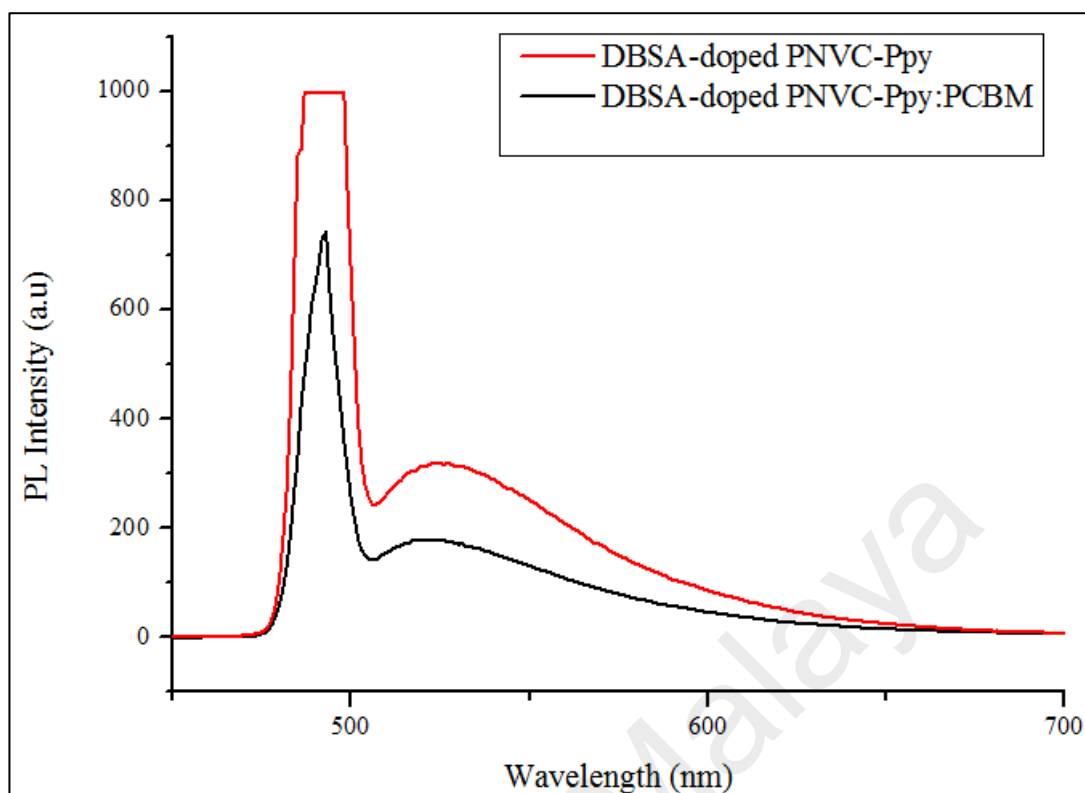


**Figure 4.1. Photoluminescence (PL) spectra of DBSA-doped PNVC-Ppy, DBSA-doped PNVC-Ppy:PC<sub>60</sub>BM**

### 4.3.3 Photovoltaic properties

The BHJ solar cell devices having the structure ITO/PEDOT:PSS/copolymer:PC<sub>60</sub>BM/Al were fabricated following the conventional technique. The hole transporting layer of PEDOT:PSS was spin-coated onto ITO, the hole collecting electrode. The active layer, a blend of the copolymer (donor) and PC<sub>60</sub>BM (acceptor) was dissolved in chloroform and spin-coated on the top of PEDOT:PSS. Table 4.3 presents the photovoltaic performance of the cells based on ratio 1:1 and 1:2 of the donor to the acceptor. Figure 4.4 shows the (J-V) characteristics of the solar cells based on DBSA-doped PNVC-Ppy, and DBSA-doped PNVC-Ppy:PC<sub>60</sub>BM (1:1 after annealing) in the dark and under illumination. The J-V curve of the devices shows no current response in the dark. However, under illumination, the device with only DBSA-doped PNVC-Ppy as the active layer shows the values of open circuit voltage ( $V_{oc}$ ), short-circuit current ( $J_{sc}$ ), and fill factor ( $FF$ ), and power conversion efficiency (PCE,  $\eta$ ) as



0.0005, 0.103, 0.56, and 0.23 respectively. The PCE of the solar cell based on DBSA-doped PNVC-Ppy: PC<sub>60</sub>BM was 0.62 % with  $V_{oc} = 0.56$  V,  $FF = 0.53$ , and  $J_{sc} = 1.5$  mA/cm<sup>2</sup>. The cell based on a blend of the copolymer and PC<sub>60</sub>BM shows a better overall performance compares with the one based on the pristine copolymer indicating charge transfer between the copolymer (donor) and PC<sub>60</sub>BM (acceptor). Blending the copolymer(donor) with PC<sub>60</sub>BM increases the photovoltaic performance of the solar cell because the lower symmetry of PC<sub>60</sub>BM allows high optical absorption coefficient with the visible region.

Although, the solar cell based on a blend of DBSA-doped PNVC-Ppy: PC<sub>60</sub>BM displayed better photovoltaic properties with regards to the pristine copolymer, its power conversion efficiency is lower than expected perhaps due to the quality of the photoactive layer film. Meanwhile, several investigations have shown that annealing treatment can improve PCE of polymer solar cells. Thus, blends of the active layer, copolymer: PC<sub>60</sub>BM (1:1 and 1:2 w/w) were prepared and then spin coated at high-speed spin (1000 rpm) and low-speed spin (500 rpm). Figure 4.4 (c) and 4.4 (d) show device performances before and after annealing (180 °C, 10 min), the detailed are summarized in table 2. It can be seen that the device with active layer composition of 1:2, spin coated at 500 rpm possesses higher PCEs (0.6 % and 0.4 %) before and after annealing. This can be attributed to better donor-acceptor blend ratio and an increased film thickness to accommodate better charge carrier mobility. After annealing, the device with donor-acceptor composition of 1:2 shows the highest PCE due to the increase in  $J_{sc}$  and  $V_{oc}$ . The D–A blend ratio strongly affects the performance of BHJ solar cells. The D–A blend ratio influences the sizes and distributions of the phases, thereby changing the size of the interface available for exciton dissociation and charge carrier transport. The increased PCE after annealing treatment is due to active layer re-ordering of the donor and acceptor phases to increase the size of the domain. Vanlaeke *et al.* [80] demonstrated that optimized thermal annealing of the BHJ

layer can improve its photon absorption properties, blend morphology and the hole mobility by inducing the stacking of P3HT in coplanar conjugated segments.

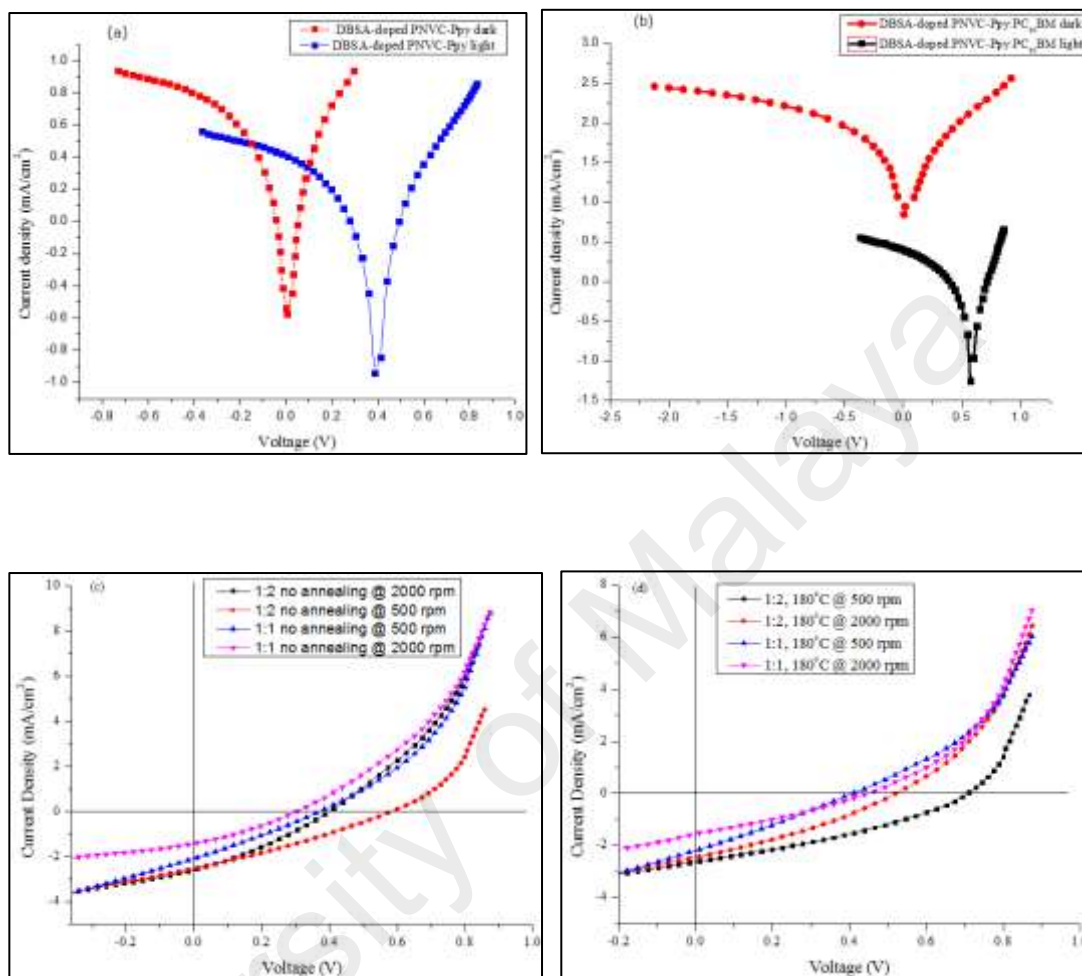


**Figure 4.2:** a, b) logarithmic  $J$ - $V$  characteristics of the photovoltaic devices based on DBSA-doped PNVC-Ppy and DBSA-doped PNVC-Ppy:PC<sub>60</sub>BM in the dark and under illumination. c, d)  $J$ - $V$  characteristics of the photovoltaic devices with different ratio of PC<sub>60</sub>BM under illumination without annealing, with annealing at 180°C for 10 min.

**Table 4.3. Photovoltaic performance of the solar cell based on DBSA-doped PNVC-Ppy:PC<sub>60</sub>BM thin film spin coated at 1000 or 500 rpm before and after annealing at 180 °C for 10 min.**

| (copolymer:PC <sub>60</sub> BM) | FF    | $J_{sc}$<br>(mA/cm <sup>2</sup> ) | $V_{oc}$ (V) | PCE (%) |
|---------------------------------|-------|-----------------------------------|--------------|---------|
| <b>1:0</b>                      | 0.029 | 1.44                              | 0.051        | 0.0021  |
| <b>1:1<sup>a</sup></b>          | 0.31  | 1.44                              | 0.30         | 0.13    |
| <b>1:1<sup>a*</sup></b>         | 0.29  | 1.54                              | 0.46         | 0.21    |
| <b>1:1<sup>b</sup></b>          | 0.27  | 2.04                              | 0.38         | 0.21    |
| <b>1:1<sup>b*</sup></b>         | 0.26  | 2.22                              | 0.41         | 0.24    |
| <b>1:2<sup>a</sup></b>          | 0.35  | 2.59                              | 0.35         | 0.32    |
| <b>1:2<sup>a*</sup></b>         | 0.32  | 2.45                              | 0.52         | 0.40    |
| <b>1:2<sup>b</sup></b>          | 0.29  | 2.52                              | 0.58         | 0.43    |
| <b>1:2<sup>b*</sup></b>         | 0.34  | 2.6                               | 0.71         | 0.62    |

<sup>a</sup> Spin coated at 1000 rpm, no annealing.

<sup>a\*</sup> Spin coated at 1000 rpm, annealing at 180°C.

<sup>b</sup> Spin coated at 500 rpm, no annealing.

<sup>b\*</sup> Spin coated at 500 rpm, annealing at 180°C.

#### 4.3.4 Conclusion

In conclusion, a solution processable conducting polymer based on DBSA-doped PNVC-Ppy was used as the donor material in organic BHJ photovoltaic cells with PC<sub>60</sub>BM as the electron acceptor. The copolymer displayed a moderate absorption curve with an absorption maximum at 525 nm and comparable optical and electrochemical band gaps of 1.91 and 1.93 eV respectively. Blending the copolymer with PC<sub>60</sub>BM resulted to quenching of the DBSA-doped PNVC-Ppy photoluminescence, showing a photoinduced

electrons transfer between the copolymer and PC<sub>60</sub>BM makes the blend applicable as an active layer in polymer solar cells. BHJ solar cells based on DBSA-doped PNVC-Ppy:PC<sub>60</sub>BM were fabricated. The power conversion efficiency of the devices based on DBSA-doped PNVC-Ppy:PC<sub>60</sub>BM (1:2) under AM1.5G, 100 mW/cm<sup>2</sup> was 0.43% with an open-circuit voltage ( $V_{oc}$ ) of 0.58 V, and a short circuit current ( $J_{sc}$ ) of 2.52 mA/cm<sup>2</sup>. Reducing the spin coating speed from 1000 to 500 rpm and subsequent annealing the device at 180 °C for 20 min enhanced the power conversion efficiency to 0.64%, with an open-circuit voltage ( $V_{oc}$ ) of 0.71 V, a short circuit current ( $J_{sc}$ ) of 2.60 mA/cm<sup>2</sup> and a fill factor ( $FF$ ) of 0.34. Owing to ease of synthesizing the copolymer and its solubility in selected organic solvents, more efforts are needed to study the paths to improve the performance of the device fabricated from this novel material, including fine control of the active layer morphology, band gap engineering, increasing the molecular weight of the copolymer, and using better fullerene derivatives.

## CHAPTER 5: ENHANCING THE ELECTRICAL CONDUCTIVITY OF DBSA-DOPED POLY(N-VINYL CARBAZOLE)-POLY(PYRROLE) COPOLYMER

### 5.1 Introduction

Polymer nanocomposite has emerged as an important area in nanoscience and nanotechnology enhancing the thermal, mechanical, electrical, and gas barrier properties of polymers (Jancar et al., 2010; Zeng et al., 2005). This new class of composite materials becomes popular owing to its wide application areas such as supercapacitors (Frackowiak et al., 2006), electronic devices (Holder et al., 2008), rechargeable batteries (Parvin et al., 2015), sensors (Sauerbrunn et al., 2015), including solar cells (Chen et al., 2015). Polymer nanocomposites have attracted great scientific interest for their design uniqueness that ordinary composites lack. Meanwhile, earlier investigations of polymer nanocomposites were on nanoscale fillers such as silica and clay. However, poor thermal and electrical conductivity of silica-based nanofillers enable investigations into other materials. For instance, nanomaterials prepared from carbon nanotube (CNT), carbon black, and expanded graphite are among the earlier candidates with improved properties (Yan et al., 2016).

Graphene, a single-atom-thick is a two-dimensional (2-D) honeycomb structure made of  $sp^2$ -hybridized carbon atoms. Graphene has displayed many intriguing properties, including high thermal and chemical tolerance, high charge carrier mobility (Loh et al., 2010; Malig et al., 2011; Soldano et al., 2010), high surface area, and good mechanical strength (Prezhdo et al., 2011). Nevertheless, forming homogeneous dispersions is a major challenge when working with graphene for large-scale production. For instance, to prepare polymer-graphene composites, one important step is to exfoliate graphite sheets into thin graphitic layers. However, pristine graphene does not disperse either in organic or inorganic media, hence working with pristine graphene proves difficult. Graphene oxide (GO), the oxidized form of graphene whose basal planes and edges contain various

oxygen-bearing functional groups, has attracted much attention. Today, using GO as a precursor is an effective approach to prepare dispersible graphene (Dreyer et al., 2010). The ease of exfoliation and reduction of GO to graphene in a large-scale makes GO a preferred choice to other expensive fillers such as CNTs and carbon nanofibers (Putz et al., 2010). In addition, GO is rich in oxygen-bearing groups (–OH, –COOH, –CHO, epoxy groups) as a result, it is not only tunable but readily soluble in solvents making it an effectiveness nanofiller (Bose et al., 2010; Cassagneau et al., 2000). One advantage of GO is its hydrophilicity that makes it disperse readily in aqueous solutions. Likewise, GO interacts covalently or non-covalently with polymers to form GO intercalated nanocomposites. Nevertheless, graphene dispersed in an organic medium is required in most of its proposed application areas (nanocomposite, organic electrodes, sensors, organic solar cells, and so on). Thus, it is important to develop an easy route to exfoliate and disperse graphene in common organic solvents. Many findings have shown that incorporation of GO improves the thermal stability of nanocomposites remarkably (ref). To date, researchers have made great efforts to develop GO-based nanocomposites for improved solubility and dispersion in organic solvents (Aleshin et al., 2015; Bindumadhavan et al., 2015; Li et al., 2011). Poly (N-vinyl carbazole) (PNVC) is readily soluble in common organic solvents and possesses good thermal stability, though a poor electrical conductor. Some of its dispersible nanocomposites with GO have been prepared without further modification of the polymer nor functionalization of graphene. As an example, Santos et al. prepared a well-dispersed PNVC/GO nanocomposite via solution mixing process. Such a dispersible nanocomposite displayed an excellent storage stability for up to 30 days in N-methyl pyrrolidone (NMP) and N-cyclohexyl-2-pyrrolidone (CHP) (Santos et al., 2011). Similarly, solution processable GO-PNVC has been fabricated by covalently attaching GO to PNVC. The material displayed good optical and electronic properties making it an excellent material for optoelectronic devices (Zhang et al., 2010).

Meanwhile, nanocomposites based on polypyrrole (Ppy) and GO are characterized with good thermal stability and enhanced electrical conductivity. However, owing to the insolubility of Ppy, Ppy-GO nanocomposites are often prepared as-deposited films and obtained in a form of free-standing papers (Li, Xia, et al., 2012). Earlier, there were reports about using DBSA as a protonating agent and an emulsifier for the synthesis of PANI/GO (Imran et al., 2014) and PANI/GOR (Basavaraja et al., 2012) nanocomposites. As a result, the nanocomposites exhibited an enhanced thermal and electrical properties and were dispersible in organic solvents making them a good candidate in several application areas such as functional coatings, electric devices, and sensors. Meanwhile, our group has prepared DBSA-doped PNVC-Ppy copolymer, soluble in some selected organic solvents. The copolymer displayed an improved thermal stability compared to polypyrrole and better electrical conductivity relative to PNVC. Although the copolymer was soluble in organic solvents, there is need to improve the electrical conductivity further to meet the demand of its potential applications. Therefore, if the copolymer is made as a composite with GO, based on the reports that  $\pi$ -electron rich polymers can form  $\pi$ -stacking with the graphene sheets (Gu et al., 2010; Pernites et al., 2011; Santos et al., 2011), the nanocomposite will not only possess enhanced electrical conductivity but stable dispersibility in organic solvent.

In this respect, we report a simple approach to prepare organic solvents dispersible PNVC-Ppy/GO nanocomposite by in-situ chemical oxidative polymerization. Ammonium persulfate was used as the oxidant while dodecylbenzene sulfonic acid (DBSA), an anionic surfactant, was used as a dopant and an emulsifier to the copolymer and GO, respectively. The obtained nanocomposite exhibits appropriate optical and electrical properties to be used an active layer in polymer electronics.

## **5.2 Experimental**

### **5.2.1 Materials**

Natural flake graphite, n-vinyl carbazole, pyrrole monomer and ammonium persulfate (oxidant) were purchased from Sigma-Aldrich Chemicals. Sulfuric acid, hydrochloric acid, ethanol and hydrogen peroxide were purchased from Merck, Germany. Dodecyl benzene sulfonic acid (DBSA, Acros Organics) was used as received. N,N-dimethylformamide (DMF), dimethyl sulfoxide (DMSO), and acetonitrile were of analytical grade and used without further purification.

### **5.2.2 Instrument**

The FTIR measurement of nanocomposites was carried out using a ThermoScientific NICOLET 5700 Spectrometer. Raman spectra were recorded in a confocal Raman spectrometer (Renishaw RM 1000, Ar+ 514.5 nm). The SEM images were obtained using an FEI Sirion Microscope. The powdered samples were subjected to a wide angle X-ray diffraction study with a PHILIPS PW/1710/00 X-ray diffractometer using CuK- $\alpha$  radiation. UV-vis spectra were recorded using an Agilent 8453 spectrometer.

### **5.2.3 Preparation of graphene oxide (GO)**

GO was prepared from natural graphite flakes by an improved Hummers method (Marcano et al., 2010). A 1:6 ratio mixture of graphite flakes and  $\text{KMnO}_4$  was dissolved in  $\text{H}_2\text{SO}_4/\text{H}_3\text{PO}_4$  (9:1) and the mixture was stirred for 12hr at room temperature. To terminate the oxidation reaction, 30%  $\text{H}_2\text{O}_2$  was added and the mixture was filtered. Then, the filtrate was centrifuged (4000 rpm), and the supernatant was decanted away. The deposit after the separation was washed with de-ionized water, ethanol, and hydrochloric acid in several times. The product was then coagulated and dried under a vacuum at room temperature.



#### 5.2.4 Synthesis of PNVC-Ppy/GO Composites

In a typical polymerization reaction, pyrrole (0.1 mol), NVC (0.15 mol), and DBSA (0.01 mol) were separately dissolved in acetonitrile. All the mixtures were further transferred to a beaker. Then, 0.50 g of GO nanoparticle was dissolved in water and finally added to the above reaction mixture and sonicated for 5 min. Afterward, 0.3 mol  $\text{FeCl}_3 \cdot 6\text{H}_2\text{O}$  was dissolved in water then added dropwise to the mixture above. The reaction mixture was subjected to a continuous shaking for 6 hours at room temperature. The PNVC-PPy/GO nanocomposites so obtained was washed several times with a mixture of water and ethanol until the washing solvents became colourless. Finally, the washing solvents were filtered off and the composite was obtained as a residue, dried in a vacuum at  $80^\circ\text{C}$  for 24 h. For comparison, the neat PNVC-PPy was polymerized by a similar method without GO suspension.

#### 5.2.5 Characterization

Electrical conductivities of the nanocomposite were measured at room temperature using a Jandel RM3000 Test Unit with typical probe spacing  $\sim 1$  mm. The following equation was used to calculate the electrical conductivity:

$$\sigma = V^{-1} I \left( \frac{\ln 2}{\pi d_n} \right) \quad (5.1)$$

where  $V$  is the applied potential measured in volt,  $d_n$  is the thickness of the pellet measured in cm, and  $I$  is the current in ampere. The pellets (0.15 g, diameter 1cm) were measured by using four-point probe method, compressed (pressure, 15 bar) from respectively powdered samples. Morphologies of the samples were studied by Field-emission scanning electron microscopy (FE-SEM, Hitachi SU-8220, Japan) while Fourier transform infrared (FT-IR) spectra were measured using an FTIR-Spotlight 400 spectrometer (Perkin Elmer, USA). The UV-Vis spectra were recorded using a UV-2600 (Shimadzu, USA) spectrophotometer, in the range of 200-1100 nm. X-ray diffraction

(XRD) measurements were performed using a PANalytical EMPYREAN model diffractometer with a Cu-K $\alpha$  radiation source ( $\lambda = 0.15418$  nm) at an accelerating voltage of 50 kV and current of 100 mA. Thermogravimetric analysis (TGA) was performed on a Perkin Elmer TGA 6 model instrument from 25 – 900 °C, a heating rate of 10 °C / min under atmospheric condition.

### 5.3 Results and discussion

In chapter 3, NVC and Py were copolymerized to obtain a new solution processable material that possesses both individual properties of PNVC and Ppy. DBSA was utilized as a stearic stabilizer that expanded the Ppy backbone to allow diffusion of solvents into the inter-molecular spaces created by the DBSA. Although the copolymer was soluble in DMSO, DMF, and chloroform and exhibited good thermal stability, its electrical conductivity can be further improved. Therefore, in this study we attempt to form a polymer nanocomposite by introducing GO as a nanomaterial, perhaps the  $\pi$ - $\pi$  interaction between the polymer and GO can improve the electrical conductivity and organic medium dispersibility of the resulting nanocomposite. For comparison, the nanocomposite prepared with and without DBSA were dispersed separately in DMF and then sonicated for 20 min. The dispersibility of the samples (Figure 5.1) were observed 30 min after sonication. The sample prepared without DBSA aggregates and suspends in the DMF while the one with DBSA dispersed well in the solvent.



**Figure 5.1: Photograph of (a) DBSA-doped PNVC-Ppy/GO dispersed in DMF; (b) PNVC-Ppy/GO (without DBSA) dispersed in DMF**

The in situ chemical oxidative polymerization of NVC and Py with GO allows intimate participation of GO forming the DBSA-doped PNVC-Ppy/GO nanocomposite as revealed by the FESEM images (Figure 5.2). The FESEM image of GO (Figure 5.2 (a)) shows the usual stacked, multi-layered structure as reported earlier (Mkhoyan et al., 2009) while DBSA-doped PNVC-Ppy (Figure 5.2 (b)) shows a densely packed globular structure with uniformly arranged particles of similar diameters. The DBSA-doped PNVC-Ppy globules disappeared to show a wrinkled, flaked morphology with some globules (Figure 5.2 (c)) during the in-situ chemical oxidative polymerization with GO. The image revealed an expanded GO layers, later exfoliated owing to the random insertion and deposition of PNVC-Ppy during the chemical oxidative polymerization resulting to a partially disordered solid (PNVC-Ppy/GO) with uneven morphology.

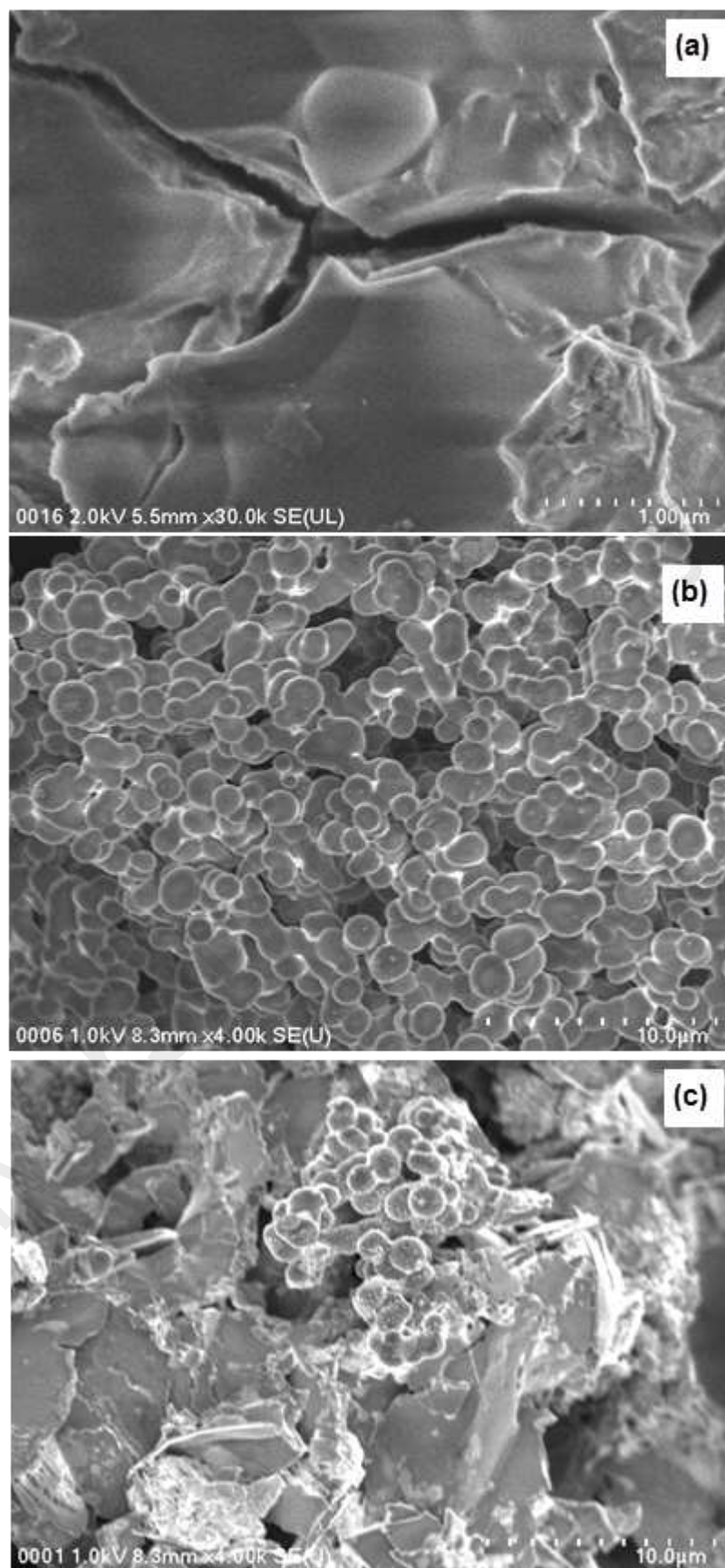


**Figure 5.2: FESEM images of (a) GO, (b) DBSA-doped PNVC-PPy, and (c) DBSA-doped PNVC-PPy/GO**

### 5.3.1 Fourier transformed infrared spectroscopy (FTIR) analysis

The appearance of characteristic C = O ( $1702\text{ cm}^{-1}$ ) and OH ( $3329\text{ cm}^{-1}$ ) stretching in the DBSA-doped PNVC-Ppy/GO (Figure. 5.3 a) confirmed that the nanocomposite has been synthesized. These peaks, the hallmarks of oxidized graphene (GO), revealed that GO was effectively incorporated into the PNVC-Ppy matrix forming the nanocomposite. The copolymer showed absorption bands at  $2916, 2848, 1626, 1378, 1287, 1155, 790, 743,$  and  $718\text{ cm}^{-1}$ . These bands bore the characteristic bands of PNVC and Ppy, shifted into new wavelengths (Figure 5.3 c). Meanwhile, most of these bands were retained in the composite spectra but with lower intensities. In the nanocomposite spectrum, the disappearance of the PNVC-Ppy bands at  $1603, 3049, 3418\text{ cm}^{-1}$  and the formation of new bands at  $1015$  and  $1147\text{ cm}^{-1}$  showed that a new product with different structural features was formed. Moreover, bands ( $1035$  and  $1008\text{ cm}^{-1}$ ) (Han et al., 2005) corresponding to R-SO<sup>3-</sup> and S=O of DBSA observed in the copolymer spectrum, shifted to  $1075$  and  $1010\text{ cm}^{-1}$  in the spectrum of PNVC-Ppy/GO.

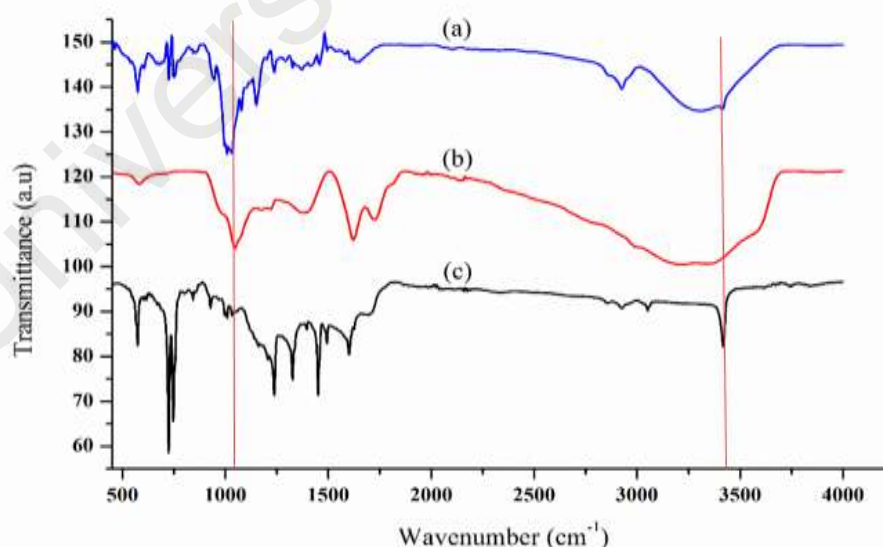


**Figure 5.3: FTIR spectra of (a) DBSA-doped PNVC-Ppy/GO, (b) GO, and (c) PNVC-Ppy copolymer**

### 5.3.2 XRD study

The XRD pattern of PNVC-Ppy/GO (Figure. 5.4 a) nanocomposite revealed that GO layers were exfoliated into the nanocomposite. GO has a sharp diffraction peak centred at  $2\theta = 10.16^\circ$  (Figure 5.4 c), indicating its laminated structure with an interlayer spacing of 8.706 Å. The XRD pattern of PNVC-Ppy (Figure 5.4 b) displayed a pattern typical of Ppy and PNVC. It revealed a combination of a broad amorphous and a partially crystalline structure with a pattern at  $2\theta = 19.79^\circ$ . However, for Ppy–PNVC/GO nanocomposite, the characteristic peak has shifted to  $23.1^\circ$  and the peak intensity has reduced. Also, GO peak was absent in the nanocomposite peak, indicating that GO layers are well exfoliated.

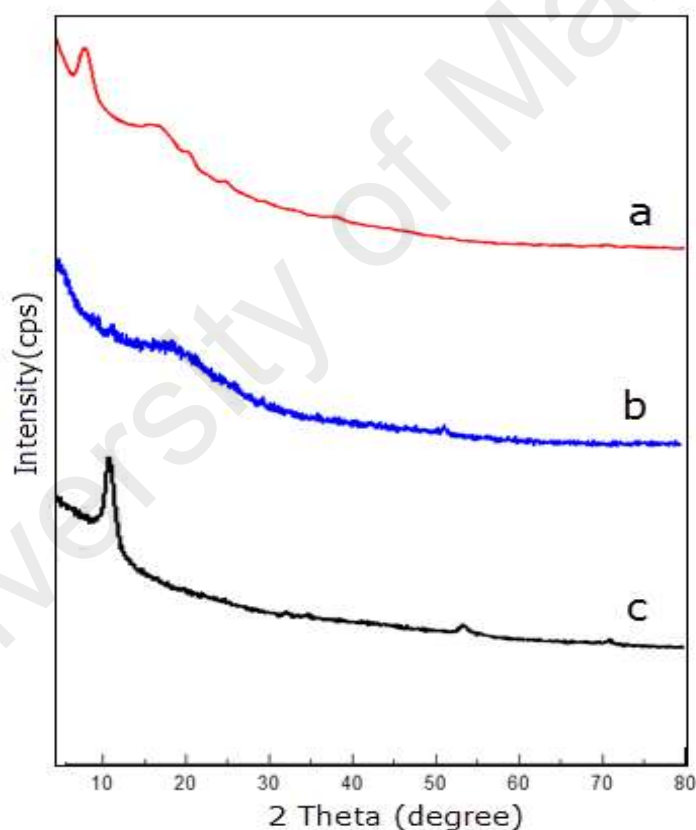


**Figure 5.4: X-RD spectra of (a) DBSA-doped PNVC-PPy/GO nanocomposite, (b) DBSA-doped PNVC-PPy copolymer and (c) GO.**

### 5.3.3 Raman spectroscopy

Raman spectroscopy is often used to determine the structural defects and electronic properties of carbon-based materials. The PNVC-Ppy/GO nanocomposite is expected to

possess good electrical conductivity because its conjugation length was enhanced by GO. The degree of graphite layer disorderliness depends on the intensity ratio between the D and G bands ( $I_D/I_G$ ) and the closer the intensities the more structurally disordered GO is (Bora & Dolui, 2012). Also, high Raman intensity depends on the extent of conjugation length (Bora & Dolui, 2012). The GO spectrum (Figure 5.5 c) displays characteristic D and G bands at 1352 and 1601  $\text{cm}^{-1}$  with peak intensity ratio almost unity (0.94). This indicates a significant structural defect due to oxidation of graphene to graphene oxide. The Raman spectrum of PNVC-Ppy copolymer shows two bands at 1594  $\text{cm}^{-1}$  and 1341  $\text{cm}^{-1}$ . The bands are assigned to C=C backbone stretching and ring stretching respectively. In the Raman spectrum PNVC-Ppy/GO nanocomposite, the C=C has shifted to 1591  $\text{cm}^{-1}$  compared with that of PNVC-Ppy. The higher ( $I_D/I_G$ ) ratio of the nanocomposite (0.205) to the copolymer (0.165) indicates a higher conjugation chain length that can induce an enhanced electrical conductivity. This shows that  $\pi$ - $\pi$  stacking has been established between the PNVC-Ppy and GO and more delocalized electrons are present in the aromatic ring of graphene or in the PNVC-Ppy chain.

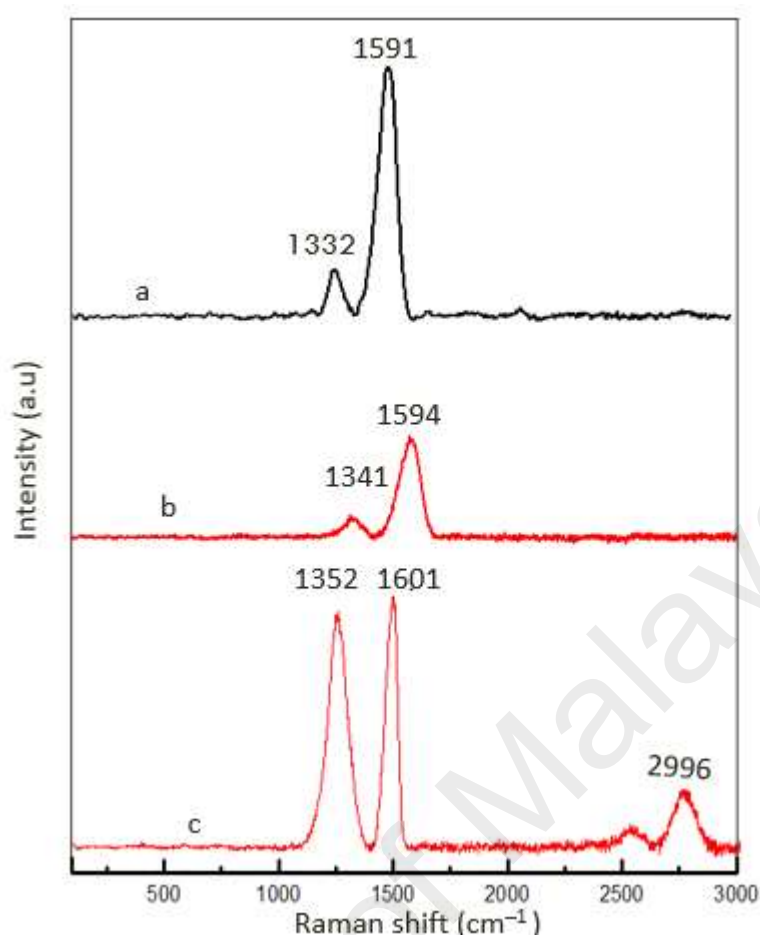


**Figure 5.5: Raman spectroscopy of (a) nanocomposite PNVC-PPy/GO, (b) copolymer PNVC-PPy and (c) graphene oxide**

#### 5.3.4 Optical properties of PNVC-Ppy nanocomposite

The UV-vis spectra of GO, PNVC-Ppy, and PNVC-Ppy/GO nanocomposite are displayed in Figure 5.6. GO displays an absorption peak at 227 nm, owing to the  $\pi$ - $\pi^*$  electronic transition of the benzene ring (Deshmukh et al., 2015). Meanwhile, the UV-vis spectrum of DBSA-doped PNVC-Ppy/GO nanocomposite shows similar features as that of DBSA-doped PNVC-Ppy. However, the nanocomposite spectrum intensity is lower compared to PNVC-Ppy spectrum. This reduced intensity shows that GO is present in the PNVC-Ppy polymer matrix (Obreja et al., 2013). To further confirm the PNVC-Ppy being attached to the surface of the exfoliated GO, we examined the photoluminescence properties of the nanocomposite dispersed in DMF. By applying 239 nm excitation wavelength, PNVC-Ppy/GO emission band was quenched suggesting intramolecular



quenching from PNVC-Ppy to GO. Such an intramolecular quenching may involve energy and electron transfer between the excited singlet states of the PNVC-Ppy moiety and the GO moiety. For the PNVC-Ppy copolymer, the emission peak is at 359 (3.62 eV) nm with a shoulder peak at 345 (3.80 eV) nm. Whereas for PNVC-Ppy/GO composite, the emission peak is at 362 (3.25eV) nm with a shoulder peak at 348 (3.5eV) nm.

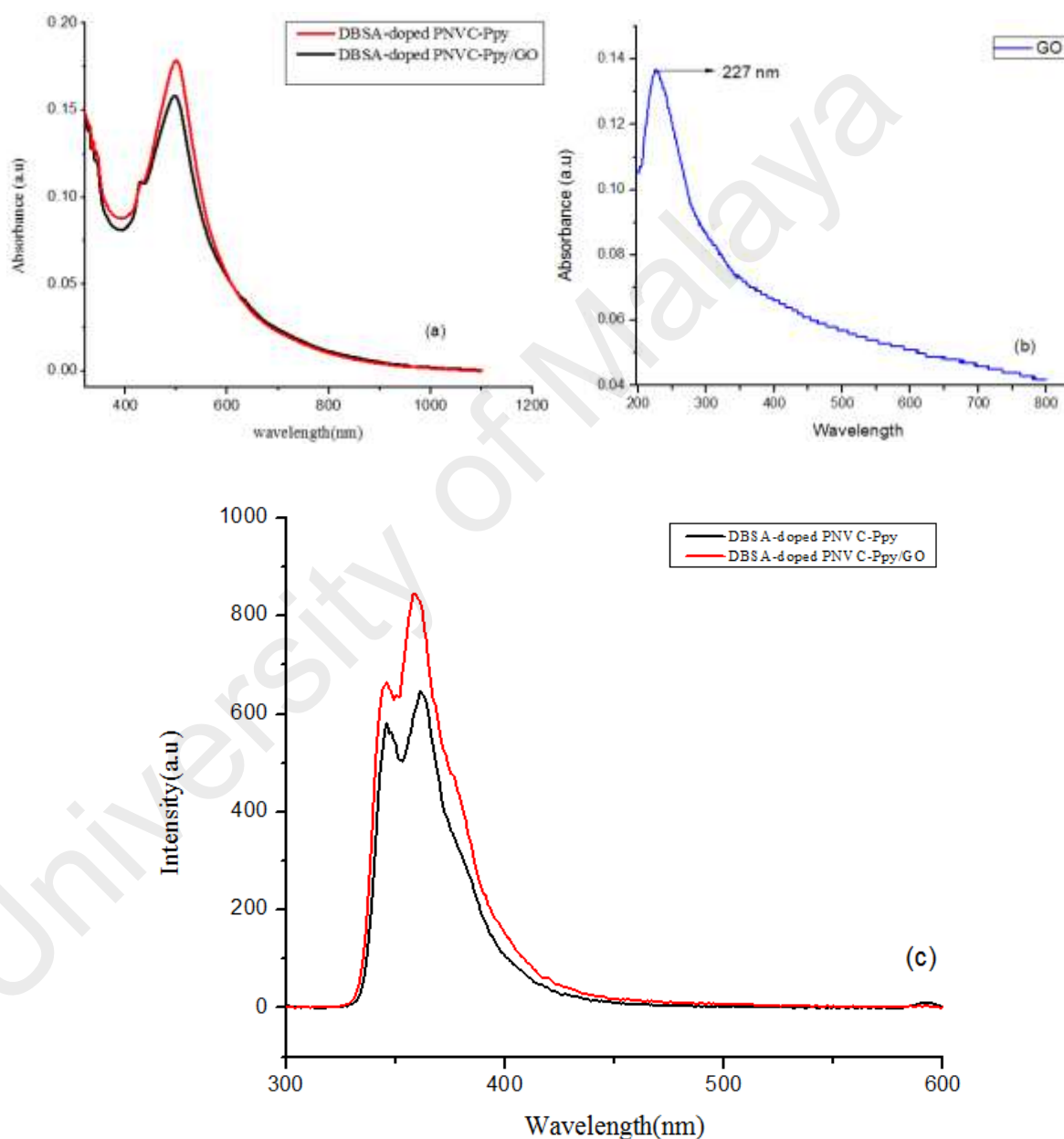


**Figure 5.6: Optical absorption spectra of (a) DBSA-doped PNVC-Ppy copolymer and DBSA-doped PNVC-Ppy nanocomposite, (b) GO, (c) Photoluminescence excitation of copolymer and nanocomposite.**

### 5.3.5 Electrical conductivity

The room temperature conductivity of PNVC-Ppy/GO nanocomposite is 0.102 S/cm. This value is, however, lower than that of Ppy homopolymer (0.286 S/cm) but higher than the value of DBSA-dope PNVC-Ppy copolymer (0.095 S/cm). The enhanced conductivity of DBSA-doped PNVC-Ppy/GO confirms the XRD report that GO exfoliated into the nanocomposite as GO films usually display insulating property. Therefore, the part of the exfoliated GO not oxidized might have established  $\pi$ - $\pi$  electron stacking with PNVC-Ppy rings to allow effective electron mobility thus increase the electrical conductivity of the nanocomposite. The PNVC-Ppy copolymer is a good electron donor while GO is an electron acceptor, thus, possibly, the charge transfer complex between the PNVC-Ppy copolymer chains and GO might also contribute to the improved conductivity.

### 5.4 Conclusion

DBSA, an anionic surfactant can be used to prepare organic medium dispersible PNVC-Ppy/GO nanocomposites to widen the applications of conducting polymer/GO nanocomposites. Because the nanocomposite dispersed well in DMSO, it was possible to determine its optical absorption and photoluminescence properties. Surprisingly, the extended  $\pi$ - $\pi$  electrons stacking between the PNVC-Ppy and GO-enabled the nanocomposite to display better electrical conductivity than copolymer and GO.

DBSA has already been used to improve the dispersibility of PANI/GO nanocomposites with enhanced electroconductivity. As our result demonstrates for the first time, improved organic dispersibility and enhanced electrical conductivity can be obtained using PNVC-Ppy as the polymer matrix. In-situ chemical oxidative polymerization with GO is an easy synthetic route to exfoliate layered GO into conducting polymers and DBSA can render the nanocomposite dispersible in various organic

solvents. We anticipated that solution processable PNVC-Ppy/GO with improved electrical properties can be a good active layer material in organic optoelectronic devices.

University of Malaya

## CHAPTER 6: REDUCED GRAPHENE OXIDE-POLY(N-VINYL CARBAZOLE)-POLY(PYRROLE) COMPOSITES—SYNTHESIS AND CHARACTERIZATION FOR OPTOELECTRONIC APPLICATIONS

### 6.1 Introduction

Oxidation of graphite to graphite oxide and subsequent chemical exfoliation to obtain graphene oxide, a soluble precursor of graphene, is among the most convenient methods to obtaining dispersible graphene for extensive applications. Many efforts are focused on obtaining graphene in various forms amenable for solution processability due to the potential of graphene as the conductor of the future. Because GO is naturally insulating especially if the graphite is subjected to a high degree of chemical oxidation, nano-conducting application of GO oxide is, therefore, limited. There are reports on the electrical conductivity of GO-based nanocomposites (Gao et al., 2011), as proved in the previous chapter of the present work, the conductivity of conducting polymer/GO nanocomposite is due to  $\pi$ - $\pi$  stacking between the conducting polymer backbone and the unoxidized region of the GO sheet (Gu et al., 2010). Imran et al. (2014) reported that the synthesis and characterization of highly conductive (474 S/m) PANI/GO nanocomposites with varying GO concentration. By applying high pressure on the nanocomposite pellet, voids created by trapped air were eliminated to allow close-packing thus conductive paths were established for the flow of electrons. Despite the initially measured conductivities of PVK ( $\sim 7 \times 10^{-10}$  S/cm) and GO ( $\sim 2 \times 10^{-6}$  S/cm), the nanocomposite fabricated from both materials exhibited an enhanced electrical conductivity as a result of intramolecular charge transfer interactions (Aleshin et al., 2015). On many occasions, owing to the insulating property of GO, conducting polymer/GO nanocomposites are fabricated for synergistic properties such as thermal stability, organic/inorganic phase dispersibility or mechanical strength (Liu et al., 2015; Ma et al., 2014; Zhang et al., 2010).

Chemical oxidation via Hummers' method is the pioneer and the most common method of preparing GO by exposing graphite to a mixture of strong oxidants ( $\text{KMnO}_4$

and  $\text{NaNO}_3$ ) in the presence of concentrated  $\text{H}_2\text{SO}_4$  followed by sonication. Compared to previous methods, Hummers' method is considered safe with higher efficiency. However, this method is defective as it releases harmful toxic gases;  $\text{NO}_2$  and  $\text{N}_2\text{O}_4$  and involves high thermal processing. To address these problems, researchers have come up with improved methods by increasing  $\text{KMnO}_4$  concentrations, excluding  $\text{NaNO}_3$ , and introducing mixtures of acids ( $\text{H}_2\text{SO}_4/\text{H}_3\text{PO}_4$  or  $\text{H}_2\text{SO}_4/\text{HNO}_3$ ) to obtain products that are free from toxic gases (Chen et al., 2013; Marcano et al., 2010).

Research and industrial focuses on graphene are increasing due to its excellent chemical, electrochemical, optical, optoelectronic, and sensing properties (Liao et al., 2010; Mueller et al., 2010). These unique behaviours of graphene have allowed its applications in solar cells, polymer nanocomposites, supercapacitor, nanofluids, etc (Choudhary et al., 2012; Sangchul et al., 2012; Wu et al., 2011). Among these, optimization of graphene for optoelectronic application has demanded wider attention both in the industrial and academic community. Graphene, especially the two-dimensional (2D) form exhibits great optical and electrical properties useful as a transparent electrode (Park et al., 2012; Suk et al., 2013). Throughout the graphene sheets,  $\pi$ -electrons are delocalized causing ballistic charge transport with a very little or no optical absorption. Meanwhile, solution processable functionalized graphene sheets are typically prepared via redox reactions. The reduction process introduces multiple grain boundaries and includes lattice defects on the surface of the product thereby increases its electrical resistance (Marinho et al., 2012; Sangchul et al., 2012). The obtained solution-processed functionalized graphene sheets are extensively used in optoelectronic devices such as a dye-sensitized solar cell (DSSC), organic solar cells (OSC), organic light-emitting diodes and organic photodetectors (Chang et al., 2013; He et al., 2012; Verma et al., 2010).

In order to utilize most of the unique properties of graphene in its proposed areas of applications, GO needs to be exfoliated to produce chemically converted graphene (CCG) sheets. Via chemical reduction, the oxygen-bearing moieties are largely removed generating a weak electrostatic repulsion against the strong  $\pi$ - $\pi$  interaction between rGO sheets. Thus, the electrical conductivity close to that of pristine graphene is restored. The resulting material called a reduced graphene oxide (rGO) or chemically converted graphene (CCG) suffers from many different kinds of structural defects due to the harsh oxidation process. Nevertheless, reduced graphene oxide is quite similar to the original graphene, and as a result, the restored electrical conductivities were reported to be as high as 1000 S/cm but the value still falls short of that of pristine graphene (Sun & Shi, 2013). Due to the ability of rGO to exhibit, to a good extent, the intriguing properties of graphene, large-scale production, and application, it has been found useful for energy applications especially when used as fillers for polymers. As the epoxy, hydroxyl, and carboxyl groups are not fully removed from the surface of GO upon reduction, the rGO nanosheets formed after the reduction facilitate interfacial interactions such as  $\pi$ - $\pi$  stacking, electrostatic interactions, van der Waals forces, and hydrogen bonding between the polymer matrix and rGO (Mitra et al., 2015). Factors such as filler-polymer matrix interaction, morphology, and filler concentration determine the properties of polymer nanocomposites. These factors are also governed by the methods of nanocomposite preparation. Conducting polymer/graphene nanocomposites can be prepared chemically or electrochemical via in-situ polymerization. Conducting polymers are applicable in areas of supercapacitors, biosensors, field-effect transistors (FET), solar cells, etc. However, problems such as low electrical conductivity, poor environmental and electrochemical stability, and low chemical resistance have made reinforcement with carbon-based materials especially graphene important to achieve their potential applications.

Till date conducting polymer /graphene nanocomposites have been developed by several research groups and their optoelectronic applications had equally been demonstrated. In optoelectronics, especially polymer solar cells, graphene can be employed as a transparent electrode (Choe et al., 2010; Choi et al., 2012; Eda et al., 2008) or as an active layer material. Liu et al. fabricated bulk heterojunction (BHJ) polymer photovoltaic cells based on poly (3-hexylthiophene) (P3HT) donor and solution-processable functionalized graphene (SPFGraphene) acceptor. The successful fabrication showed that graphene-based PSC with good power conversion efficiency can be realized (Liu et al., 2010). GO or rGO is also applicable as a hole transporting material in polymer BHJ solar cells. Although, poly(3,3-ethylenedioxythiophene):poly(styrene sulfonate) (PEDOT:PSS) is commonly used in this regard, however, according to a report by Jeon et al. (2012), rGO film obtained via thermal reduction of GO, when used as a hole transporting layer in PSC, yielded a better power conversion efficiency than PSC containing PEDOT:PSS.

Successful functionalization of graphene with phenyl isocyanate or dodecylbenzene sulfonic acid (DBSA) makes graphene dispersible in polar organic solvents such dimethyl sulfoxide (DMSO), N,N-dimethylformamide (DMF), and 1-methyl-2-pyrrolidinone (NMP). Since the reduction of GO yields rGO with electrical conductivity comparable to that of graphene and easily dispersed conducting polymer/GO nanocomposites have been reported with high electrical and thermal conductivity with good solubility in polar organic solvents; conducting polymer/rGO could display an enhanced performance when applied in optoelectronics or electrochemical sensing.

Hence, this chapter investigates in-situ polymerization of PNVC-Ppy in the presence of DBSA rGO to obtain DBSA-doped PNVC-Ppy/rGO using ammonium persulfate as the oxidant and acetonitrile as the reaction medium. Structural and optical properties of

the polymer nanocomposites were elucidated using Fourier transformation infrared (FTIR) and RAMAN, photoluminescence, and UV-vis spectroscopy analyses. In addition, the thermal stability of the nanocomposites was examined at different rGO loadings. The DC electrical conductivities obtained in the present study were enhanced and the nanocomposite dispersed well some selected organic solvents.

## **6.2 Experimental**

### **6.2.1 Preparation of rGO**

Reduced graphene oxide was prepared via chemical reduction of GO with hydrazine hydrate (Stankovich et al., 2007). Approximately 400 mg of GO was dispersed in 400 ml distilled water and ultrasonicated for 30 min to obtain a brown homogeneous aqueous GO suspension. Then, 1 ml hydrazine hydrate ( $N_2H_4.H_2O$ ) was added into the aqueous suspension and the mixture was heated at  $80^\circ C$  for 24 h to yield a black precipitate. After the reaction completed, the mixture was filtered and the black residue repeatedly washed with methanol followed by distilled water. The final product was dried in a vacuum at  $80^\circ C$  for 24 h.

### **6.2.2 Preparation of PNVC-PPy/rGO nanocomposites**

Firstly, rGO was dispersed in 20 mL of water by ultrasonication for 20 min. Equally, 0.1 M DBSA, Py (1 M) and NVC (1M) were separately dissolved in 20 and 30 ml of acetonitrile respectively. The reduced graphene oxide was varied as 0.1, 0.3, and 0.5g the resulting nanocomposites which were designated as DBSA-doped PNVC-Ppy/rGO-1, DBSA-doped PNVC-Ppy/rGO-2, and DBSA-doped PNVC-Ppy/rGO-3. The monomers solution was added to the solution of DBSA in acetonitrile and the mixture was ultrasonicated for 20 min. The solution obtained was added to the dispersed rGO under sonication. The ultrasonication continued for another 30 min and afterwards, 0.4 M of APS in 20 ml ACN/water (1:1) mixture was added at a time to the mixture of DBSA,



NVC, Py, and rGO. The polymerization proceeded immediately and the reaction was allowed to continue for 24 h under vigorous stirring. The polymer nanocomposite thus obtained was washed several times with mixtures of chloroform, acetonitrile, ethanol and water and dried under vacuum at 65°C for 24 h.

### 6.3 Results and discussion

Graphene easily re-stacks so do rGO due to the very high surface area of graphene. Attempts to produce easily dispersed graphene proved abortive and most graphene-polymer nanocomposites are applied where soluble graphene or its composites are not desired. To apply graphene in optoelectronics, a soluble or easily dispersed form is needed.

#### 6.3.1 FTIR analysis

Figure 6.1 shows the FTIR spectra of GO, rGO, DBSA-doped PNVC-Ppy, and DBSA-doped PNVC-Ppy/rGO nanocomposite. For GO, the broad peak centred at 3363  $\text{cm}^{-1}$  is assigned to the O—H stretching vibrations while the peaks at 1732, 1616 and 1225  $\text{cm}^{-1}$  are attributed to C=O stretching  $\text{sp}^2$  hybridized C=C group and O—H bending, C—OH stretching. The rGO showed absorption bands at 2927 and 2856  $\text{cm}^{-1}$  which can be attributed to asymmetric and symmetric stretching vibrations of  $\text{CH}_2$ . The peaks at 1456 and 1743  $\text{cm}^{-1}$  in the rGO spectrum are recognized as the C—O stretching vibration of the epoxy and alkoxy groups, respectively. These peaks showed that the rGO still contains some remnants of oxygen-bearing groups as a result of oxidation of graphene to GO. In the copolymer-rGO spectrum, the new peaks at 2927 and 2989  $\text{cm}^{-1}$  are from the reduced graphene oxide confirming the presence of rGO in the polymer matrix. These peaks revealed that rGO was effectively incorporated into the copolymer matrix to form the nanocomposite. The FTIR analysis indicates that the DBSA-doped PNVC-Ppy/rGO nanocomposite could display a better electrical conductivity than nanocomposite based

on GO because most of the oxygen bearing groups that are covalently linked to graphene in GO have been removed when GO undergoes reduction process with hydrazine. This phenomenon is further confirmed by Raman spectroscopy as revealed below.

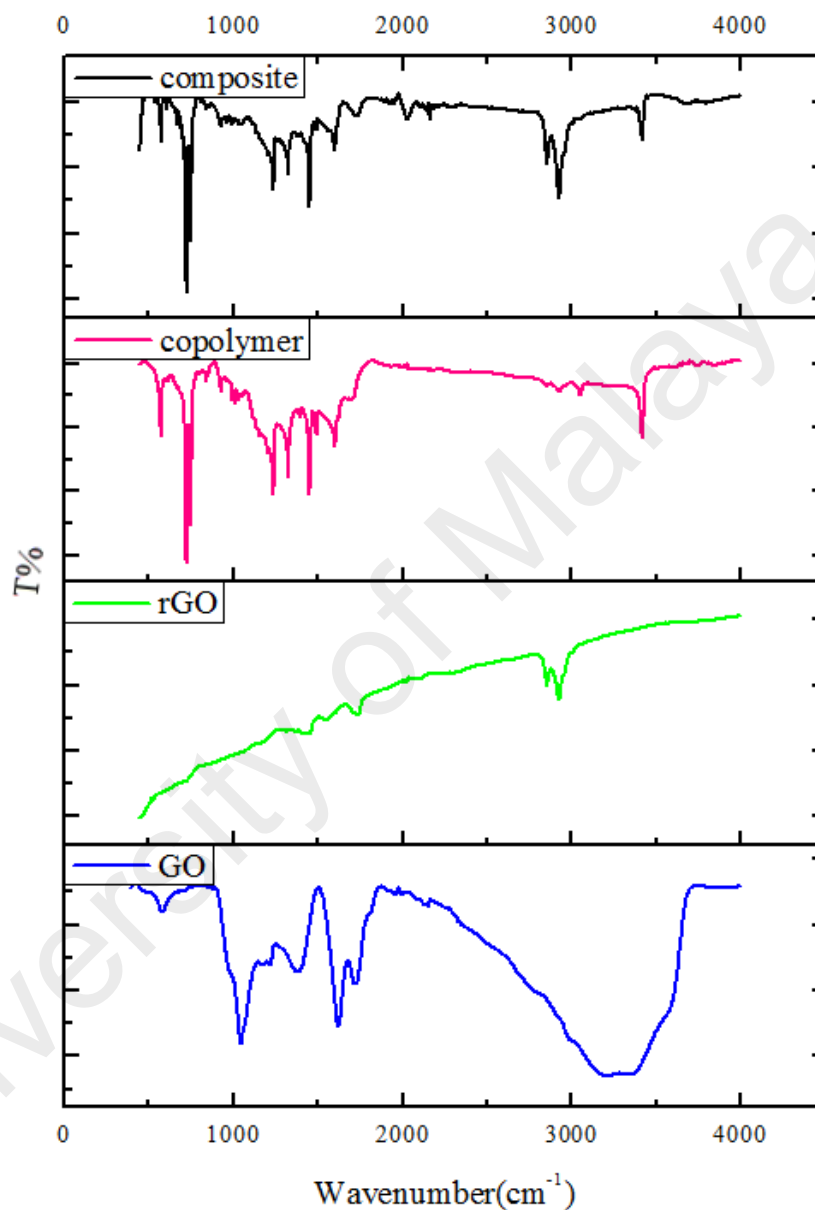


**Figure 6.1: FTIR of GO, rGO, DBSA-doped PNVC-Ppy, and DBSA-doped PNVC-PPy/rGO nanocomposite.**

### 6.3.2 Raman spectroscopy

The Raman spectra (Figure 6.2 a-f) of GO and rGO contain two characteristic peaks both with high intensity. The peaks appear at 1350, 1600  $\text{cm}^{-1}$  and 1358 and 1598  $\text{cm}^{-1}$  corresponding to the D-bands (defect or edge areas) and G-bands (the vibration of  $\text{sp}^2$

hybridized carbon) respectively. One of the G bands of each spectrum also represents GO (1600  $\text{cm}^{-1}$ ) and rGO (1592  $\text{cm}^{-1}$ ) absorption respectively. The bands were due to either asymmetric vibrations of the carboxylate groups or ketones. Furthermore, the 2D bands of GO at 2934  $\text{cm}^{-1}$  (C-H stretching) shifted to 2989  $\text{cm}^{-1}$  upon reduction of GO to rGO. However, in the Raman spectra of PNVC-PPy/rGO composite, the appearance of a new peak 2978  $\text{cm}^{-1}$  can be attributed to the 2D peak of rGO in composite. The broad 2D band indicates that rGO in the composite may be a multilayer structure. The D/G band intensity ratio expresses the atomic ratio of  $\text{sp}^3/\text{sp}^2$  carbons, which is a measure of the extent of disordered graphite. The intensity ratio of D to G band in the GO spectrum is calculated to be 1.23, indicating that increased number of  $\text{sp}^2$  domains formed during the chemical reduction process. By increasing the concentration of rGO in the nanocomposite, the D/G band intensity significantly increased and this corresponds to an increase in conjugation length. Therefore, this result, confirming what was obtained FTIR analysis, further proved the DBSA-doped PNVC-Ppy is expected to display a much higher electrical conductivity compares to the nanocomposite based on GO.

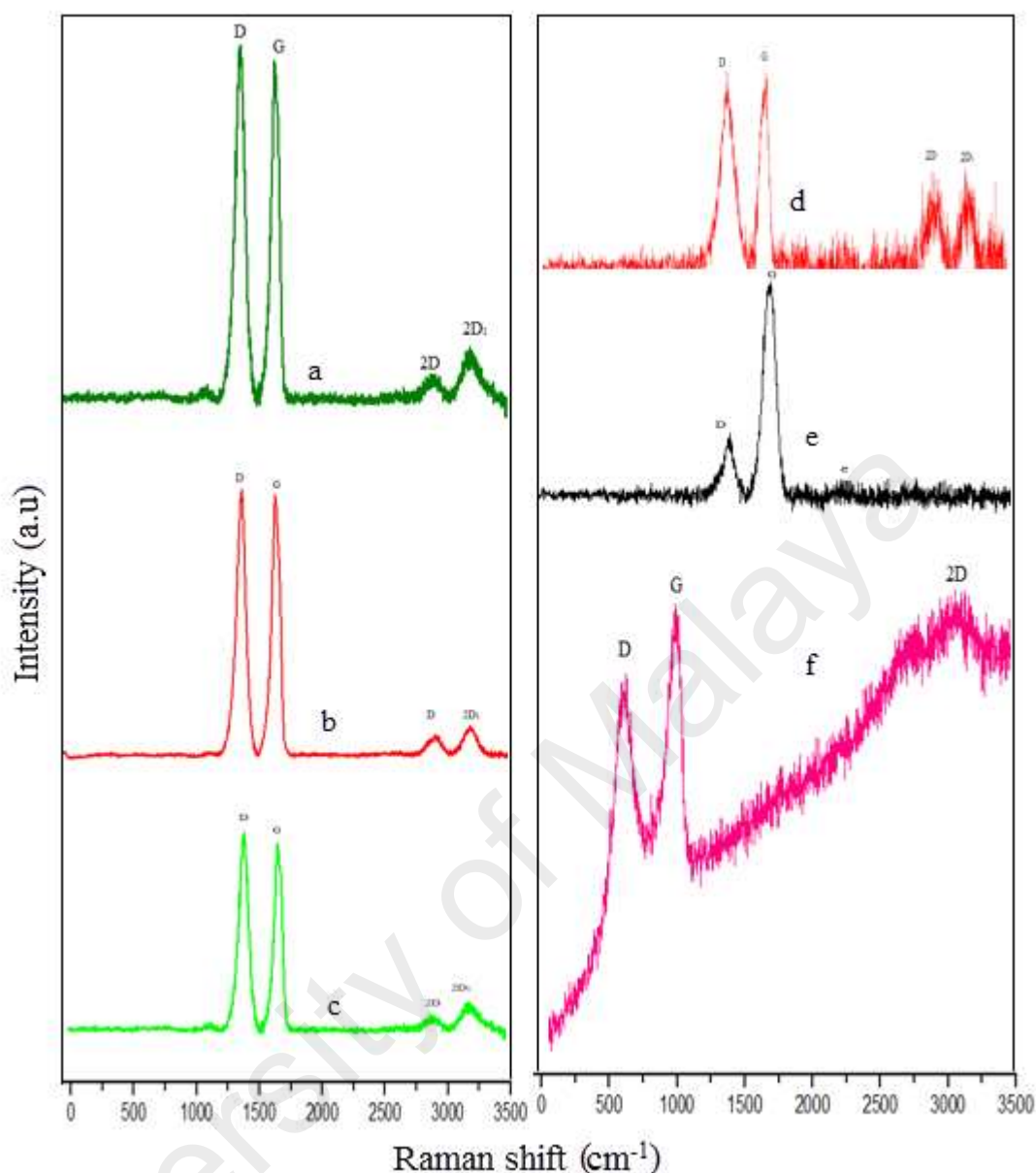


**Figure 6.2: Raman spectra of a) DBSA-doped PNVC-Ppy/rGO-3, b) DBSA-doped PNVC-Ppy/rGO-2, c) DBSA-doped PNVC-Ppy/rGO-1 d) rGO, e) DBSA-doped PNVC-Ppy, and f) GO**

### 6.3.3 FESEM study

Figure 6.3 a-c shows the FESEM images of the DBSA-doped PNVC-Ppy, pure rGO, and DBSA-doped PNVC-Ppy/rGO nanocomposite. GO is hydrophilic due to the presence of polar groups on its edges and surface. However, the rough morphology of rGO due to the formation of agglomerate as GO is being converted to a hydrophobic rGO indicating the loss of most of the oxygen bearing groups. The non-uniform globular structure of DBSA-doped PNVC-Ppy/rGO shows that the rGO is incorporated into the copolymer

matrix as there are observable differences between the morphology of the copolymer and that of the composite.

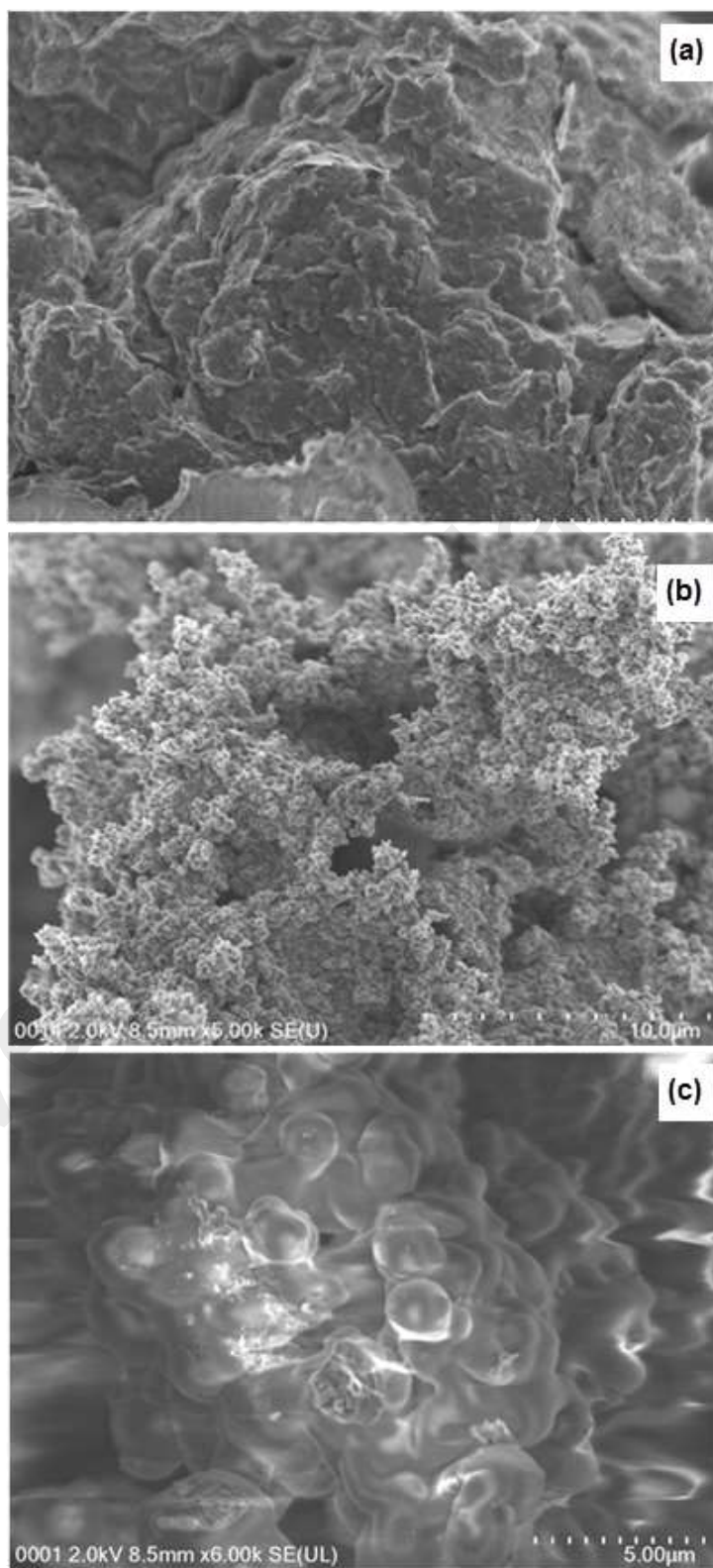


**Figure 6.3: FESM image of a) rGO, b) DBSA-doped PNVC-Ppy, and c) DBSA-doped PNVC-Ppy/rGO**

### 6.3.4 Electrical conductivity

Reduction of GO restores the high conductivity of graphene. One of the aims of forming graphene/polymer nanocomposite is to obtain synergetic materials having the properties of both components of the composite. A composite of conducting polymer with rGO is therefore expected to display a better conductivity as regard the conducting polymer. The average conductivities of the nanocomposites obtained in this study are presented in Table 6.1. The rGO shows a very high conductivity value (46.7 S/cm). For the nanocomposites, conductivities increase with an increase in rGO loadings. The conductivity of DBSA-doped PNVC-Ppy/GO, as described in chapter 5, is due  $\pi$ - $\pi$  stacking between the copolymer matrix and GO nanoparticles. However, the conductivities increased dramatically after reduction as shown in Table 6.1. The significant increase in conductivity is perhaps due to higher surface area of rGO which increases the number of conductive paths for electrons and charge carriers and the removal of most of the oxygen-bearing groups that are covalently linked to GO before reduction. It should be noted that the polymers matrix is in a doped state. Thus, the conductivity of the composite is enhanced by several factors; formation of polarons and bipolarons upon oxidation, presence of delocalized  $\pi$ -electrons in the polymer backbone, high aspect ratio surface area of the rGO.

**Table 6.1: Electrical conductivity of rGO compared to GO, copolymer and DBSA-doped PNVC-Ppy/rGO**

| Sample                           | Thickness (g) | Conductivity (S/cm) |
|----------------------------------|---------------|---------------------|
| <b>DBSA-doped PNVC-Ppy</b>       | 0.15          | 0.095               |
| <b>GO</b>                        | 0.15          | 0.102               |
| <b>rGO</b>                       | 0.15          | 46.7                |
| <b>DBSA-doped PNVC-Ppy/rGO-1</b> | 0.15          | 27                  |
| <b>DBSA-doped PNVC-Ppy/rGO-2</b> | 0.15          | 28                  |
| <b>DBSA-doped PNVC-Ppy/rGO-3</b> | 0.15          | 30                  |

### 6.3.5 X-RD analysis

The XRD pattern of the rGO and DBSA-doped PNVC-Ppy nanocomposites are presented in Figure 6.4. rGO exhibits a characteristic peak at  $2\theta = 20.85, 24.88,$  and  $28.99^\circ$ . Meanwhile, the copolymer is mainly amorphous so it displays only a broad peak at  $2\theta = 19.79^\circ$ . Whereas, the appearance of peaks at  $20.85, 24.88$  and  $28.99^\circ$  in the XRD pattern of the DBSA-doped PNVC-PPy/rGO composites are the evidence that the unit structures of rGO are retained after the formation of the composite with the copolymer. The peak intensity increases with increase in rGO nanoparticles and becomes more tapered as a result of the  $\pi$ - $\pi$  stacking of the benzene ring of the copolymer with rGO. The increase in the intensity of the first peak with increasing rGO concentration confirms the formation of well-ordered planes of rGOs. It is observed that peaks at  $15.53^\circ$  and  $20.62^\circ$  become slender and intense with increasing percentages of rGO. The formation of the nanocomposite enhances the charge carrier transport thus confirming the results obtained from electrical conductivity measurements.

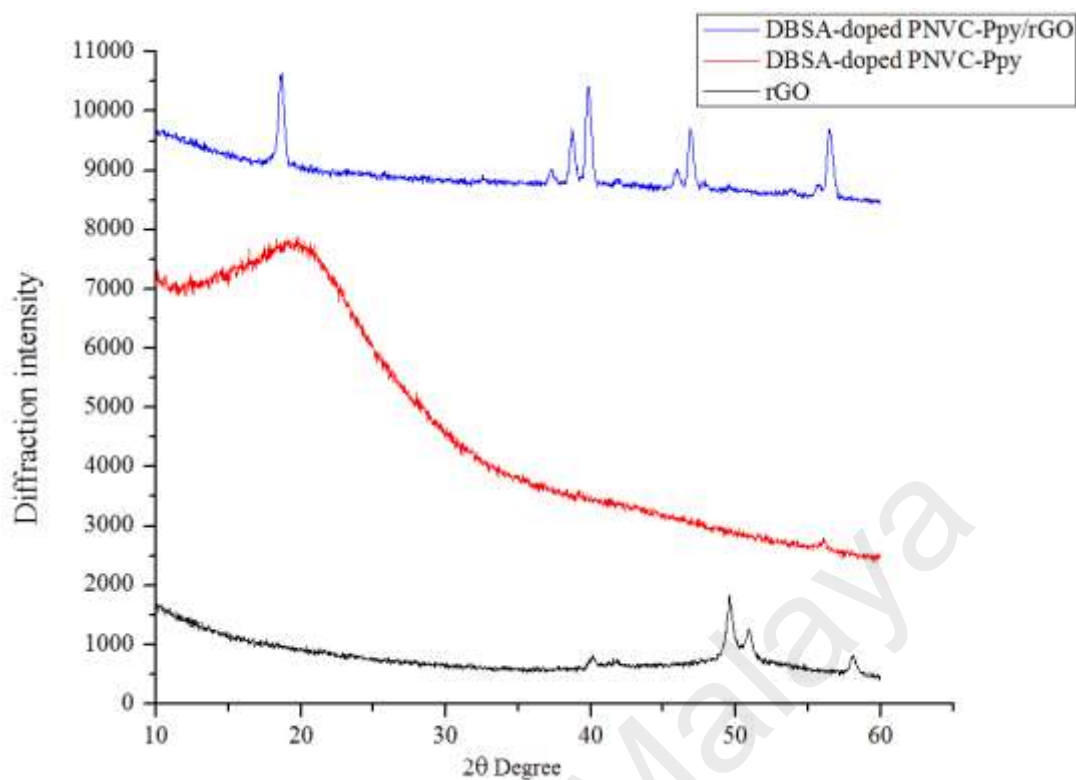


**Figure 6.4: X-RD spectra of a) PNVC-Ppy b) rGO c) PNVC-Ppy/rGO-1, d) PNVC-Ppy/rGO-2 and d) PNVC-Ppy/rGO-3**

### 6.3.6 TGA analysis

The thermal stability of rGO, DBSA-doped PNVC-Ppy copolymer, and DBSA-doped PNVC-Ppy/rGO nanocomposite were measured using by TGA curves under  $N_2$  atmosphere and the results are shown in Figure 6.5. All the samples undergo initial weight loss as a result of the loss of residual water molecule. The copolymer lost almost half of the original sample between 50 and 250°C. rGO decomposes over three more stages to leave a residue which is 78% of the starting mass. The result shows that rGO is thermally stable perhaps due to loss of hydroxides, epoxides, and ketones during chemical reduction of GO. On the other hand, the copolymer undergoes two decomposition steps leaving behind 34% of the initial mass as the residue. From this result, it is obvious that rGO is more thermally stable than the copolymer. Therefore, the nanocomposite is expected to possess a better thermal stability compares to the copolymer. Interestingly, after the initial loss of water, the nanocomposite retains up to 56% of the original mass. The thermal



stability of the copolymer has been enhanced by the presence of rGO which possesses little or no thermally unstable labile oxygen.

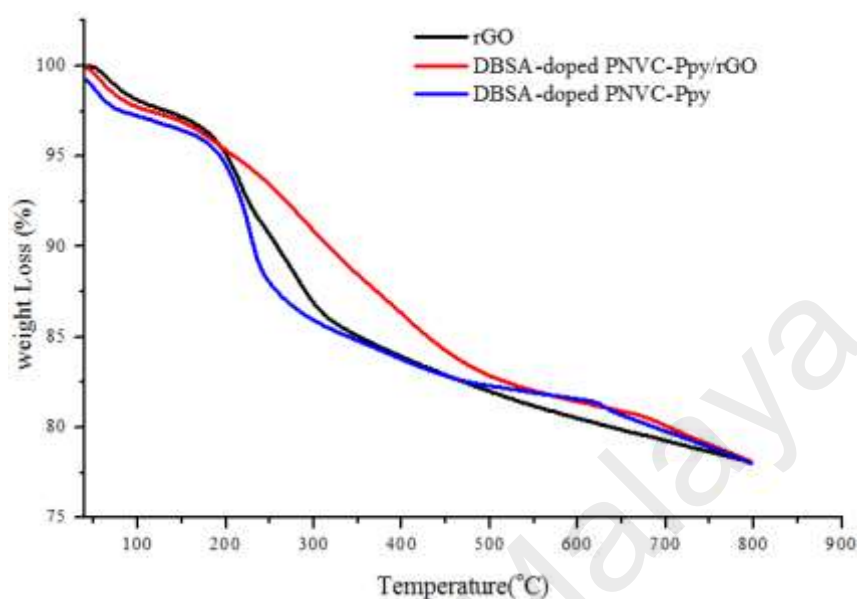


**Figure 6.5: Thermogravimetry (TGA) micrograph of rGO, composite, and copolymer**

### 6.3.7 Optical study of PNVC-PPy/rGO nanocomposite

The optical properties of the DBSA-doped PNVC-Ppy with and without rGO were investigated using UV-vis and photoluminescence spectroscopy. Figure 6.6 shows the UV-vis absorption spectra (a) and PL (b) spectra of the nanocomposites measured in DMF. The reduction of GO by hydrazine and the enhanced conductivity of rGO was further confirmed by UV-vis spectra of rGO. The single absorption peak of GO (Figure 5.6b, in Chapter 5) at 227 nm red shifted to 279 nm indicating the restoration of conjugation and an increase in electron density within the rGO layers. In the case of DBSA-doped PNVC-Ppy/rGO composites, the peak at 337 nm red shifted to 425 nm which may be due to an interaction between DBSA-doped PNVC-Ppy and rGO sheets in the composite. The interaction between the copolymer and the rGO sheets increases the presence mobile electrons along the polymer chain and therefore enhanced the electrical

conductivity observed earlier. The nanocomposite exhibited an optical band gap comparable to that of the copolymer.

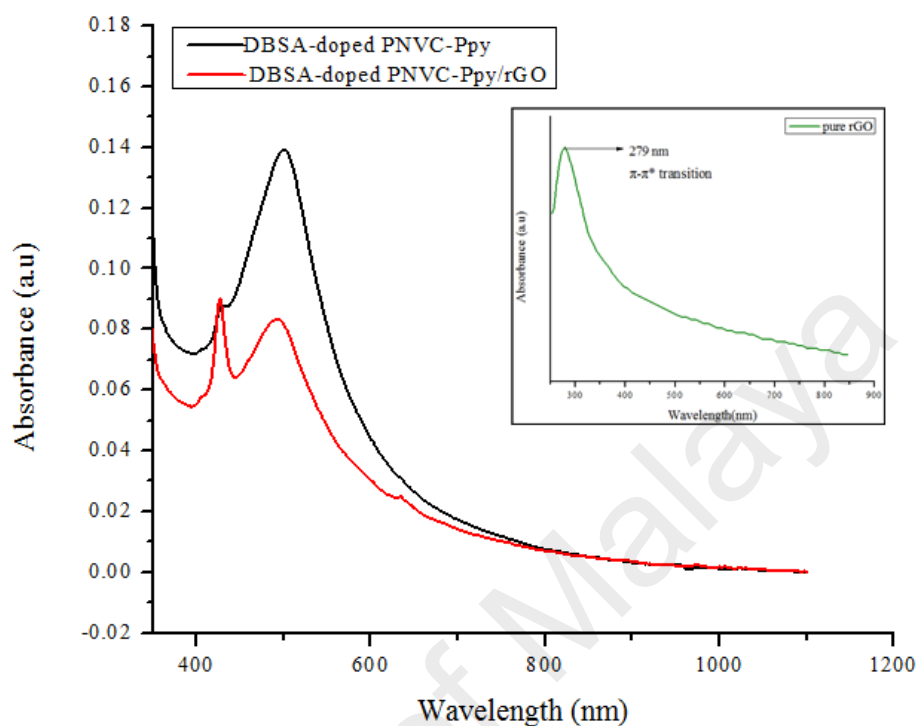


**Figure 6.6: Optical absorption spectra of DBSA-doped PNVC-Ppy, DBSA-doped PNVC-Ppy/rGO, and rGO (in-set)**

The PL spectra of the composites in DMF solutions (Figure 6.7) shows that the intensity of the emission band of DBSA-doped PNVC-Ppy/rGO at around 360 nm was both blue-shifted and quenched as the concentrations of rGO in the composites increased. The quenching effect of rGO on the copolymer shows the effective photoinduced charge transfer from the copolymer to rGO (Heeger, 1998; Sariciftci et al., 1992). This implies that the composite can be applied in optoelectronics as a transparent electrode or as a donor-acceptor blend in the active layer of polymer-based solar cells. Also, the result confirms the potential of graphene as an important electron acceptor or a hole transporting material in optoelectronics.

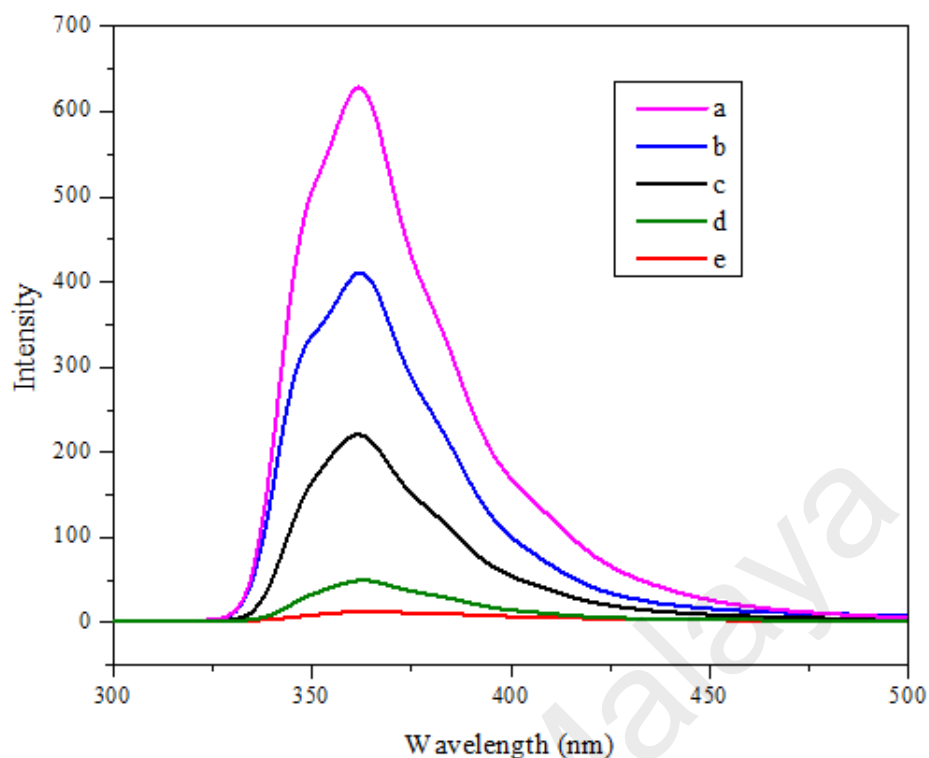


**Figure 6.8 :** Photoluminescence spectra of a) PNVC-Ppy, b) PNVC-Ppy/rGO-1, c) PNVC-PPy/rGO-2, d) PNVC-Ppy/rGO-3, e) rGO

#### 6.4 Conclusion

Composites of DBSA-doped PNVC-Ppy and rGO with good optical and electrical properties have been prepared via in situ chemical oxidative polymerization. UV-vis, Raman, FTIR, and XRD spectra show that rGO nanoparticles interacted with copolymer chains and the copolymers chains were more ordered than with the presence of rGO which is due to the  $\pi$ - $\pi$  interaction between the polymer matrix and the rGO nanocomposite. The charge carrier mobility of the composite was enhanced compared to the copolymer and the nanocomposite of the polymer with GO because the copolymer acted as an electron donor and rGO an acceptor. The acceptor capability of rGO in the composite was further endorsed by photoluminescence measurement of the composite. The copolymer luminesces was significantly quenched by rGO due to charge transfer from the copolymer to the rGO, as a result, the DBSA-doped PNVC-Ppy/rGO composite showed better electrical and thermal conductivity compared with the copolymer or its composite with

GO. In conclusion, the result suggests that dispersible DBSA-doped PNVC-Ppy/rGO nanocomposite possesses the properties useful for photovoltaic applications.

University of Malaya

## CHAPTER 7: CONCLUSION AND RECOMMENDATION

### 7.1 Conclusions

The discovery of electrical conductivity in doped conjugated polymers has extended their potential application beyond electrical insulators. Conducting polymers are now among the frontier materials notable for their interesting electrical and optical properties with a range of potential applications. Particularly, conducting polymer-based solar cells are emerging as a potential alternative to solar cells fabricated from inorganic materials. Among the notable conducting polymers is polypyrrole and poly n-vinyl carbazole. Polypyrrole is renowned owing to its environmental stability and excellent electrical conductivity. On the other hand, as an excellent hole conductor which has also demonstrated electron mobility, poly n-vinyl carbazole is capable of displaying charge transfer properties when used as an active layer material in optoelectronics.

Solution processability is a cornerstone to various applications of conjugated polymers, especially in polymer solar cells where the active layer materials are fabricated from solutions. Meanwhile, most conjugated polymers are inherently intractable and as well insoluble owing to increasing conjugation as the chain grows which tends to increase their rigidity. Many synthetic routes to obtain conjugated polymers have little or no connection with their solution processability and thus some conducting polymer products will remain insoluble even after tremendous synthetic efforts.

Being able to synthesise solution processable conducting polymers via relatively easy synthetic route is of great importance for their photovoltaic applications. The work described in this thesis concerns synthesis, characterization and photovoltaic applications of solution processable conjugated polymers. It focused on using DBSA as a dopant and stabilizing agent in the polymerization of NVC and Py to obtain copolymers processable from organic solutions as well as testing the photovoltaic properties of a device fabricated

based on the copolymers. This thesis also examined the effect of graphene oxide on the electrical properties of the DBSA-doped PNVC-Ppy by synthesizing PNVC-Ppy/GO nanocomposite and established the photovoltaic application of the solution processable nanocomposite.

The effects of DBSA concentration on the solubility and electrical conductivity of the copolymer was described. It is known that film of active layer materials in bulk heterojunction solar cells are processed from organic solution, and good solubility of the donor material plays a key role in fabricating efficient polymer BHJ solar cells. Therefore, the results provide compelling evidence that due to counterion effect of DBSA, a functionalized protonic acid, on the copolymer chain, the intractable copolymer of NVC and polypyrrole could be made soluble especially in polar organic solvents to give DBSA-doped PNVC-Ppy. The simple synthetic route, which is chemical oxidative polymerization in the presence of a controlled amount of functionalized protonic acid may thus be used to obtain solution processable conducting polymers. The interactions between the optical absorption spectrum of the individual homopolymers resulted in a copolymer with moderately low band gap. Because the copolymer has been rendered soluble, upon doping with DBSA, a film of the copolymer could be spin cast to be used as a donor material in or a transparent electrode in optoelectronics.

Based on the successful chemical synthesis of soluble conducting polymer of PNVC and Ppy, the hypothesis that DBSA can facilitate deeper interaction between the copolymer and GO and that the resulting nanocomposite could be dispersed in various organic solvents was tested. By preparing a nanocomposite of the copolymer and GO using in situ chemical oxidative polymerization, a DBSA-doped/GO nanocomposite that dispersed well in some selected organic solvents was obtained. The obtained nanocomposite dispersed well in DMSO and its optical absorption and

photoluminescence properties were determined. Because GO sheets are covalently decorated with hydrophilic functional groups, its tendency to be electrically conductive is low. The results show that the electrical conductivity of the DBSA-doped PNVC-Ppy/GO nanocomposite was enhanced when GO formed extended  $\pi$ - $\pi$  electrons stacking with the copolymer. Further investigation of a reduced form of graphene oxide showed that DBSA-doped PNVC-Ppy/rGO possesses better electrical properties than the nanocomposites based on GO.

The potential of conducting polymers as electron donor materials in BHJ solar cells could only be realized if the polymer is solution processable. Making conjugated polymer solution processable via side-chain functionalization has already been established in the literature. Meanwhile, intractable polypyrrole and polyaniline have been rendered soluble upon doping with DBSA, a functional protonic acid. To demonstrate that solution processable conducting polymer synthesized via a simple chemical oxidative polymerization could be used as a donor material, photovoltaic performance of solar cell device based on a blend of DBSA-doped PNVC-Ppy: PC<sub>60</sub>BM was exhibited. The results demonstrated for the first time, that an appreciable power conversion efficiency could be realized from solar cell device based on DBSA-doped PNVC-Ppy: PC<sub>60</sub>BM.

## **7.2 Recommendations**

The processing route for obtaining solution processable conducting polymer established in this project is simple yet effective. However, the efficiency of polymer solar cell fabricated from a blend of DBSA-doped PNVC-Ppy and PC<sub>60</sub>BM is low. To enhance the efficiency of the device, further investigations into the structure-property relations *vis-à-vis* the microstructure of the of the copolymer is needed. The difficulties involved in the film casting of the DBSA-doped copolymer was suspected to be a major reason why the recorded efficiency of the solar cell is quite low. This is often attributed

to the low molecular weight of the DBSA-doped copolymer as the polymer chain is not large enough to facilitate adequate adherence of the spin coated film to the PEDOT:PSS layer.

University of Malaya



## REFERENCES

- Adams, W. G., & Day, R. (1876). The Action of Light on Selenium. *Proceedings of the Royal Society of London*, 25(171-178), 113-117.
- Aleshin, A. N., Shcherbakov, I. P., Komolov, A. S., Petrov, V. N., & Trapeznikova, I. N. (2015). Poly(9-vinylcarbazole)–graphene oxide composite field-effect transistors with enhanced mobility. *Organic Electronics*, 16, 186-194.
- Allemand, P. M., Koch, A., Wudl, F., Rubin, Y., Diederich, F., Alvarez, M. M., . . . Whetten, R. L. (1991). Two different fullerenes have the same cyclic voltammetry. *Journal of the American Chemical Society*, 113(3), 1050-1051.
- Andrey, P. T., Vladimir, S. S., Evgenii, D. P., & Vladislav, A. K. (2006). Charge carrier transport in polyvinylcarbazole. *Journal of Physics: Condensed Matter*, 18(27), 6365.
- Armes, S. P. (1987). Optimum reaction conditions for the polymerization of pyrrole by iron(III) chloride in aqueous solution. *Synthetic Metals*, 20(3), 365-371.
- Asadian, E., Shahrokhian, S., zad, A. I., & Jokar, E. (2014). In-situ electro-polymerization of graphene nanoribbon/polyaniline composite film: Application to sensitive electrochemical detection of dobutamine. *Sensors and Actuators B: Chemical*, 196, 582-588.
- Ates, M. (2013). A review study of (bio)sensor systems based on conducting polymers. *Materials Science and Engineering: C*, 33(4), 1853-1859.
- Bakhshi, A., Kaur, A., & Arora, V. (2012). Molecular engineering of novel low band gap conducting polymers. *Indian Journal of Chemistry-Part A InorganicPhysical Theoretical and Analytical*, 51(1), 57.
- Balderrama, V., Estrada, M., Formentin, P., Viterisi, A., Ferre-Borrull, J., Pallares, J., . . . Marsal, L. (2011). *Influence and relationship of film morphology on Organic Solar Cells manufactured with different P3HT: PC[70]BM blend solutions*. Paper presented at the Electrical Engineering Computing Science and Automatic Control (CCE), 2011 8th International Conference on.
- Ballav, N., & Biswas, M. (2003). A conducting composite of polyN-vinylcarbazole and polythiophene. *Synthetic Metals*, 132(2), 213-218.
- Basavaraja, C., Kim, W. J., & Kim, D. G. (2011). Synthesis and characterization of soluble polypyrrole–poly ( $\epsilon$ -caprolactone) polymer blends with improved electrical conductivities. *Materials Chemistry and Physics*, 129(3), 787-793.
- Basavaraja, C., Kim, W. J., Kim, D. G., & Huh, D. S. (2012). Behavior of polyaniline–dodecylbenzene sulfonic acid/reduced graphene oxide nanocomposite films. *Polymer Composites*, 33(3), 388-396.

- Beaujuge, P. M., & Frechet, J. M. J. (2011). Molecular Design and Ordering Effects in pi-Functional Materials for Transistor and Solar Cell Applications. *Journal of the American Chemical Society*, 133(50), 20009-20029.
- Becquerel, A. E. (1839). Recherches sur les effets de la radiation chimique de la lumiere solaire au moyen des courants electriques. *Comptes Rendus de L'Academie des Sciences*, 9.
- Bedeloglu, A. (2011). Progress in organic photovoltaic fibers research. *Solar Cells—New Aspects and Solutions*, 255-286.
- Bhattacharya, A., & De, A. (1999). Conducting Polymers in Solution—Progress Toward Processibility. *Journal of Macromolecular Science, Part C*, 39(1), 17-56.
- Bilal, S., Sohail, M., & Shah, A. (2014). Synthesis and Characterization of Soluble and Thermally Stable Polypyrrole-DBSA Salts. *Journal of the Chemical Society of Pakistan*, 36(6).
- Bindumadhavan, K., Roy, S., Srivastava, S. K., & Nayak, B. B. (2015). Synthesis and Characterization of Poly (N-vinylcarbazole)/Graphene Nanocomposites. *Journal of nanoscience and nanotechnology*, 15(5), 3733-3742.
- Bispo-Fonseca, I., Aggar, J., Sarrazin, C., Simon, P., & Fauvarque, J. (1999). Possible improvements in making carbon electrodes for organic supercapacitors. *Journal of power sources*, 79(2), 238-241.
- Biswas, M., & Roy, A. (1993a). Thermal stability, morphological, dielectric, and conductivity characteristics of pyrrole modified poly-N-vinyl carbazole. *Journal of Applied Polymer Science*, 49(12), 2189-2196.
- Biswas, M., & Roy, A. (1993b). Thermal stability, morphological, dielectric, and conductivity characteristics of pyrrole modified poly-N-vinyl carbazole. *Journal of Applied Polymer Science*, 49(12), 2189-2196.
- Biswas, M., & Roy, A. (1994). Thermal, stability, morphological, and conductivity characteristics of polypyrrole prepared in aqueous medium. *Journal of Applied Polymer Science*, 51(9), 1575-1580.
- Biswas, M., & Roy, A. (1995). O-chloranil initiated polymerization of pyrrole in presence of N-vinylcarbazole and some properties of the polymer. *European Polymer Journal*, 31(8), 725-731.
- Biswas, M., & Roy, A. (1996). Ferric chloride-initiated polymerization of pyrrole in presence of N-vinyl carbazole in aqueous suspension. *Journal of Applied Polymer Science*, 60(1), 143-146.
- Bolink, H. J., Coronado, E., Forment-Aliaga, A., Lenes, M., La Rosa, A., Filippone, S., & Martin, N. (2011). Polymer solar cells based on diphenylmethanofullerenes with reduced sidechain length. *Journal of Materials Chemistry*, 21(5), 1382-1386.

- Bolto, B., McNeill, R., & Weiss, D. (1963). Electronic Conduction in Polymers. III. Electronic Properties of Polypyrrole. *Australian Journal of Chemistry*, 16(6), 1090-1103.
- Bolto, B., & Weiss, D. (1963). Electronic Conduction in Polymers. II. The Electrochemical Reduction of Polypyrrole at Controlled Potential. *Australian Journal of Chemistry*, 16(6), 1076-1089.
- Bora, C., & Dolui, S. K. (2012). Fabrication of polypyrrole/graphene oxide nanocomposites by liquid/liquid interfacial polymerization and evaluation of their optical, electrical and electrochemical properties. *Polymer*, 53(4), 923-932.
- Bose, S., Kuila, T., Uddin, M. E., Kim, N. H., Lau, A. K. T., & Lee, J. H. (2010). In-situ synthesis and characterization of electrically conductive polypyrrole/graphene nanocomposites. *Polymer*, 51(25), 5921-5928.
- Brabec, C. J., Cravino, A., Meissner, D., Sariciftci, N. S., Rispens, M. T., Sanchez, L., . . . Fromherz, T. (2002). The influence of materials work function on the open circuit voltage of plastic solar cells. *Thin Solid Films*, 403-404, 368-372.
- Brunner, K., van Dijken, A., Börner, H., Bastiaansen, J. J. A. M., Kiggen, N. M. M., & Langeveld, B. M. W. (2004). Carbazole Compounds as Host Materials for Triplet Emitters in Organic Light-Emitting Diodes: Tuning the HOMO Level without Influencing the Triplet Energy in Small Molecules. *Journal of the American Chemical Society*, 126(19), 6035-6042.
- Bundgaard, E., & Krebs, F. C. (2007). Low band gap polymers for organic photovoltaics. *Solar Energy Materials and Solar Cells*, 91(11), 954-985.
- Camurlu, P., & Guven, N. (2015). Optoelectronic properties of thiazole-based polythiophenes. *Journal of Applied Polymer Science*, 132(27).
- Cao, W., & Xue, J. (2014). Recent progress in organic photovoltaics: device architecture and optical design. *Energy & Environmental Science*, 7(7), 2123-2144.
- Cao, Y., Smith, P., & Heeger, A. J. (1993). Proceedings of the International Conference on Science and Technology of Synthetic Metals Counter-ion induced processibility of conducting polyaniline. *Synthetic Metals*, 57(1), 3514-3519.
- Cao, Y., Treacy, G. M., Smith, P., & Heeger, A. J. (1992). Solution-cast films of polyaniline: Optical-quality transparent electrodes. *Applied Physics Letters*, 60(22), 2711-2713.
- Cassagneau, T., Guérin, F., & Fendler, J. H. (2000). Preparation and Characterization of Ultrathin Films Layer-by-Layer Self-Assembled from Graphite Oxide Nanoplatelets and Polymers. *Langmuir*, 16(18), 7318-7324.
- Chandrasekaran, J., Nithyaprakash, D., Ajjan, K. B., Maruthamuthu, S., Manoharan, D., & Kumar, S. (2011). Hybrid solar cell based on blending of organic and inorganic materials—An overview. *Renewable and Sustainable Energy Reviews*, 15(2), 1228-1238.

- Chandrasekhar, P. (2013). *Conducting polymers, fundamentals and applications: a practical approach*: Springer Science & Business Media.
- Chang, L.-H., Hsieh, C.-K., Hsiao, M.-C., Chiang, J.-C., Liu, P.-I., Ho, K.-K., . . . Tsai, C.-H. (2013). A graphene-multi-walled carbon nanotube hybrid supported on fluorinated tin oxide as a counter electrode of dye-sensitized solar cells. *Journal of power sources*, 222, 518-525.
- Chapin, D. M., Fuller, C. S., & Pearson, G. L. (1954). A new silicon p-n junction photocell for converting solar radiation into electrical power [3]. *Journal of Applied Physics*, 25(5), 676-677.
- Chemek, M., Khlaifia, D., Massuyeau, F., Duvail, J., Faulques, E., Wéry, J., & Alimi, K. (2014). A copolymer of PVK and P3HT and its nanocomposite with single-walled carbon nanotubes. *Synthetic Metals*, 197, 246-251.
- Chemek, M., Massuyeau, F., Wéry, J., Hlel, A., Ayachi, S., Faulques, E., . . . Alimi, K. (2012). Photoluminescence properties of new poly(N-vinylcarbazole)-3-methylthiophene (PVK-3MeT) graft copolymer. *Journal of Applied Polymer Science*, 125(1), 126-132.
- Chemek, M., Wéry, J., Bouachrine, M., Paris, M., Lefrant, S., & Alimi, K. (2010). Synthesis and characterization of novel graft copolymers of Poly(N-vinylcarbazole) and Poly(3-methylthiophene) for optoelectronic applications. *Synthetic Metals*, 160(21-22), 2306-2314.
- Chen, D., Liu, F., Wang, C., Nakahara, A., & Russell, T. P. (2011). Bulk Heterojunction Photovoltaic Active Layers via Bilayer Interdiffusion. *Nano Letters*, 11(5), 2071-2078.
- Chen, H.-C., Lin, S.-W., Jiang, J.-M., Su, Y.-W., & Wei, K.-H. (2015). Solution-Processed Zinc Oxide/Polyethylenimine Nanocomposites as Tunable Electron Transport Layers for Highly Efficient Bulk Heterojunction Polymer Solar Cells. *ACS Applied Materials & Interfaces*, 7(11), 6273-6281.
- Chen, J., Yao, B., Li, C., & Shi, G. (2013). An improved Hummers method for eco-friendly synthesis of graphene oxide. *Carbon*, 64, 225-229.
- Chen, Y., Huang, Z. E., & Cai, R. F. (1996). The synthesis and characterization of C60 chemically modified poly (N-vinylcarbazole). *Journal of Polymer Science Part B: Polymer Physics*, 34(4), 631-640.
- Cheng, Y. J., Yang, S. H., & Hsu, C. S. (2009). Synthesis of Conjugated Polymers for Organic Solar Cell Applications. *Chemical reviews*, 109(11), 5868-5923.
- Chiang, C. K., Fincher, C. R., Park, Y. W., Heeger, A. J., Shirakawa, H., Louis, E. J., . . . MacDiarmid, A. G. (1977). Electrical Conductivity in Doped Polyacetylene. *Physical Review Letters*, 39(17), 1098-1101.
- Choe, M., Lee, B. H., Jo, G., Park, J., Park, W., Lee, S., . . . Lee, T. (2010). Efficient bulk-heterojunction photovoltaic cells with transparent multi-layer graphene electrodes. *Organic Electronics*, 11(11), 1864-1869.

- Choi, S., Zhou, Y., Haske, W., Shim, J. W., Fuentes-Hernandez, C., & Kippelen, B. (2015). ITO-free large-area flexible organic solar cells with an embedded metal grid. *Organic Electronics*, 17, 349-354.
- Choi, Y.-Y., Kang, S. J., Kim, H.-K., Choi, W. M., & Na, S.-I. (2012). Multilayer graphene films as transparent electrodes for organic photovoltaic devices. *Solar Energy Materials and Solar Cells*, 96, 281-285.
- Choudhary, S., Mungse, H. P., & Khatri, O. P. (2012). Dispersion of alkylated graphene in organic solvents and its potential for lubrication applications. *Journal of Materials Chemistry*, 22(39), 21032-21039.
- Coughlin, J. E., Henson, Z. B., Welch, G. C., & Bazan, G. C. (2014). Design and Synthesis of Molecular Donors for Solution-Processed High-Efficiency Organic Solar Cells. *Accounts of Chemical Research*, 47(1), 257-270.
- Croce, F., Passerini, S., Selvaggi, A., & Scrosati, B. (1990). Properties and applications of lithium ion-conducting polymers. *Solid State Ionics*, 40, 375-379.
- Dang, M. T., Hirsch, L., & Wantz, G. (2011). P3HT:PCBM, Best Seller in Polymer Photovoltaic Research. *Advanced Materials*, 23(31), 3597-3602.
- Das, T. K., & Prusty, S. (2012). Review on conducting polymers and their applications. *Polymer-Plastics Technology and Engineering*, 51(14), 1487-1500.
- De Paoli, M.-A., Zanelli, A., Mastragostino, M., & Rocco, A. M. (1997). An electrochromic device combining polypyrrole and WO<sub>3</sub> II: solid-state device with polymeric electrolyte. *Journal of Electroanalytical Chemistry*, 435(1), 217-224.
- Deshmukh, K., Ahamed, M. B., Pasha, S. K. K., Deshmukh, R. R., & Bhagat, P. R. (2015). Highly dispersible graphene oxide reinforced polypyrrole/polyvinyl alcohol blend nanocomposites with high dielectric constant and low dielectric loss. *RSC Advances*, 5(76), 61933-61945.
- Donnet, J.-B., & Bansal, R. C. (1998). *Carbon fibers*: CRC Press.
- Dou, L., You, J., Hong, Z., Xu, Z., Li, G., Street, R. A., & Yang, Y. (2013). 25th Anniversary Article: A Decade of Organic/Polymeric Photovoltaic Research. *Advanced Materials*, 25(46), 6642-6671.
- Dreyer, D. R., Park, S., Bielawski, C. W., & Ruoff, R. S. (2010). The chemistry of graphene oxide. *Chemical Society Reviews*, 39(1), 228-240.
- Eda, G., Lin, Y.-Y., Miller, S., Chen, C.-W., Su, W.-F., & Chhowalla, M. (2008). Transparent and conducting electrodes for organic electronics from reduced graphene oxide. *Applied Physics Letters*, 92(23), 233305.
- Facchetti, A. (2010).  $\Pi$ -conjugated polymers for organic electronics and photovoltaic cell applications†. *Chemistry of Materials*, 23(3), 733-758.
- Forrest, S. R. (2005). The limits to organic photovoltaic cell efficiency. *MRS bulletin*, 30(01), 28-32.

- Frackowiak, E., Khomenko, V., Jurewicz, K., Lota, K., & Béguin, F. (2006). Supercapacitors based on conducting polymers/nanotubes composites. *Journal of power sources*, 153(2), 413-418.
- Gao, J., Heeger, A. J., Lee, J. Y., & Kim, C. Y. (1996). Soluble polypyrrole as the transparent anode in polymer light-emitting diodes. *Synthetic Metals*, 82(3), 221-223.
- Gao, Y., Yip, H.-L., Chen, K.-S., O'Malley, K. M., Acton, O., Sun, Y., . . . Jen, A. K. Y. (2011). Surface Doping of Conjugated Polymers by Graphene Oxide and Its Application for Organic Electronic Devices. *Advanced Materials*, 23(16), 1903-1908.
- Geissler, U., Hallensleben, M. L., & Toppare, L. (1991). Conductive polymer composites and copolymers of pyrrole and N-vinylcarbazole. *Synthetic Metals*, 40(2), 239-246.
- Gómez, H., Ram, M. K., Alvi, F., Villalba, P., Stefanakos, E., & Kumar, A. (2011). Graphene-conducting polymer nanocomposite as novel electrode for supercapacitors. *Journal of power sources*, 196(8), 4102-4108.
- Gong, J., Darling, S. B., & You, F. (2015). Perovskite photovoltaics: life-cycle assessment of energy and environmental impacts. *Energy & Environmental Science*.
- Govindraj, S., Ntholeng, N., Ranganathan, K., Moloto, M., Sikhwivhilu, L., & Moloto, N. (2016). The effect of structural properties of Cu<sub>2</sub>Se/polyvinylcarbazole nanocomposites on the performance of hybrid solar cells. *Journal of Nanomaterials*, 2016, 90.
- Green, M. A., Emery, K., Hishikawa, Y., Warta, W., & Dunlop, E. D. (2015). Solar cell efficiency tables (Version 45). *Progress in photovoltaics: research and applications*, 23(1), 1-9.
- Green, R. A., Baek, S., Poole-Warren, L. A., & Martens, P. J. (2010). Conducting polymer-hydrogels for medical electrode applications. *Science and Technology of Advanced Materials*, 11(1), 014107.
- Gross, M., Müller, D. C., Nothofer, H.-G., Scherf, U., Neher, D., Bräuchle, C., & Meerholz, K. (2000). Improving the performance of doped  $\pi$ -conjugated polymers for use in organic light-emitting diodes. *Nature*, 405(6787), 661-665.
- Gu, Z., Li, C., Wang, G., Zhang, L., Li, X., Wang, W., & Jin, S. (2010). Synthesis and characterization of polypyrrole/graphite oxide composite by in situ emulsion polymerization. *Journal of Polymer Science Part B: Polymer Physics*, 48(12), 1329-1335.
- Guo, B., Glavas, L., & Albertsson, A.-C. (2013). Biodegradable and electrically conducting polymers for biomedical applications. *Progress in Polymer Science*, 38(9), 1263-1286.

- Guo, X., Baumgarten, M., & Mullen, K. (2013). Designing pi-conjugated polymers for organic electronics. *Progress in Polymer Science*, 38(12), 1832-1908.
- Halls, J. J. M., Pichler, K., Friend, R. H., Moratti, S. C., & Holmes, A. B. (1996). Exciton diffusion and dissociation in a poly(p-phenylenevinylene)/C60 heterojunction photovoltaic cell. *Applied Physics Letters*, 68(22), 3120-3122.
- Halls, J. J. M., Walsh, C. A., Greenham, N. C., Marseglia, E. A., Friend, R. H., Moratti, S. C., & Holmes, A. B. (1995). Efficient photodiodes from interpenetrating polymer networks. *Nature*, 376(6540), 498-500.
- Hammed, W. A., Yahya, R., Bola, A. u. L., & Mahmud, H. N. M. E. (2013). Recent approaches to controlling the nanoscale morphology of polymer-based bulk-heterojunction solar cells. *Energies*, 6(11), 5847-5868.
- Han, C. C., & Elsenbaumer, R. L. (1989). Protonic acids: Generally applicable dopants for conducting polymers. *Synthetic Metals*, 30(1), 123-131.
- Han, D., Chu, Y., Yang, L., Liu, Y., & Lv, Z. (2005). Reversed micelle polymerization: a new route for the synthesis of DBSA-polyaniline nanoparticles. *Colloids and Surfaces A: Physicochemical and Engineering Aspects*, 259(1-3), 179-187.
- Hau, S. K., O'Malley, K. M., You-Jung, C., Yip, H.-L., Ma, H., & Jen, A. K. Y. (2010). Optimization of Active Layer and Anode Electrode for High-Performance Inverted Bulk-Heterojunction Solar Cells. *Selected Topics in Quantum Electronics, IEEE Journal of*, 16(6), 1665-1675.
- Haugeneder, A., Neges, M., Kallinger, C., Spirkl, W., Lemmer, U., Feldmann, J., . . . Müllen, K. (1999). Exciton diffusion and dissociation in conjugated polymer/fullerene blends and heterostructures. *Physical Review B*, 59(23), 15346-15351.
- Huang, S. H., Lu, P. Y., Chung, C. L., & Fu, S. L. (2010, 24-26 Aug. 2010). *Preparation of active layer of solar cells device by F8T2 blending with PCBM*. Paper presented at the CPMT Symposium Japan, 2010 IEEE.
- He, B., Tang, Q., Luo, J., Li, Q., Chen, X., & Cai, H. (2014). Rapid charge-transfer in polypyrrole-single wall carbon nanotube complex counter electrodes: Improved photovoltaic performances of dye-sensitized solar cells. *Journal of power sources*, 256, 170-177.
- He, M., Jung, J., Qiu, F., & Lin, Z. (2012). Graphene-based transparent flexible electrodes for polymer solar cells. *Journal of Materials Chemistry*, 22(46), 24254-24264.
- Heeger, A. J. (1998). Photo-induced electron transfer from a conducting polymer to buckminsterfullerene: A molecular approach to high efficiency photovoltaic cells. Final report (pp. Medium: ED; Size: 4 p.): ; Univ. of California, Santa Barbara, CA (United States).
- Heeger, A. J. (2001). Semiconducting and metallic polymers: the fourth generation of polymeric materials (Nobel lecture). *Angewandte Chemie International Edition*, 40(14), 2591-2611.

- Heeger, A. J. (2010). Semiconducting polymers: the third generation. *Chemical Society Reviews*, 39(7), 2354-2371.
- Heeger, A. J., MacDiarmid, A., & Shirakawa, H. (2000). The nobel prize in chemistry 2000. *The Nobel Foundation*.
- Holder, E., Tessler, N., & Rogach, A. L. (2008). Hybrid nanocomposite materials with organic and inorganic components for opto-electronic devices. *Journal of Materials Chemistry*, 18(10), 1064-1078.
- Horowitz, G. (1998). Organic field-effect transistors. *Advanced Materials*, 10(5), 365-377.
- Hu, B., & Karasz, F. E. (2003). Blue, green, red, and white electroluminescence from multichromophore polymer blends. *Journal of Applied Physics*, 93(4), 1995-2001.
- Huo, M., Yuan, J., Tao, L., & Wei, Y. (2014). Redox-responsive polymers for drug delivery: from molecular design to applications. *Polymer Chemistry*, 5(5), 1519-1528.
- Imran, S. M., Kim, Y., Shao, G. N., Hussain, M., Choa, Y.-h., & Kim, H. T. (2014). Enhancement of electroconductivity of polyaniline/graphene oxide nanocomposites through in situ emulsion polymerization. *Journal of Materials Science*, 49(3), 1328-1335.
- Inzelt, G. (2012). *Conducting polymers: a new era in electrochemistry*: Springer Science & Business Media.
- Jancar, J., Douglas, J. F., Starr, F. W., Kumar, S. K., Cassagnau, P., Lesser, A. J., . . . Buehler, M. J. (2010). Current issues in research on structure–property relationships in polymer nanocomposites. *Polymer*, 51(15), 3321-3343.
- Jang, J., Nam, Y., & Yoon, H. (2005). Fabrication of Polypyrrole– Poly(N-vinylcarbazole) Core–Shell Nanoparticles with Excellent Electrical and Optical Properties. *Advanced Materials*, 17(11), 1382-1386.
- Jeon, Y.-J., Yun, J.-M., Kim, D.-Y., Na, S.-I., & Kim, S.-S. (2012). High-performance polymer solar cells with moderately reduced graphene oxide as an efficient hole transporting layer. *Solar Energy Materials and Solar Cells*, 105, 96-102.
- Kallmann, H., & Pope, M. (1959). Photovoltaic Effect in Organic Crystals. *The Journal of Chemical Physics*, 30(2), 585-586.
- Kholmanov, I. N., Domingues, S. H., Chou, H., Wang, X., Tan, C., Kim, J.-Y., . . . Ruoff, R. S. (2013). Reduced Graphene Oxide/Copper Nanowire Hybrid Films as High-Performance Transparent Electrodes. *ACS Nano*, 7(2), 1811-1816.
- Kido, J., Hongawa, K., Okuyama, K., & Nagai, K. (1994). White light-emitting organic electroluminescent devices using the poly(N-vinylcarbazole) emitter layer doped with three fluorescent dyes. *Applied Physics Letters*, 64(7), 815-817.



- Kido, J., Shionoya, H., & Nagai, K. (1995). Single-layer white light-emitting organic electroluminescent devices based on dye-dispersed poly(N-vinylcarbazole). *Applied Physics Letters*, 67(16), 2281-2283.
- Kiebooms, R., Menon, R., & Lee, K. (2001). Chapter 1 - Synthesis, electrical, and optical properties of conjugated polymers A2 - Nalwa, Hari Singh *Handbook of Advanced Electronic and Photonic Materials and Devices* (pp. 1-102). Burlington: Academic Press.
- Kim, B. G., Jeong, E. J., Chung, J. W., Seo, S., Koo, B., & Kim, J. (2013). A molecular design principle of lyotropic liquid-crystalline conjugated polymers with directed alignment capability for plastic electronics. *Nat Mater*, 12(7), 659-664.
- Kim, I. W., Lee, J. Y., & Lee, H. (1996). Solution-cast polypyrrole film: the electrical and thermal properties. *Synthetic Metals*, 78(2), 177-180.
- Kim, J.-K., Manuel, J., Lee, M.-H., Scheers, J., Lim, D.-H., Johansson, P., . . . Jacobsson, P. (2012). Towards flexible secondary lithium batteries: polypyrrole-LiFePO<sub>4</sub> thin electrodes with polymer electrolytes. *Journal of Materials Chemistry*, 22(30), 15045-15049.
- Kim, J. S., Kim, W. J., Cho, N., Shukla, S., Yoon, H., Jang, J., . . . Lee, K.-S. (2009). Synthesis and Properties of Quantum Dot-Polypyrrole Nanotube Composites for Photovoltaic Application. *Journal of nanoscience and nanotechnology*, 9(12), 6957-6961.
- Kim, S., Yim, J., Wang, X., Bradley, D. D. C., Lee, S., & deMello, J. C. (2010). Spin- and Spray-Deposited Single-Walled Carbon-Nanotube Electrodes for Organic Solar Cells. *Advanced Functional Materials*, 20(14), 2310-2316.
- Krebs, F. C. (2009). Fabrication and processing of polymer solar cells: a review of printing and coating techniques. *Solar Energy Materials and Solar Cells*, 93(4), 394-412.
- Krebs, F. C., Jørgensen, M., Norrman, K., Hagemann, O., Alstrup, J., Nielsen, T. D., . . . Kristensen, J. (2009). A complete process for production of flexible large area polymer solar cells entirely using screen printing—First public demonstration. *Solar Energy Materials and Solar Cells*, 93(4), 422-441.
- Kroon, R., Lenes, M., Hummelen, J. C., Blom, P. W. M., & de Boer, B. (2008). Small Bandgap Polymers for Organic Solar Cells (Polymer Material Development in the Last 5 Years). *Polymer Reviews*, 48(3), 531-582.
- Kumar, P., & Chand, S. (2012). Recent progress and future aspects of organic solar cells. *Progress in Photovoltaics*, 20(4), 377-415.
- Kwon, J.-D., Kim, P.-H., Keum, J.-H., & Kim, J. S. (2004). Polypyrrole/titania hybrids: synthetic variation and test for the photovoltaic materials. *Solar Energy Materials and Solar Cells*, 83(2-3), 311-321.

- Lai, L., Wang, L., Yang, H., Sahoo, N. G., Tam, Q. X., Liu, J., . . . Lin, J. (2012). Tuning graphene surface chemistry to prepare graphene/polypyrrole supercapacitors with improved performance. *Nano Energy*, 1(5), 723-731.
- Lang, X., Wan, Q., Feng, C., Yue, X., Xu, W., Li, J., & Fan, S. (2010). The role of anthraquinone sulfonate dopants in promoting performance of polypyrrole composites as pseudo-capacitive electrode materials. *Synthetic Metals*, 160(15-16), 1800-1804.
- Lee, G., Lee, S., Ahn, K., & Kim, K. (2002). Synthesis and characterization of soluble polypyrrole with improved electrical conductivity. *Journal of Applied Polymer Science*, 84(14), 2583-2590.
- Lee, J., Kim, D., & Kim, C. (1995). Synthesis of soluble polypyrrole of the doped state in organic solvents. *Synthetic Metals*, 74(2), 103-106.
- Lee, Y. H., Lee, J. Y., & Lee, D. S. (2000). A novel conducting soluble polypyrrole composite with a polymeric co-dopant. *Synthetic Metals*, 114(3), 347-353.
- Li, G., Zhu, R., & Yang, Y. (2012). Polymer solar cells. *Nature Photonics*, 6(3), 153-161.
- Li, L., Xia, K., Li, L., Shang, S., Guo, Q., & Yan, G. (2012). Fabrication and characterization of free-standing polypyrrole/graphene oxide nanocomposite paper. *Journal of Nanoparticle Research*, 14(6), 1-8.
- Li, P.-P., Chen, Y., Zhu, J., Feng, M., Zhuang, X., Lin, Y., & Zhan, H. (2011). Charm-Bracelet-Type Poly(N-vinylcarbazole) Functionalized with Reduced Graphene Oxide for Broadband Optical Limiting. *Chemistry – A European Journal*, 17(3), 780-785.
- Li, Y., Ban, H., & Yang, M. (2016). Highly sensitive NH<sub>3</sub> gas sensors based on novel polypyrrole-coated SnO<sub>2</sub> nanosheet nanocomposites. *Sensors and Actuators B: Chemical*, 224, 449-457.
- Li, Y., Yang, J., Xu, J., Li, S., Li, J., & Wan, M. (1995). Poly (N-vinylcarbazole) and polypyrrole composites synthesized by laser-electrochemical polymerization. *Synthetic Metals*, 72(1), 41-44.
- Liao, L., Lin, Y.-C., Bao, M., Cheng, R., Bai, J., Liu, Y., . . . Duan, X. (2010). High-speed graphene transistors with a self-aligned nanowire gate. *Nature*, 467(7313), 305-308.
- Lin, J., Tang, Q., Wu, J., & Sun, H. (2008). Synthesis, characterization, and properties of polypyrrole/expanded vermiculite intercalated nanocomposite. *Journal of Applied Polymer Science*, 110(5), 2862-2866.
- Liu, S., Ma, X., Wang, B., Shang, X., Wang, W., & Yu, X. (2015). Nanostructure-Dependent Interfacial Interactions between Poly(3-hexylthiophene) and Graphene Oxide. *Macromolecules*, 48(16), 5791-5798.

- Liu, Z., He, D., Wang, Y., Wu, H., & Wang, J. (2010). Solution-processable functionalized graphene in donor/acceptor-type organic photovoltaic cells. *Solar Energy Materials and Solar Cells*, 94(7), 1196-1200.
- Livi, F., Carlé, J. E., & Bundgaard, E. (2014). Thiophene in conducting polymers: synthesis of poly (thiophene) s and other conjugated polymers containing thiophenes, for application in polymer solar cells *Thiophenes* (pp. 203-226): Springer.
- Loh, K. P., Bao, Q., Ang, P. K., & Yang, J. (2010). The chemistry of graphene. *Journal of Materials Chemistry*, 20(12), 2277-2289.
- Lu, L., Zheng, T., Wu, Q., Schneider, A. M., Zhao, D., & Yu, L. (2015). Recent Advances in Bulk Heterojunction Polymer Solar Cells. *Chemical reviews*.
- Ma, L., Niu, H., Cai, J., Zhao, P., Wang, C., Bai, X., . . . Wang, W. (2014). Photoelectrochemical and electrochromic properties of polyimide/graphene oxide composites. *Carbon*, 67, 488-499.
- MacDiarmid, A. G. (2001). Synthetic metals: a novel role for organic polymers. *Synthetic Metals*, 125(1), 11-22.
- MacDiarmid, A. G., & Epstein, A. J. (1994). Workshop on the Metallic Phase of Conducting Polymers The concept of secondary doping as applied to polyaniline. *Synthetic Metals*, 65(2), 103-116.
- Malig, J., Englert, J. M., Hirsch, A., & Guldi, D. M. (2011). Wet chemistry of graphene. *Interface-Electrochemical Society*, 20(1), 53.
- Marcano, D. C., Kosynkin, D. V., Berlin, J. M., Sinitskii, A., Sun, Z., Slesarev, A., . . . Tour, J. M. (2010). Improved synthesis of graphene oxide. *ACS nano*, 4(8), 4806-4814.
- Marinho, B., Ghislandi, M., Tkalya, E., Koning, C. E., & de With, G. (2012). Electrical conductivity of compacts of graphene, multi-wall carbon nanotubes, carbon black, and graphite powder. *Powder Technology*, 221, 351-358.
- Marks, R. N., Halls, J. J. M., Bradley, D. D. C., Friend, R. H., & Holmes, A. B. (1994). The photovoltaic response in poly(p-phenylene vinylene) thin-film devices. *Journal of Physics: Condensed Matter*, 6(7), 1379.
- Mbarek, M., Massuyeau, F., Duvail, J.-L., Wery, J., Faulques, E., & Alimi, K. (2013). New copolymer of poly(N-vinylcarbazole) and poly(p-phenylenevinylene) for optoelectronic devices. *Journal of Applied Polymer Science*, 130(4), 2839-2847.
- McCullough, R. D., & Jayaraman, M. (1995). The tuning of conjugation by recipe: the synthesis and properties of random head-to-tail poly(3-alkylthiophene) copolymers. *Journal of the Chemical Society, Chemical Communications*(2), 135-136.

- McNeill, R., Siudak, R., Wardlaw, J., & Weiss, D. (1963). Electronic Conduction in Polymers. I. The Chemical Structure of Polypyrrole. *Australian Journal of Chemistry*, 16(6), 1056-1075.
- McNeill, R., & Weiss, D. (1959). A Xanthene Polymer with Semiconducting Properties. *Australian Journal of Chemistry*, 12(4), 643-656.
- Mitra, M., Kulsi, C., Chatterjee, K., Kargupta, K., Ganguly, S., Banerjee, D., & Goswami, S. (2015). Reduced graphene oxide-polyaniline composites-synthesis, characterization and optimization for thermoelectric applications. *RSC Advances*, 5(39), 31039-31048.
- Mkhoyan, K. A., Contryman, A. W., Silcox, J., Stewart, D. A., Eda, G., Mattevi, C., . . . Chhowalla, M. (2009). Atomic and Electronic Structure of Graphene-Oxide. *Nano letters*, 9(3), 1058-1063.
- Morita, S., Zakhidov, A. A., & Yoshino, K. (1992). Doping effect of buckminsterfullerene in conducting polymer: Change of absorption spectrum and quenching of luminescence. *Solid state communications*, 82(4), 249-252.
- Mueller, T., Xia, F., & Avouris, P. (2010). Graphene photodetectors for high-speed optical communications. *Nat Photon*, 4(5), 297-301.
- Narayan, K. S., & Murthy, G. L. (1997). Emission studies of poly(N-vinylcarbazole) / poly(3-hexylthiophene) bilayer devices. *Chemical Physics Letters*, 276(5), 441-444.
- Nel, A., Xia, T., Mädler, L., & Li, N. (2006). Toxic Potential of Materials at the Nanolevel. *Science*, 311(5761), 622-627.
- Nicholson, P. G., & Castro, F. A. (2010). Organic photovoltaics: principles and techniques for nanometre scale characterization. *Nanotechnology*, 21(49), 492001.
- Nishino, H., Yu, G., Heeger, A. J., Chen, T. A., & Rieke, R. D. (1995). Electroluminescence from blend films of poly(3-hexylthiophene) and poly(N-vinylcarbazole). *Synthetic Metals*, 68(3), 243-247.
- Obreja, A. C., Cristea, D., Gavrilă, R., Schiopu, V., Dinescu, A., Danila, M., & Comanescu, F. (2013). Isocyanate functionalized graphene/P3HT based nanocomposites. *Applied Surface Science*, 276, 458-467.
- Oh, E. J., Jang, K. S., & MacDiarmid, A. G. (2001). High molecular weight soluble polypyrrole. *Synthetic Metals*, 125(3), 267-272.
- Park, O.-K., Hahm, M. G., Lee, S., Joh, H.-I., Na, S.-I., Vajtai, R., . . . Ajayan, P. M. (2012). In situ synthesis of thermochemically reduced graphene oxide conducting nanocomposites. *Nano letters*, 12(4), 1789-1793.
- Parvin, M. H., Pirnia, M., & Arjomandi, J. (2015). Electrochemical synthesis, in situ spectroelectrochemistry of conducting indole-titanium dioxide and zinc oxide

polymer nanocomposites for rechargeable batteries. *Electrochimica Acta*, 185, 276-287.

Pernites, R., Vergara, A., Yago, A., Cui, K., & Advincula, R. (2011). Facile approach to graphene oxide and poly(N-vinylcarbazole) electro-patterned films. *Chemical Communications*, 47(35), 9810-9812.

Pettersson, L. A., Roman, L. S., & Inganäs, O. (1999). Modeling photocurrent action spectra of photovoltaic devices based on organic thin films. *Journal of Applied Physics*, 86(1), 487.

Po, R., Maggini, M., & Camaioni, N. (2010). Polymer Solar Cells: Recent Approaches and Achievements. *Journal of Physical Chemistry C*, 114(2), 695-706.

Prasad, P. N., & Ulrich, D. R. (2012). *Nonlinear optical and electroactive polymers*: Springer Science & Business Media.

Prezhdo, O. V., Kamat, P. V., & Schatz, G. C. (2011). Virtual Issue: Graphene and Functionalized Graphene. *The Journal of Physical Chemistry C*, 115(8), 3195-3197.

Price, S. C., Stuart, A. C., Yang, L., Zhou, H., & You, W. (2011). Fluorine Substituted Conjugated Polymer of Medium Band Gap Yields 7% Efficiency in Polymer–Fullerene Solar Cells. *Journal of the American Chemical Society*, 133(12), 4625-4631.

Putz, K. W., Compton, O. C., Palmeri, M. J., Nguyen, S. T., & Brinson, L. C. (2010). High-Nanofiller-Content Graphene Oxide–Polymer Nanocomposites via Vacuum-Assisted Self-Assembly. *Advanced Functional Materials*, 20(19), 3322-3329.

Rahimi, R., Roberts, A., Narang, V., & Korakakis, D. (2013). Investigate the role of the active layers' structures and morphology in the performance of the organic solar cell devices. *Applied Physics Letters*, 102(7), 073105.

Ramanavičius, A., Ramanavičienė, A., & Malinauskas, A. (2006). Electrochemical sensors based on conducting polymer—polypyrrole. *Electrochimica Acta*, 51(27), 6025-6037.

Ramar, A., & Saraswathi, R. (2015). Synthesis and characterization of a charm-bracelet-type poly (N-vinylcarbazole)–C60 double-cable polymer. *Journal of Materials Science*, 50(10), 3740-3749.

Ramasamy, M. S., Mahapatra, S. S., & Cho, J. W. (2015). Functionalization of graphene with self-doped conducting polypyrrole by click coupling. *Journal of Colloid and Interface Science*, 455, 63-70.

Rapi, S., Bocchi, V., & Gardini, G. P. (1988). Conducting polypyrrole by chemical synthesis in water. *Synthetic Metals*, 24(3), 217-221.

- Rasmussen, S. C. (2011). Electrically Conducting Plastics: Revising the History of Conjugated Organic Polymers *100+ Years of Plastics*. *Leo Baekeland and Beyond* (Vol. 1080, pp. 147-163): American Chemical Society.
- Rodrigues, P. C., Fontes, B. D., Torres, B., Sousa, W. S., Faria, G. C., Balogh, D. T., . . . Akcelrud, L. (2015). Synthesis of a PPV-fluorene derivative: Applications in luminescent devices. *Journal of Applied Polymer Science*, *132*(38).
- Roncali, J. (2007). Molecular Engineering of the Band Gap of  $\pi$ -Conjugated Systems: Facing Technological Applications. *Macromolecular Rapid Communications*, *28*(17), 1761-1775.
- Roncali, J., Frère, P., Blanchard, P., de Bettignies, R., Turbiez, M., Roquet, S., . . . Nicolas, Y. (2006). Molecular and supramolecular engineering of  $\pi$ -conjugated systems for photovoltaic conversion. *Thin Solid Films*, *511*, 567-575.
- Safoula, G., Bernede, J. C., Alimi, K., Molinie, P., & Touihri, S. (1996). Study of the evolution of the conductivity of iodine-doped poly(N-vinylcarbazole) as a function of annealing treatment. *Journal of Applied Polymer Science*, *60*(10), 1733-1739.
- Sangchul, L., Jun-Seok, Y., Yongsung, J., Chunhum, C., Dong-Yu, K., Seok-In, N., . . . Takhee, L. (2012). Flexible organic solar cells composed of P3HT:PCBM using chemically doped graphene electrodes. *Nanotechnology*, *23*(34), 344013.
- Santos, C. M., Tria, M. C. R., Vergara, R. A. M. V., Cui, K. M., Pernites, R., & Advincula, R. C. (2011). Films of Highly Disperse Electrodeposited Poly(N-vinylcarbazole)–Graphene Oxide Nanocomposites. *Macromolecular Chemistry and Physics*, *212*(21), 2371-2377.
- Sarac, A. S., Ates, M., & Parlak, E. A. (2005). Comparative Study of Chemical and Electrochemical Copolymerization of N-Methylpyrrole with N-Ethylcarbazole Spectroscopic and Cyclic Voltammetric Analysis. *International Journal of Polymeric Materials and Polymeric Biomaterials*, *54*(9), 883-897.
- Sariciftci, N., Smilowitz, L., Heeger, A. J., & Wudl, F. (1992). Photoinduced electron transfer from a conducting polymer to buckminsterfullerene. *Science*, *258*(5087), 1474-1476.
- Sauerbrunn, E., Chen, Y., Didion, J., Yu, M., Smela, E., & Bruck, H. A. (2015). Thermal imaging using polymer nanocomposite temperature sensors. *physica status solidi (a)*, *212*(10), 2239-2245.
- Scharber, M. C., & Sariciftci, N. S. (2013). Efficiency of bulk-heterojunction organic solar cells. *Progress in Polymer Science*, *38*(12), 1929-1940.
- Sezer, E., Ustamehmetoğlu, B., & Saraç, A. S. (1999). Chemical and electrochemical polymerisation of pyrrole in the presence of N-substituted carbazoles. *Synthetic Metals*, *107*(1), 7-17.
- Shattuck, M. D., & Vahtra, U. (1969). Organic photoconductive compositions and their use in electrophotographic processes: US Patent 3,484,237.

- Shen, Y., & Wan, M. (1998). In situ doping polymerization of pyrrole with sulfonic acid as a dopant. *Synthetic Metals*, 96(2), 127-132.
- Shirakawa, H. (2001). The discovery of polyacetylene film: the dawning of an era of conducting polymers (Nobel lecture). *Angewandte Chemie International Edition*, 40(14), 2574-2580.
- Shirakawa, H., Louis, E. J., MacDiarmid, A. G., Chiang, C. K., & Heeger, A. J. (1977). Synthesis of electrically conducting organic polymers: halogen derivatives of polyacetylene, (CH)<sub>x</sub>. *Journal of the Chemical Society, Chemical Communications*(16), 578-580.
- Silinsh, E. A., Belkind, A. I., Balode, D. R., Biseniece, A. J., Grechov, V. V., Taure, L. F., . . . Bok, I. (1974). Photoelectrical properties, energy level spectra, and photogeneration mechanisms of pentacene. *physica status solidi (a)*, 25(1), 339-347.
- Singh, K., Ohlan, A., & Dhawan, S. (2012). *Polymer-graphene nanocomposites: preparation, characterization, properties, and applications*: INTECH Open Access Publisher.
- Skotheim, T. A., & Reynolds, J. (2006). *Conjugated polymers: theory, synthesis, properties, and characterization*: CRC press.
- Snook, G. A., Kao, P., & Best, A. S. (2011). Conducting-polymer-based supercapacitor devices and electrodes. *Journal of power sources*, 196(1), 1-12.
- Soldano, C., Mahmood, A., & Dujardin, E. (2010). Production, properties and potential of graphene. *Carbon*, 48(8), 2127-2150.
- Song, K. T., Lee, J. Y., Kim, H. D., Kim, D. Y., Kim, S. Y., & Kim, C. Y. (2000). Solvent effects on the characteristics of soluble polypyrrole. *Synthetic Metals*, 110(1), 57-63.
- Song, M.-K., Kim, Y.-T., Kim, B.-S., Kim, J., Char, K., & Rhee, H.-W. (2004). Synthesis and characterization of soluble polypyrrole doped with alkylbenzenesulfonic acids. *Synthetic Metals*, 141(3), 315-319.
- Song, Z., Xu, T., Gordin, M. L., Jiang, Y.-B., Bae, I.-T., Xiao, Q., . . . Wang, D. (2012). Polymer-Graphene Nanocomposites as Ultrafast-Charge and -Discharge Cathodes for Rechargeable Lithium Batteries. *Nano letters*, 12(5), 2205-2211.
- Spanggaard, H., & Krebs, F. C. (2004). A brief history of the development of organic and polymeric photovoltaics. *Solar Energy Materials and Solar Cells*, 83(2-3), 125-146.
- Stankovich, S., Dikin, D. A., Piner, R. D., Kohlhaas, K. A., Kleinhammes, A., Jia, Y., . . . Ruoff, R. S. (2007). Synthesis of graphene-based nanosheets via chemical reduction of exfoliated graphite oxide. *Carbon*, 45(7), 1558-1565.
- Suk, J. W., Lee, W. H., Lee, J., Chou, H., Piner, R. D., Hao, Y., . . . Ruoff, R. S. (2013). Enhancement of the electrical properties of graphene grown by chemical vapor

- deposition via controlling the effects of polymer residue. *Nano letters*, 13(4), 1462-1467.
- Sun, Y., & Shi, G. (2013). Graphene/polymer composites for energy applications. *Journal of Polymer Science Part B: Polymer Physics*, 51(4), 231-253.
- Sun, Y., Welch, G. C., Leong, W. L., Takacs, C. J., Bazan, G. C., & Heeger, A. J. (2012). Solution-processed small-molecule solar cells with 6.7% efficiency. *Nature materials*, 11(1), 44-48.
- Takagi, S., Makuta, S., Veamatahau, A., Otsuka, Y., & Tachibana, Y. (2012). Organic/inorganic hybrid electrochromic devices based on photoelectrochemically formed polypyrrole/TiO<sub>2</sub> nanohybrid films. *Journal of Materials Chemistry*, 22(41), 22181-22189.
- Talaie, A., Lee, J. Y., Lee, Y. K., Jang, J., Romagnoli, J. A., Taguchi, T., & Maeder, E. (2000). Dynamic sensing using intelligent composite: an investigation to development of new pH sensors and electrochromic devices. *Thin Solid Films*, 363(1-2), 163-166.
- Tang, C. W. (1986). Two-layer organic photovoltaic cell. *Applied Physics Letters*, 48(2), 183-185.
- Tat'yana, V. V., & Oleg, N. E. (1997). Polypyrrole: a conducting polymer; its synthesis, properties and applications. *Russian Chemical Reviews*, 66(5), 443.
- Thinh, P. X., Basavaraja, C., & Kim, D. (2012). Characterization and electrochemical behaviors of honeycomb-patterned poly (N-vinylcarbazole)/polystyrene composite films. *Polymer bulletin*, 69(1), 81-94.
- Thomassin, J.-M., Jérôme, C., Pardoën, T., Bailly, C., Huynen, I., & Detrembleur, C. (2013). Polymer/carbon based composites as electromagnetic interference (EMI) shielding materials. *Materials Science and Engineering: R: Reports*, 74(7), 211-232.
- Turco, A., Corvaglia, S., & Mazzotta, E. (2015). Electrochemical sensor for sulfadimethoxine based on molecularly imprinted polypyrrole: Study of imprinting parameters. *Biosensors and Bioelectronics*, 63, 240-247.
- Udum, Y. A., Ergun, Y., Sahin, Y., Pekmez, K., & Yildiz, A. (2009). Electrochemical synthesis and characterization of a new soluble conducting polymer. *Journal of Materials Science*, 44(12), 3148-3155.
- Van der Sanden, M. (1997). Counter-ion induced processibility of conducting Polymers: 1. Acid-assisted oxidative doping and solubilization. *Synthetic Metals*, 87(2), 137-140.
- Verma, V. P., Das, S., Lahiri, I., & Choi, W. (2010). Large-area graphene on polymer film for flexible and transparent anode in field emission device. *Applied Physics Letters*, 96(20), 203108.



- Vyas, M. K., & Chandra, A. (2016). Ion-electron conducting polymer composites: Promising electromagnetic interference shielding material. *ACS Applied Materials & Interfaces*.
- Walton, D. J., Hall, C. E., & Chyla, A. (1991). Functional dopants in conducting polymers. *Synthetic Metals*, 45(3), 363-371.
- Wang, C., Zheng, W., Yue, Z., Too, C. O., & Wallace, G. G. (2011). Buckled, Stretchable Polypyrrole Electrodes for Battery Applications. *Advanced Materials*, 23(31), 3580-3584.
- Wang, J., Chen, J., Konstantinov, K., Zhao, L., Ng, S. H., Wang, G. X., . . . Liu, H. K. (2006). Sulphur-polypyrrole composite positive electrode materials for rechargeable lithium batteries. *Electrochimica Acta*, 51(22), 4634-4638.
- Wang, K., Wu, H., Meng, Y., & Wei, Z. (2014). Conducting Polymer Nanowire Arrays for High Performance Supercapacitors. *Small*, 10(1), 14-31.
- Wang, X., Yang, C., Li, H., & Liu, P. (2013). Synthesis and electrochemical performance of well-defined flake-shaped sulfonated graphene/polypyrrole composites via facile in situ doping polymerization. *Electrochimica Acta*, 111, 729-737.
- Weerakoon, K. A., Auad, M., Horikawa, S., & Chin, B. A. (2012). Effect of Active Layer Morphology on Poly3-Hexylthiophene Phytochemical Chemiresistor Sensor Performance. *Sensors Journal, IEEE*, 12(10), 3062-3068.
- Wen, Q., Pan, X., Hu, Q.-x., Zhao, S.-j., Hou, Z.-f., & Yu, Q.-z. (2013). Structure-property relationship of dodecylbenzenesulfonic acid doped polypyrrole. *Synthetic Metals*, 164, 27-31.
- Wienk, M. M., Kroon, J. M., Verhees, W. J. H., Knol, J., Hummelen, J. C., van Hal, P. A., & Janssen, R. A. J. (2003). Efficient Methano[70]fullerene/MDMO-PPV Bulk Heterojunction Photovoltaic Cells. *Angewandte Chemie International Edition*, 42(29), 3371-3375.
- Wu, Y., Lin, Y.-m., Bol, A. A., Jenkins, K. A., Xia, F., Farmer, D. B., . . . Avouris, P. (2011). High-frequency, scaled graphene transistors on diamond-like carbon. *Nature*, 472(7341), 74-78.
- Yan, Q.-L., Gozin, M., Zhao, F.-Q., Cohen, A., & Pang, S.-P. (2016). Highly energetic compositions based on functionalized carbon nanomaterials. *Nanoscale*, 8(9), 4799-4851.
- Ye, L., Zhang, S., Huo, L., Zhang, M., & Hou, J. (2014). Molecular Design toward Highly Efficient Photovoltaic Polymers Based on Two-Dimensional Conjugated Benzodithiophene. *Accounts of Chemical Research*, 47(5), 1595-1603.
- Yeo, J.-S., Yun, J.-M., Kim, D.-Y., Kim, S.-S., & Na, S.-I. (2013). Successive solvent-treated PEDOT:PSS electrodes for flexible ITO-free organic photovoltaics. *Solar Energy Materials and Solar Cells*, 114, 104-109.

- Yu, G., Gao, J., Hummelen, J. C., Wudl, F., & Heeger, A. J. (1995). Polymer photovoltaic cells: enhanced efficiencies via a network of internal donor-acceptor heterojunctions. *Science-AAAS-Weekly Paper Edition*, 270(5243), 1789-1790.
- Zaidi, B., Bouzayen, N., Wéry, J., & Alimi, K. (2010). Grafting of oligo-N-vinyl carbazole on single walled carbon nanotubes. *Journal of Molecular Structure*, 971(1-3), 71-80.
- Zeng, Q. H., Yu, A. B., Lu, G. Q., & Paul, D. R. (2005). Clay-Based Polymer Nanocomposites: Research and Commercial Development. *Journal of nanoscience and nanotechnology*, 5(10), 1574-1592.
- Zhang, B., Chen, Y., Zhuang, X., Liu, G., Yu, B., Kang, E.-T., . . . Li, Y. (2010). Poly(N-vinylcarbazole) chemically modified graphene oxide. *Journal of Polymer Science Part A: Polymer Chemistry*, 48(12), 2642-2649.
- Zhang, D., Xie, F., Lin, P., & Choy, W. C. H. (2013). Al-TiO<sub>2</sub> Composite-Modified Single-Layer Graphene as an Efficient Transparent Cathode for Organic Solar Cells. *ACS Nano*, 7(2), 1740-1747.
- Zhao, Y., Liu, J., Hu, Y., Cheng, H., Hu, C., Jiang, C., . . . Qu, L. (2013). Highly Compression-Tolerant Supercapacitor Based on Polypyrrole-mediated Graphene Foam Electrodes. *Advanced Materials*, 25(4), 591-595.
- Zhou, C., Zhang, Y., Li, Y., & Liu, J. (2013). Construction of High-Capacitance 3D CoO@Polypyrrole Nanowire Array Electrode for Aqueous Asymmetric Supercapacitor. *Nano letters*, 13(5), 2078-2085.
- Zhou, J., Wan, X., Liu, Y., Zuo, Y., Li, Z., He, G., . . . Su, X. (2012). Small molecules based on benzo [1, 2-b: 4, 5-b'] dithiophene unit for high-performance solution-processed organic solar cells. *Journal of the American Chemical Society*, 134(39), 16345-16351.
- Zhou, X., Ma, P., Wang, A., Yu, C., Qian, T., Wu, S., & Shen, J. (2015). Dopamine fluorescent sensors based on polypyrrole/graphene quantum dots core/shell hybrids. *Biosensors and Bioelectronics*, 64, 404-410.
- Zhou, Z.-G., Zhao, Y., Zhang, C., Zhou, D., Chen, Y., Lin, Z., . . . Ling, Q. (2017). A facile one-pot synthesis of hyper-branched carbazole based polymer as hole-transporting material for perovskite solar cells. *Journal of Materials Chemistry A*.
- Zhuang, X., Chen, Y., Wang, L., Neoh, K.-G., Kang, E.-T., & Wang, C. (2014). A solution-processable polymer-grafted graphene oxide derivative for nonvolatile rewritable memory. *Polym. Chem.*, 5(6), 2010-2017.

## LIST OF PUBLICATIONS AND PAPERS PRESENTED

- 1. Recent Approaches to Controlling the Nanoscale Morphology of Polymer-Based Bulk-Heterojunction Solar Cells**  
Wasiu Adebayo Hammed, Rosiyah Yahya, Abdulra'uf Lukman Bola and Habibun Nabi Muhammad Ekramul Mahmud  
Available online: 8 November 2013  
*Energies* 2013, 6, 5847-5868
- 2. Prospects of conducting polymer and graphene as counter electrodes in dye-sensitized solar cells**  
Muhammad Shafiqur Rahman, Wasiu Adebayo Hammed, Rosiyah Binti Yahya, Habibun Nabi Muhammad Ekramul Mahmud  
Available online: 17 August 2016  
*J Polym Res* (2016) 23: 192
- 3. One-step facile synthesis of poly (N-vinylcarbazole)-polypyrrole/graphene oxide nanocomposites: Enhanced solubility and good electrical conductivity**  
*International Journal of Polymeric Materials* (Article under review)
- 4. Processable dodecylbenzene sulfonic acid (DBSA) doped poly(N-vinyl carbazole)-poly(pyrrole) for optoelectronic applications**  
WA Hammed, MS Rahman, H Mahmud, R Yahya, K Sulaiman  
*Designed Monomers and Polymers* 20 (1), 368-377
- 5. Optoelectrical and Photoluminescence Quenching Properties of Poly(N-vinyl carbazole)-Polypyrrole/Reduced Graphene Oxide Nanocomposites**  
Muhammad Shafiqur Rahman, Wasiu Adebayo Hammed, Rosiyah Binti Yahya, Habibun Nabi Muhammad Ekramul Mahmud  
*Synthetic Metals* Volume 226, April 2017, Pages 188–194  
**Synthesis of conducting polymers based on poly(n-vinyl carbazole pyrrole) and their optoelectronic applications**  
(Seminar presentation)
- 6. Small band gap polymers for organic photovoltaics**  
1st International Conference on the Science & Engineering of Materials 13-14 November 2013, Sunway Putra Hotel, Kuala Lumpur, Malaysia